THE
PHYSICAL REVIEW
A journal of experimental and theoretical physics established by E. L. Nichols in 1893

SECOND SERIES, VOL. 71, No. 8 APRIL 15, 1947

Electron Affinity of Positronium

EGIL A. HYLLERAAS
Institute of Theoretical Physics, University of Oslo, Oslo, Norway
(Received November 9, 1946)

By use of the variational method as previously applied to the mathematically similar problem of the negative atomic hydrogen ion, the energy of a compound of two electrons and one positron has been calculated. The resulting (third approximation) value of roughly 0.19 ev binding energy of this system with respect to dissociation into a free electron and a system of one electron and one positron corresponds to the value already found by J. A. Wheeler. On the basis of higher approximations obtained for H^- the exact binding energy of the tri-electron has been estimated to be 0.203 ev.

1.

THE properties of the hypothetical *positronium* atom or *bi-electron*, a compound of one electron and one positron, have been studied by various physicists.[1] Thus, for example, the energy levels of this system are

$$E_n = -R'h/n^2, \quad R' = \tfrac{1}{2}R,$$

where R is the Rydberg constant.

J. A. Wheeler first extended the investigations to electron-positron clusters of higher complexity.[1] Wheeler concludes that the three-particle system $(++-)$ or $(+--)$ is stable by at least 0.19 ev against dissociation of any kind.

Shortly after the calculations which are presented below had been completed the author was informed about the method employed and the numerical results obtained by Wheeler. The two treatments are very much the same, both being based on that previously developed by the present author for the negative atomic hydrogen ion.[2] As a matter of fact, the eigenfunctions used by the two investigators are identical up to the third approximation, which is the highest approximation considered by Wheeler.

Nevertheless, I believe the present publication to be of some interest in demonstrating the agreement between the numerical results, and, furthermore, because of the attempt which has been made in this paper to estimate the exact value of the binding energy of the tri-electron on the basis of the higher approximations previously found by the author for the hydrogen ion. Again, the results recently reported[3] on the dynamic stability of the four-electron system might also make the publication of this paper desirable.

2.

A compound of two electrons and one positron (or two positrons and one electron) is closely related to the negative hydrogen ion. In atomic

[1] The name 'positronium' has been proposed by A. E. Ruark, Phys. Rev. 68, 278 (1945) and the name 'bi-electron' by J. A. Wheeler, Ann. New York Acad. Sci. 48, 219 (1946).

[2] E. A. Hylleraas, Zeits. f. Physik 60, 624 (1930).

[3] E. A. Hylleraas and A. Ore, Phys. Rev. 71, 493 (1947).

units, with e, m, and $\hbar$ as fundamental units and a_H and $2Rh$ the corresponding units of length and energy, the wave equation for such systems may be written as

$$\left\{\frac{1}{2}\left(\nabla_1^2+\nabla_2^2+\frac{m}{m_3}\nabla_3^2\right)+E+\frac{1}{r_1}+\frac{1}{r_2}-\frac{1}{r_{12}}\right\}\psi=0,$$

r_1 and r_2 being the distances of the two electrons from the positive particle of mass m_3.

For the hydrogen ion we take $m_3=\infty$ and change the unit of length from a_H to $\frac{1}{2}a_H$, the unit of energy becoming $4Rh$. In energy units Rh, the wave equation of H^- then reads

$$\left\{\nabla_1^2+\nabla_2^2+\frac{E}{4}+\frac{1}{r_1}+\frac{1}{r_2}-\frac{1}{r_{12}}\right\}\psi=0$$

compared to

$$\left\{\tfrac{1}{2}(\nabla_1^2+\nabla_2^2+\nabla_3^2)+\frac{E}{4}+\frac{1}{r_1}+\frac{1}{r_2}-\frac{1}{r_{12}}\right\}\psi=0$$

for the tri-electron in units a_H and $\frac{1}{2}Rh$.

Considering only states of zero total linear and angular momentum it is easily seen that the wave function depends only on the three distances appearing in the potential energy of the particles. As shown in reference 2 the energy of the ground state is given by the minimum value of $E=-L^2/4NM$, where

$$N=\int\psi^2 d\tau,\quad L=4\int\left(\frac{1}{r_1}+\frac{1}{r_2}-\frac{1}{r_{12}}\right)\psi^2 d\tau,$$

$$M=4\int\{(\nabla_1\psi)^2+(\nabla_2\psi)^2\}d\tau$$

$$\text{or}\quad 4\int\tfrac{1}{2}\{(\nabla_1\psi)^2+(\nabla_2\psi)^2+(\nabla_3\psi)^2\}d\tau.$$

It is understood, however, that in the function $\psi(r_1, r_2, r_{12})$ used here we have to replace each r by kr in order to get the actual eigenfunction. The expression for E given above has been obtained by minimizing E with respect to k in the expression $NE=-kL+k^2M$.

The two expressions for M refer to the hydrogen ion and the tri-electron, respectively. The difference in the two M-values

$$\Delta M=4\int\tfrac{1}{2}\{(\nabla_3\psi)^2-(\nabla_1\psi)^2-(\nabla_2\psi)^2\}d\tau$$

vanishes when ψ is independent of r_{12}. Consequently, in that case there is no mathematical difference at all between the two problems—apart from the difference in energy units.

If we consider a function

$$\psi=e^{-\frac{1}{2}s}(1+c_1u+c_2t^2+c_4t^4+c_6t^6+\cdots),$$

$$s=r_1+r_2,\quad t=-r_1+r_2,\quad u=r_{12},$$

and put $c_1=c_4=c_6=0$, we get in the first and second approximation $E=-0.9453$ and $E=-1.0246$ when we take $c_2=0$, and $c_2=0.05$, respectively. For the hydrogen ion this value is better than the second approximation $E=-1.0176$ obtained by variation of c_1 only. The corresponding variation for the tri-electron leads to the value $E=-0.9607$; hence it is evident that the variable $u=r_{12}$ plays a less important role in the case of the tri-electron.

In order to investigate the convergence by r_{12}-independent functions the third and forth approximations have been calculated, giving

$$E=-1.02665 \text{ for } c_2=0.045,$$

$$c_4=0.00025 \quad\text{and}\quad E=-1.02762 \text{ for } c_2=0.048,$$

$$c_4=0.00011,\quad c_6=0.0000011.$$

On the other hand the wave function

$$\psi=e^{-\frac{1}{2}s}\cosh\beta t/2$$

gives $E=-1.02660$, with $\beta=0.33$, corresponding approximately to the above third approximation. The difference between the third and fourth approximations is rather astonishing, but certainly does not mean that the limiting value is still far away.

Postponing the evaluation of ΔM, we give at once the third approximation minimum value when $c_4=c_6=0$. Putting $c_1=0.05$, $c_2=0.05$, the result is $E=-1.0276$, the corresponding value for H^- being (-1.0506). Thus the contributions of the term c_1u are (-0.0030) and (-0.0260), respectively. Now the minimum energy value of H^- has been found[4] to be (-1.05284), an im-

[4] E. A. Hylleraas, Zeits. f. Physik 65, 209 (1930).

provement amounting to (-0.00224) reckoned from the third approximation. Adding the same value to the third approximation of the tri-electron the result is $E=-1.02984$. On the other hand, adding the contribution (-0.0030) from c_1u in the third approximation to the fourth approximation with u-independent functions the result is $E=-1.0306$. But the contribution of c_1u must be smaller in this approximation than in the third one. We therefore infer that the energy of the positronium ion is very near to $E=-1.0300$, corresponding to an electron affinity of positronium of

$$W=0.0300R'h=0.203 \text{ ev}.$$

As to the various terms of M, it is easier to evaluate $\int(\nabla_3\psi)^2 d\tau$ than the difference ΔM. Putting

$$M_1=4\int\{(\nabla_1\psi)^2+(\nabla_2\psi)^2\}d\tau$$

and

$$M_2=4\int(\nabla_3\psi)^2 d\tau$$

and considering only terms of the form

$$\psi_{lm}=e^{-\frac{1}{2}t}t^l u^m$$

in the eigenfunction one finds

$$(M_2)_{lm}{}^{l'm'}=\left\{\frac{l+l'+m+m'+4}{l+l'+1}+\frac{4ll'}{(l+l'-1)(l+l'+1)}\right\}\cdot\Pi(l+l'+m+m'+2),$$

where M_1, N, and L have already been given in the paper[4] on H^-. In order to have just this numerical value the volume element is taken to be $d\tau=\frac{1}{2}r_1r_2r_{12}dr_1dr_2dr_{12}=\frac{1}{16}u(s^2-t^2)dsdudt$, corresponding to $dt=r_1^2r_2^2dr_1dr_2$ when the eigenfunction is independent of r_{12}.

It is easy to find general formulae for all matrix elements but, because of the complexity of M_1, we shall not give them here but take the values from the paper cited above. The result is

$$N=4+35c_1+48c_2+96c_1^2+308c_1c_2+576c_2^2 \qquad L=11+88c_1+156c_2+218c_1^2+928c_1c_2+1992c_2^2$$

$$M_1=8+50c_1+96c_2+128c_1^2+584c_1c_2+1920c_2^2 \qquad M_2=8+60c_1+96c_2+144c_1^2+560c_1c_2+1920c_2^2$$

$$M=\tfrac{1}{2}(M_1+M_2)=8+55c_1+96c_2+136c_1^2+572c_1c_2+1920c_2^2.$$

PHYSICAL REVIEW VOLUME 71, NUMBER 8 APRIL 15, 1947

Binding Energy of the Positronium Molecule

EGIL A. HYLLERAAS
Institute of Theoretical Physics, University of Oslo, Oslo, Norway

AND

AADNE ORE*
Sloane Physics Laboratory, Yale University, New Haven, Connecticut

(Received December 26, 1946)

A system of two electrons and two positrons is shown to possess dynamic stability. The variational calculation performed leads to a binding energy of at least 0.11 ev for this cluster. The approximate wave function which yields this value depends on the four electron-positron distances only. Neglect of the two distances between particles of the same kind permits an essential mathematical simplification which might be of interest in other problems.

INTRODUCTION

THE question of the stability of a compound of two electrons and two positrons is of particular interest, since it may be considered fundamental in a theoretical investigation of the stability of large poly-electrons.[1]

A first approximation calculation of the

* F. E. Loomis Fellow.

[1] J. A. Wheeler, Ann. New York Acad. Sci. 48, 219 (1946).

binding energy of the quadri-electron or "positronium molecule" $(++--)$ was performed by Wheeler[1] who employed the variational method with a ground-state harmonic oscillator function. The investigations have been extended to higher approximations by Ore,[2] who considered oscillator functions of higher degree of excitation as well as functions of more "hydrogenic" character. The results failed to furnish evidence for the stability of this four-particle system with respect to dissociation into two separate bi-electrons or "positronium atoms."

These investigations were not conclusive, and there were reasons why it seemed worth while to re-examine the problem in question. The cluster $(++-)$ forms a stable particle[1,3] capable of exerting an attractive coulomb force on a distant electron. Furthermore, it is easily found that the energy arising from the attractive van der Waals force between two distant bi-electrons is appreciably larger than that for two hydrogen atoms. But an attempt to study the stability of the four-particle system from this point of view leads to a difficulty of principle, *viz.*, the combination of short range exchange forces with long range van der Waals forces when all component particles of the interacting structures are of equal mass. In point of fact, a precisely similar difficulty arises when one treats the problem of the interaction between light nuclei. It was the attempt to solve this question which led Wheeler to the invention of a "collision" matrix.[4] It would seem that the problem of interaction between two bi-electrons is of the type for which the method of resonating group structure is in principle adapted.

However, the present treatment of the quadri-electron may be considered an extension of the successful treatments of the tri-electron, which followed the scheme employed by Hylleraas for the negative hydrogen ion.[5]

THEORY

In suitable units, which differ from ordinary atomic units in that as the energy unit is taken to be $R'h=\frac{1}{2}Rh$ rather than $2Rh$, the wave equation of the four-electron may be written:

$$\{\tfrac{1}{2}[\nabla_1^2+\nabla_2^2+\nabla_a^2+\nabla_b^2]+E/4+V\}\Psi=0,$$

$$V=\frac{1}{r_{1a}}+\frac{1}{r_{2b}}+\frac{1}{r_{1b}}+\frac{1}{r_{2a}}-\frac{1}{r_{12}}-\frac{1}{r_{ab}}.$$

Here 1, 2 refer to the two electrons, and a, b to the positrons.

The motion of the center of mass of the cluster is irrelevant, and the ground state is an S state. The absence of total linear and angular momentum with respect to the center of mass reduces the number of independent variables from 12 to 6. Obviously these six variables can be taken to be the six distances appearing in the expression for the potential energy.

This means a reduction in the number of variables as compared to a total of nine scalar components of the three vectors $\mathbf{s}$, $\mathbf{t}$, and $\mathbf{u}$ employed in reference 2. It is readily seen that a function of s, t, and u involves the angle between $\mathbf{r}_{12}$ and $\mathbf{r}_{ab}$ in addition to the six interparticle distances. The ground-state harmonic oscillator function, on the other hand, contains no such irrelevant variable. Thus we see why the hydrogenic function of reference 2 turned out to be inferior to the oscillator function.

The usual procedure of minimizing the energy with respect to the parameter k, corresponding to the correct wave function $\Psi=\Psi(kr_{ij})$, $i,j=1,2,a,b$, leads to

$$EN/4=-kL+k^2M, \quad \text{or} \quad E=-L^2/NM$$

where

$$N=\int\Psi^2d\tau, \quad L=\int V\Psi^2d\tau,$$

$$M=\tfrac{1}{2}\int\textstyle\sum_i(\nabla_i\Psi)^2d\tau, \quad i=1,2,a,b; \quad \Psi=\Psi(r_{ij}).$$

For suitable new variables we choose

$$s_1=r_{1a}+r_{1b}, \quad t_1=r_{1a}-r_{1b}, \quad s_2=r_{2a}+r_{2b},$$

$$t_2=r_{2a}-r_{2b}, \quad u=r_{12}, \quad v=r_{ab}.$$

The ground state is non-degenerate and will have symmetry properties which follow from the symmetry of the Hamiltonian, that is, symmetry in both electrons and positrons, as well as, symmetry or anti-symmetry with respect to inter-

[1] A. Ore, Phys. Rev. **70**, 90 (1946).
[2] E. A. Hylleraas, Phys. Rev. **71**, 491 (1947).
[3] J. A. Wheeler, Phys. Rev. **52**, 1107 (1937).
[4] E. A. Hylleraas, Zeits. f. Physik **60**, 624 (1930).

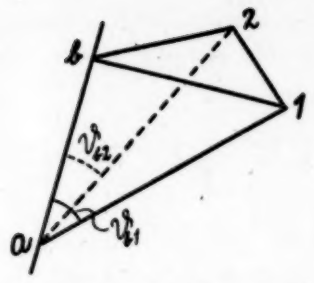

FIG. 1. Coordinate system for the positronium molecule.

change of the two electrons against the two positrons. (We are concerned with the space dependence of the wave function. The inclusion of the two anti-symmetric spin functions, one for each kind of particles, would give a total wave function in accordance with the Pauli principle.)

Thus if we consider functions of the simple form

$$\Psi=\psi_1(s_1, s_2)\psi_2(t_1, t_2)\psi_3(u)\psi_4(v)$$

the symmetry suggests

$$\psi_1=\psi_1(s_1+s_2), \quad \psi_2=\psi_2((t_1-t_2)^2) \quad \text{and} \quad \psi_3=\psi_4.$$

There will in general be no particular difficulties involved in the calculation of the integrals L, M, and N when the variational function is taken to be independent of u and v. By performing the substitution 1, $2\leftrightarrow a, b$ in the terms which involve u one can see that it is proper in that case to consider the integrands independent of u. For instance, on account of this symmetry u may be replaced by v in L. We need then retain only five variables of integration, since the integration over the sixth variable, which may be chosen to be the angle φ_{12} defined below, contributes merely the same constant factor to L, M, and N.

In order to get the proper volume element consider the edge (ab) as the main axis of the tetrahedron $(ab12)$ (in Fig. 1). Then the three angles defining the direction of (ab) and the rotation of the system as a whole around this axis may be left out of the integrations. Also the relative angle φ_{12} between the triangles $(ab1)$ and $(ab2)$ is unimportant when the integrand is independent of $r_{12}=u$.

After this reduction in the number of independent variables from 9 to 6, and next to 5, we may take the volume element to be

$$\begin{aligned}d\tau&=4r_{ab}^2dr_{ab}r_{1a}^2dr_{1a}r_{2a}^2dr_{2a}\sin\vartheta_{b1}d\vartheta_{b1}\sin\vartheta_{b2}d\vartheta_{b2}\\&=4dr_{ab}r_{1a}dr_{1a}r_{1b}dr_{1b}r_{2a}dr_{2a}r_{2b}dr_{2b}\\&=dv\tfrac{1}{4}(s_1^2-t_1^2)ds_1dt_1\tfrac{1}{4}(s_2^2-t_2^2)ds_2dt_2,\end{aligned}$$

the limits of integration being

$$v\leqq s_1,s_2\leqq\infty; \quad -v\leqq t_1,t_2\leqq v; \quad 0\leqq v\leqq\infty.$$

If we use in a first approximation the very simple function

$$\Psi=\exp[-\tfrac{1}{2}(s_1+s_2)],$$

the integrals become

$$N_1=\int_0^\infty e^{-2v}(\tfrac{1}{3}v^3+v^2+v)^2dv=33/8,$$

$$L_1=4A-2B=4\cdot21/8-2\cdot25/12=19/3,$$

$$M_1=2A=21/4,$$

$$A=\int_0^\infty e^{-2v}(\tfrac{1}{3}v^3+v^2+v)(v^2+v)dv,$$

$$B=\int_0^\infty e^{-2v}(\tfrac{1}{3}v^3+v^2+v)^2\frac{dv}{v}.$$

Hence, in this approximation,

$$E=-\frac{19^2\cdot32}{33\cdot21\cdot9}=-1.8522R'h=-12.54 \text{ ev}.$$

A better approximation is obtained when we consider a function representing each electron strongly bound to one of the two positrons and only loosely bound to the second. For instance, let

$$\begin{aligned}2\Psi=&\exp[-\tfrac{1}{2}(1+\beta)(r_{1a}+r_{2b})-\tfrac{1}{2}(1-\beta)(r_{1b}+r_{2a})]\\&+\exp[-\tfrac{1}{2}(1-\beta)(r_{1a}+r_{2b})-\tfrac{1}{2}(1+\beta)(r_{1b}+r_{2a})].\end{aligned}$$

or

$$\Psi=\exp[-\tfrac{1}{2}(s_1+s_2)]\cosh\beta/2(t_1-t_2).$$

Then $\beta=1$ will correspond to two separate bi-electrons, whereas for $\beta=0$ we have the above case of equal binding within all electron-positron pairs.

Since $\cosh^2\beta/2(t_1-t_2)=\tfrac{1}{2}(1+\cosh\beta(t_1-t_2))$ the integrals N, L, and M will now be

$$N=\tfrac{1}{2}(N_1+N_2), \quad L=\tfrac{1}{2}(L_1+L_2)$$

TABLE I. Numerical relation between the calculated total binding energy and the square of the parameter β.

β^2	0	0.25	0.5	0.75	1.0
$-E$	1.8522	1.98180	2.01681	2.00288	2.0000

and

$$M=\tfrac{1}{2}(M_1'+M_2), \quad M_1'=M_1-3\beta^2.$$

Here N_1, L_1, and M_1 are the integrals given above, while the integrals of index 2 can be obtained from those of index 1 by replacing $\frac{1}{3}v^3+v^2+v$ by

$$\left(v-\frac{1-\beta^2}{\beta^2}\right)\frac{\sinh\beta v}{\beta}+\frac{v\cosh\beta v}{\beta^2}$$

and by further replacement of v^2+v by

$$(v+1)(\sinh\beta v)/\beta \text{ in } L_2$$

and by

$$v((\sinh\beta v)\beta+\cosh\beta v) \text{ in } M_2.$$

Finally we get M_1' from M_1 by replacing v^2+v by $v^2+v-\frac{1}{3}\beta^2v^3$.

The result is

$$N_2=\frac{33/8-11\beta^2/4+5\beta^4/8}{(1-\beta^2)^3},$$

$$M_2=2\frac{21/8-3\beta^2/4+\beta^4/8}{(1-\beta^2)^3},$$

$$L_2=4\frac{21/8-9\beta^2/4+5\beta^4/8}{(1-\beta^2)^3}-\frac{2}{(1-\beta^2)^2}\left[1-\frac{5\beta^2}{8}\right.$$
$$\left.-\frac{1}{4\beta^2}+\frac{7}{8\beta^2}+\frac{(1-\beta^2)^4}{4\beta^6}\log\frac{1}{1-\beta^2}\right].$$

Among the integrations leading to these expressions we need only mention the integral involved in L_2

$$\int_0^\infty e^{-2v}\left(\frac{\sinh\beta v}{\beta}\right)^2\frac{dv}{v}=\frac{1}{4\beta^2}\log\left(\frac{1}{1-\beta^2}\right).$$

The relation between the calculated total binding energy of the system and the value of the parameter β, which determines the approximate wave function, can be read from Table I. The minimum value of E appears to be roughly -2.017 for β^2 about 0.50. The binding energy of the positronium molecule with respect to dissociation into two positronium atoms is thus in fact positive, amounting in this approximation to

$$W=0.017R'h=0.11 \text{ ev}.$$

The approximate calculation just presented is related to the well-known Heitler-London treatment of the hydrogen molecule or rather to Wang's modification of this treatment. In view of the excellent results obtained subsequently by James and Coolidge for the binding energy of that molecule we are inclined to believe that considerable improvement is possible in the value presented above for the positronium molecule.

The authors wish to express their acknowledgment to Professors H. Margenau of Yale University and J. A. Wheeler of Princeton University for their stimulating interest in the problem of the four-electron system, for suggestions incorporated in the introduction to this paper, and for other information at an early stage of the development of the theory of polyelectrons.

Photo-Neutron Sources and the Energy of the Photo-Neutrons*

A. WATTENBERG**
Argonne Laboratory, University of Chicago, Chicago, Illinois

(Received January 2, 1947)

In a preliminary study photo-neutrons were observed to be produced by the γ-rays from Na^{24}, Mn^{56}, Ga^{72}, As^{76}, and La^{140} when these artificially radioactive isotopes were placed in D_2O or Be; F^{20}, Al^{28}, Cl^{38}, In^{116}, and Sb^{124} produced neutrons only in Be. The first group of isotopes must have γ-rays with energy higher than 2.18 Mev, and the second group must have γ-rays greater than 1.63 Mev but less than 2.18 Mev. No photo-neutrons were observed from Co^{60}, Cu^{64}, Ag (225 day $\frac{1}{2}$-life), Pr^{142}, Eu^{151}, Dy^{165}, Ta^{182}, Re^{188}, Ir (19 hours $\frac{1}{2}$-life), and Au^{198} in Be; the intense γ-rays from these isotopes must have energies less than 1.63 Mev. In a second experiment the energy of the photo-neutrons from nine of these sources was determined by measuring the hydrogen scattering cross section of the emitted neutrons. Seven of the sources seem to emit homogeneous groups of neutrons; they are: Sb+Be, Ga+D_2O, La+D_2O, Mn+D_2O, Na+D_2O, La+Be, and Na+Be with neutron energies 0.024, 0.13, 0.13, 0.22, 0.22, 0.62, and 0.83 Mev, respectively, for the particular sized sources studied. Mn+Be emits three groups of neutrons of different energies, but more than 80 percent of the neutrons seem to be in a group at 0.14 Mev. The energy of the γ-rays calculated to produce neutrons of these energies are: for Na^{24}, 2.74 Mev; for Mn^{56}, 1.81 and 2.7 Mev (a third γ-ray is present); for Ga^{72}, 2.50 Mev (at least one other γ-ray is present with an energy between 2.2 and 1.63 Mev); for Sb^{124}, 1.67 Mev; and for La^{140}, 2.49 Mev. The total neutron cross section of carbon is also given for seven of these photo-neutron sources.

INTRODUCTION

HIGH energy γ-rays falling on beryllium or deuterium will cause the emission of neutrons. The threshold for this (γ, n) reaction in beryllium is approximately 1.63 Mev[1-3] and in deuterium is approximately 2.18 Mev.[2-4] Gamma-rays from artificially radioactive sodium, antimony, and yttrium have been used previously to make photo-neutron sources.[5-9]

The heavy water "Pile" at the Argonne Laboratory[10] made available very intense radioactive sources produced by means of (n, γ) reactions. The γ-rays from these radioactive sources were used to produce photo-neutrons.

The photo-neutron sources are of value because γ-rays of a single energy produce a monoenergetic group of neutrons. The energy of the emitted neutrons is from the conservation of energy and momentum

$$E_n=\frac{A-1}{A}\left[E_\gamma-Q-\frac{E_\gamma^2}{1862(A-1)}\right]+\delta. \quad (1)$$

E_n is the energy of the neutrons in Mev; A is the atomic weight of the target nucleus; E_γ is the energy of the γ-ray in Mev; and Q is the threshold energy in Mev for the (γ, n) reaction in the nucleus of mass A. δ is a small spread in energy that is a function of the angle θ between the direction of the γ-ray and the direction in which the neutron is emitted.

$$\delta \cong E_\gamma \cos\theta\left(\frac{2(A-1)(E_\gamma-Q)}{931\times A^2}\right)^{\frac{1}{2}}. \quad (2)$$

Part I of this article deals with a preliminary study that was made to determine which of the radioactive elements emit γ-rays energetic enough to produce photo-neutrons in beryllium or deuterium. Part II deals with the determination

* Based on work performed under Contract W-741-eng-37 of the Manhattan District at the Argonne Laboratory, University of Chicago.

** Now a Fellow of the Institute for Nuclear Studies of the University of Chicago.

[1] Collins, Waldman, and Guth, Phys. Rev. **56**, 878 (1939).
[2] F. E. Myers and L. C. Van Atta, Phys. Rev. **61**, 19 (1942).
[3] M. L. Wiedenbeck and C. J. Marhoef, Phys. Rev. **67**, 54 (1945).
[4] F. T. Rogers and M. M. Rogers, Phys. Rev. **55**, 263 (1939).
[5] W. E. Ogle and P. G. Kruger, Phys. Rev. **65**, 61 (1944).
[6] Goldhaber, Klaiber, and Scharff-Goldhaber, Phys. Rev. **65**, 61 (1944).
[7] G. S. Klaiber and G. Scharff-Goldhaber, Phys. Rev. **61**, 733 (1942).
[8] G. Scharff-Goldhaber, Phys. Rev. **59**, 937 (1941).
[9] G. R. Gamertsfelder, Phys. Rev. **63**, 60 (1943).
[10] H. D. Smyth, Rev. Mod. Phys. **17**, 419 (1945).

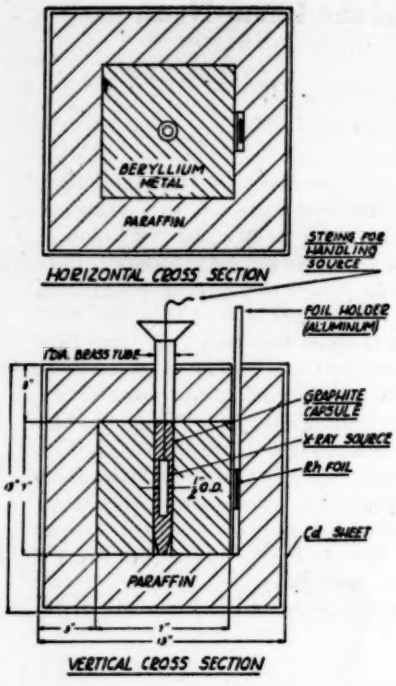

FIG. 1. Geometry used in preliminary study to find (γ, n) sources. For investigations with deuterium, a brass cylinder containing heavy water was substituted for the beryllium.

of the energy of the neutrons emitted by nine of these photo-neutron sources. The actual use of these sources in experiments will be reported in further articles.

I. PRELIMINARY STUDY

Seaborg's table[11] lists eight isotopes that emit γ-rays sufficiently energetic to produce neutrons in both deuterium and beryllium (i.e., the energy of the γ-ray is greater than 2.18 Mev). There are seven other isotopes that emit γ-rays which will produce neutrons only in beryllium (i.e., the energy of the γ-ray is greater than 1.63 Mev but less than 2.18 Mev). These artificially radioactive isotopes and the energy of their γ-rays as given by Seaborg are listed in Table I.

Method

All of the isotopes of Table I were activated except for those starred. The activity of the sources ranged from 100 to 5000 "millicuries."[12]

[11] G. T. Seaborg, Rev. Mod. Phys. 16, 1 (1944).

[12] By a "millicurie" of activity in an artificially radioactive source is meant an activity of 3.7×10^7 disintegrations per second. The activity is calculated using the values of the thermal neutron cross sections for the activation of the isotope in question and the value of the thermal neutron flux as measured by means of a small gold foil.

A test was made to observe whether neutrons were emitted when these sources were placed in beryllium or heavy water. The sources were set either at the center of a cubical box of beryllium containing 9.5 kilograms of beryllium metal or at the center of a cylinder containing 3.0 kilograms of heavy water. The beryllium and the heavy water were inclosed in paraffin (Fig. 1) in order to slow down the neutrons. A rhodium foil was placed as indicated to detect the neutrons. The activity of the rhodium foil was measured by placing it underneath an Eck and Krebs, glass wall, Geiger counter. An initial counting rate of more than 10,000 counts per minute was observed from the neutrons produced in beryllium by a 100 millicurie source of Na^{24}.

In order to be certain that the γ-ray producing the neutrons was associated with the activity of the isotope being studied and not to another isotope or to some impurity, the decay of the photo-neutrons was followed. All the half-lives observed were in reasonable agreement with those given in column 3 of Table II, which are from Seaborg's table.[11]

Results of Preliminary Study

The relative (neutron induced) activity observed from 100 millicuries of the different elements varied over a factor greater than 1000. The efficiency of the rhodium foil as a neutron detector in a geometrical arrangement of this kind undoubtedly varies with the initial energy of the photo-neutron, and the cross section for the (γ, n) reaction is a function of the energy of

TABLE I. Radioactive isotopes emitting high energy γ-rays, from Seaborg's table.

Isotopes with γ-rays above 2.18 Mev	Energy of γ-ray (in Mev)	Isotopes with γ-rays above 1.63 Mev	Energy of γ-ray (in Mev)
F^{20}	2.2	Al^{28}	1.8
Na^{24}	2.7	Sc^{44*}	1.8
Cl^{38}	2.2	Mn^{56}	2.13 and 1.8
Ga^{72}	2.65	Co^{58*}	1.74
As^{76}	3.2 and 2.2	Sb^{124}	1.75
Y^{88*}	2.8	La^{140}	1.75
In^{116}	2.3	Pr^{142}	1.9
An^{198}	2.5		

* These isotopes cannot be produced by an (n, γ) reaction.

the γ-rays. These two undetermined factors prevent any accurate quantitative interpretation of the data. However, these two factors do not account for the observed factor of 1000 as the activities observed from the high energy Na+Be neutrons (see Table IV) and the low energy Sb+Be neutrons differed by less than a factor of two. Therefore, the large variation in the relative number of neutrons emitted by different sources must be attributed to the number of energetic γ-rays emitted per disintegration.

Table II gives the radioactive isotopes whose γ-rays were observed to produce neutrons. In order to give some idea of the relative number of neutrons emitted by various sources, the sources are divided into three classes (listed in the last column of Table II). An element in class *A*, as estimated by the relative number of neutrons emitted compared to the sodium sources, emits more than 0.1 useful γ-rays per disintegration; an element in class *B* emits 0.1 to 0.01 γ-rays per disintegration; and an element in class *C* emits less than 0.01 γ-rays per disintegration. Sodium is used as the standard as approximately one γ-ray of 2.8 Mev is emitted per disintegration.[13]

No neutrons were observed from Cl^{38}, In^{116}, or Au^{198} in heavy water. This indicates that if these isotopes emit γ-rays of energy greater than 2.18 Mev that such γ-rays have intensities less than 0.01 γ-ray per disintegration. No neutrons were observed from Pr^{142} or Au^{198} in beryllium indicating that the γ-rays from these elements of energy greater than 1.63 Mev have intensities less than 0.01 γ-ray per disintegration. It is of interest that Mn^{56} and La^{140} both produced neutrons in heavy water; therefore these two isotopes belong with those on the left-hand side of Table I.

Co^{60}, Cu^{64}, Ag (225 day $\frac{1}{2}$ life), Eu^{151}, Dy^{165}, Ta^{182}, Re^{188}, and Ir (19 hr. $\frac{1}{2}$ life) were activated in the hope that the γ-ray literature was incomplete with regard to these elements. However, no neutrons were observed when these sources were placed in beryllium.

This preliminary study showed that one can produce with the aid of a pile at least nine good (class *A*) photo-neutron sources. Those sources with half-lives shorter than one hour have not been found to be very useful.

[13] Elliott, Deutsch, and Roberts, Phys. Rev. **61**, 99 (1942); **63**, 386 (1943); **64**, 321 (1943).

TABLE II. Photo-neutron sources.

Radioactive isotope	Target	Half-life	Class
F^{20}	Be	12 sec.	*A*
Na^{24}	Be	14.8 hr.	*A*
Na^{24}	D_2O	14.8 hr.	*A*
Al^{28}	Be	2.4 min.	*A*
Cl^{38}	Be	37 min.	*A*
Mn^{56}	Be	2.59 hr.	*A*
Mn^{56}	D_2O	2.59 hr.	*C*
Ga^{72}	Be	14.1 hr.	*A*
Ga^{72}	D_2O	14.1 hr.	*A*
As^{76}	Be	26.8 hr.	*B*
As^{76}	D_2O	26.8 hr.	*C*
In^{116}	Be	54 min.	*B*
Sb^{124}	Be	60 days	*A*
La^{140}	Be	40 hr.	*B*
La^{140}	D_2O	40 hr.	*B*

II. ENERGY OF THE PHOTO-NEUTRONS

Method

The neutron scattering cross section of hydrogen (σ_H) varies with the energy of the neutrons (E_n). E. Fermi suggested that the energy of the neutrons emitted by the photo-neutron sources be determined by measuring σ_H and using the relationship between σ_H and E_n. In the experiments being described σ_H was determined by measuring the transmissions of the different photo-neutrons through thin pieces of paraffin.

All of the photo-neutron sources investigated emit neutrons with energies lying between 0.01 and 1.0 Mev. The theoretical formula for the curve of σ_H as a function of E_n is given by Kittel and Breit.[14] This curve, at energies less than 1 Mev, is caused by *S* scattering and depends mainly upon the value of σ_H at $E_n=0$, hereafter designated by $\sigma_H(0)$. Kittel and Breit used the value $\sigma_H(0)=14.5\times10^{-24}$ cm^2. It now seems that the best values of $\sigma_H(0)$, as obtained from conditions of good collimation, approach $21\pm1\times10^{-24}$ cm^2.[15–18] S. Dancoff has used Kittel and Breit's Eqs. (11) and (12)[14] and has calculated three curves of σ_H *versus* E_n for values of $\sigma_H(0)$ equal

[14] C. Kittel and G. Breit, Phys. Rev. **56**, 744 (1939).
[15] Cohen, Goldsmith, and Schwinger, Phys. Rev. **55**, 106 (1939).
[16] Cohen, Goldsmith, and Hanstein, Phys. Rev. **57**, 352 (1940).
[17] Hanstein, Phys. Rev. **59**, 489 (1941).
[18] H. Carroll, Phys. Rev. **60**, 702 (1941).

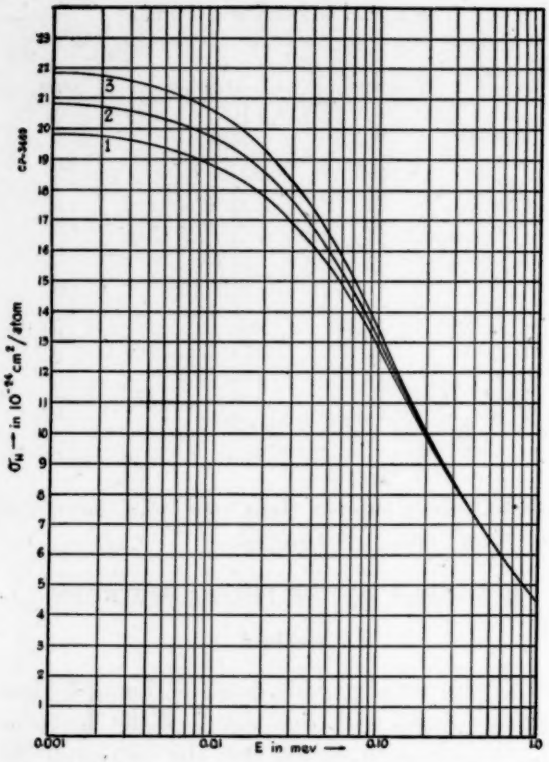

FIG. 2. Theoretical curves for the variation of hydrogen scattering cross section with the energy of the neutrons. Curves 1, 2, and 3 are for the assumed values of σ_H (at $E_n=0$) equal to 20, 21, and 22×10^{-24} cm², respectively.

to 20, 21, and 22×10^{-24} cm². These curves have been adjusted to join smoothly to a curve at higher energies that took into consideration the tensor forces.[19] Dancoff's curves are shown in Fig. 2.

In determining E_n for a measurement of σ_H, one introduces an uncertainty in E_n due to the uncertainty in the value of $\sigma_H(0)$. This uncertainty in E_n is greatest at low neutron energies (i.e., for $\sigma_H\sim20\times10^{-24}$ cm²). However, for σ_H less than 12×10^{-24} cm², the uncertainty in E_n is less than 7 percent. This uncertainty is considered for each source separately in the sections of this article dealing with the individual sources.

Description of Photo-Neutron Sources

The γ-ray emitting elements were activated at the center of the heavy water pile. The activity of the sources ranged from 1 to 75 curies. The activity that could be induced in an isotope depended upon the thermal neutron activation cross section for that isotope.

In order to keep the sources as small as possible, metal castings of the element were used in every case except that of sodium. In this case fused NaF was used in order to get the highest density of sodium atoms; the fluorine half-life is so short that the fluorine activity caused no trouble.

The γ-ray sources, in the form of cylinders 1.25 cm in diameter and 5 cm long, were encased in graphite cylinders. A thin string or wire was attached to the graphite for handling the source. The graphite cylinder containing the source was pulled up into a thin walled brass tube on which was mounted a cylinder of beryllium metal (Fig. 3) or a brass container of D_2O. The cylinders of Be or D_2O were 0.79 cm thick and 5.08 long and weighed 69.7 g and 34.5 g, respectively.

Neutron Detector

The neutron detector used in these experiments consisted of a BF_3-filled ionization cham-

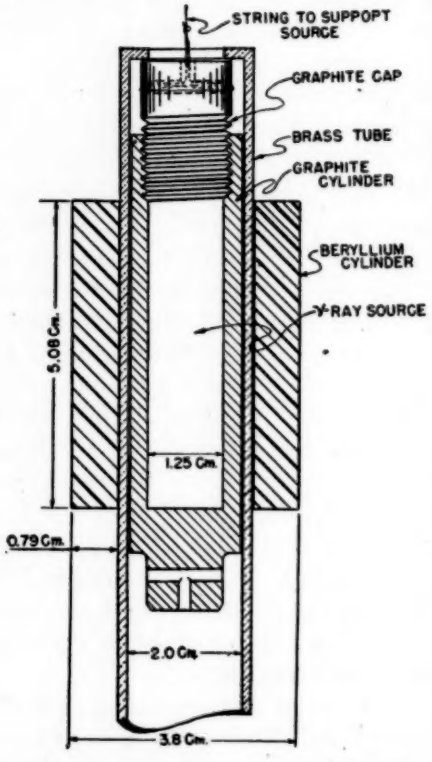

FIG. 3. Photo-neutron sources used in determining the energy of the emitted neutrons. For sources employing deuterium, an identically shaped thin walled brass cylinder of heavy water was substituted for the beryllium.

[19] Bohm and Richman (unpublished).

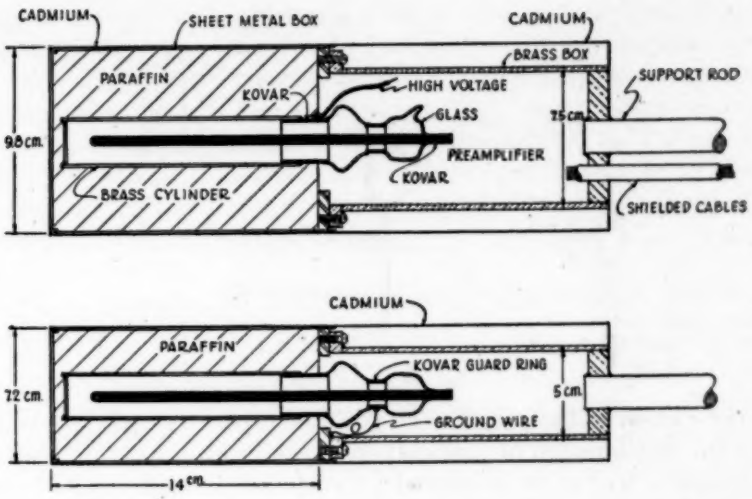

FIG. 4. Photo-neutron detector. The pulse ionization chamber was filled with BF_3 at a pressure of one atmosphere.

ber embedded in paraffin (Fig. 4). The paraffin increased the efficiency of the detector by slowing down the neutrons to a point at which the BF_3 has a high neutron absorption cross section. The electrical circuits were arranged to count the pulse produced when a neutron was absorbed and caused an (n, α) reaction in B^{10}.

The outer cylinder of the ionization chamber was made of brass and was 12.5 cm long and had a 2.5 cm I.D. The central electrode was a Kovar rod 0.50 cm O.D. At the back of the chamber the brass cylinder was insulated from the central rod by a Kovar-glass seal. In the middle of the Kovar-glass there was a grounded guard ring of Kovar metal. The chamber was filled with BF_3 to a pressure of one atmosphere. The paraffin block in which the chamber was embedded was 7.5 cm $\times$ 10 cm $\times$ 15 cm long. The paraffin was encased in a sheet metal box. The box was covered by a 0.5 mm thickness of cadmium in order to shield the detector from any slow neutrons that may have been present.

A preamplifier was attached directly to the back of the detector. A stabilized high voltage supply, a storage battery filament supply, an amplifier, an oscilloscope, and a counting unit (scale of 64) were connected to the preamplifier by shielded cables 20 feet long. These long cables permitted the person making measurements to be shielded from the γ-radiation of the sources by four feet of concrete.

It was found possible to make the scaler count only neutron pulses even when a 75-curie source was 50 cm from the face of the detector. Before making neutron measurements with any source, a test was run to make certain that no γ-rays would be counted.

Even though no counts were being produced by the γ-rays, it was feared that the presence of a large amount of ionization in the chamber due to the γ-rays might affect the counting of neutrons. To investigate this, a cylinder of lead was placed in front of the ionization chamber, and several neutron transmissions were measured. The average values of the transmissions with and without the lead were the same; this indicated that the γ-rays were not affecting the measurements of neutron transmissions.

The neutron counting rate of this detector varied slowly with changes in the high voltage; the counting rate increased by 15 percent in going from 600 to 1100 volts. The voltage normally used across the chamber was 700 volts.

Scatterers

Paraffin is supposed to be a mixture of straight-chain hydrocarbon compounds with formulas of the type C_nH_{2n+2}. The paraffin scatterers used in these transmission measurements were made from material that had a density of 0.901 at 20°C and a melting point of 56°C. For the purpose of calculations the paraffin was considered to have the formula $C_{24}H_{50}$.

In order to determine σ_H from measurements of the transmission of neutrons through paraffin, one must correct for the neutron scattering due

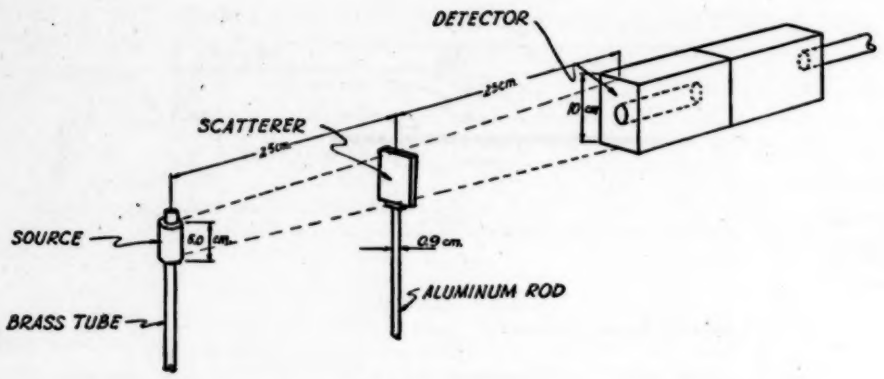

FIG. 5. Geometry used in measuring transmissions. Source and detector are detailed in Figs. 3 and 4, respectively.

to the carbon in the paraffin. To get this correction the transmission of pure carbon in the form of graphite had to be measured for each source of neutrons.

Paraffin and graphite scatterers 5.6 cm wide, 6.9 cm high, and of various thicknesses were prepared. Thin paraffin scatterers of a uniform thickness were produced by allowing molten paraffin to solidify on a water surface. The graphite and thicker paraffin scatterers were machined to size. Micrometer calipers were used to check that the thickness of a scatterer did not vary from point to point by more than 2 percent.

Geometrical Arrangement

In order to minimize the number of stray neutrons being scattered into the detector, the source and the detector were mounted two meters above the ground in the center of a large room. During the neutron measurements, nothing was near the source, the scatterer, or the detector except their means of support.

The source was supported on the brass tube shown in Fig. 3, and the brass tube was attached to a horizontal pipe 60 cm below the source. The iron rod sticking out the back of the detector (Fig. 4) was the only support for the detector. This rod was attached to a vertical pipe 60 cm behind the detector. The scatterers were supported on a small aluminum platform on top of a 1 cm aluminum rod. The platform was $1 \times 2 \times 0.2$ cm. The scatterers were held in position on the platform by two small pins that fitted into holes in the scatterers.

The source was 50 cm from the front face of the detector, and the scatterers were placed midway between the two. The scatterers completely blocked the detector's view of the source (Fig. 5). Every time a scatterer was mounted, this geometrical arrangement was checked by means of a straight edge. The center of the source and the axis of the ionization chamber were at the same height. In order to make sure that the face of a scatterer was perpendicular to this horizontal line of centers, the edges of the scatterer were brought into alignment with two vertical strings attached to plumb-bobs.

Measurements

The measurements of transmissions were made in cycles. A cycle consisted of:

1. A measurement without anything between the source and the detector (open beam reading).
2. A measurement with a paraffin or graphite scatterer.
3. A measurement with a lead plug between the source and the detector to determine the number of neutrons being scattered into the detector from the ground and walls (plug reading).
4. Another open beam reading.

These cycles were repeated several times. The natural background of the detector was measured at least every third cycle and was about one count per minute. The open beam readings ranged from 3000 to 50 counts per minute. Counts were taken for five minutes at the highest counting rates. The longest time interval used was 30 minutes, except when background or plug readings were being taken; the counting rates of the plug readings were about 10 percent of the open beam readings.

The lead plug was 30 cm long and was tapered in such a way that at any point along its length it had a cross-sectional area that would just prevent the detector from seeing the source.

The plug was mounted on the scatterer platform and aligned with a straight edge.

The natural background was subtracted from all readings first. As a check, the open beam readings from all the cycles were plotted on semi-log paper against time. The half-lives found from these graphs checked the values of Table II within our experimental accuracy.

Within each cycle all the readings were corrected for the decay of the source from the half-lives given in Table II. The two open beam readings were then averaged, and the observed transmissions (T_{obs}) were calculated from

$$T_{obs}=\frac{\text{Scatterer reading—plug reading}}{\text{Average open beam reading—plug reading}}.$$

The average values of T_{obs} and their standard errors are given in column 6 of Table III. The number of independent determinations used in calculating each average is given in column 5. The total number of counts taken with each scatterer is given in column 4. The standard errors (column 7) are listed in order to give an idea of the spread in the observed values of the transmissions.

Calculation of Hydrogen Cross Sections

Some of the neutrons that are scattered suffer only a small change in direction. Some of these (small scattering angle) neutrons will still hit the detector and be recorded as if they had not been scattered. A correction to the transmission for the neutrons scattered into the detector (scattering-in-effect) has been calculated. The

TABLE III. Observed transmissions and hydrogen cross sections.

Source	Scattering material	Scatterer g/cm²	Total counts	No. of independent determinations	Observed transmission	Standard error	Calculated transmission of hydrogen	Hydrogen cross section (in 10^{-24} cm²)
Na^{24}+Be	$C_{24}H_{50}$	0.654	40,000	6	0.710	0.007	0.743	5.1
	$C_{24}H_{50}$	.890	50,000	7	.639	.004	.679	4.9
	C	3.003	40,000	5	.653	.003		
Na^{24}+D_2O	$C_{24}H_{50}$	.258	61,000	9	.780	.004	.796	10.0
	$C_{24}H_{50}$	.449	84,000	10	.670	.005	.693	9.2
	$C_{24}H_{50}$	.654	33,000	7	.565	.005	.590	9.1
	C	1.513	54,000	7	.736	.003		
Mn^{56}+Be	$C_{24}H_{50}$	.258	56,000	5	.757	.004	.770	11.4
	$C_{24}H_{50}$	.421	114,000	13	.638	.004	.653	11.4
	$C_{24}H_{50}$	.449	67,000	5	.626	.004	.642	11.1
	$C_{24}H_{50}$	.654	53,000	5	.514	.005	.529	10.9
	$C_{24}H_{50}$	.890	52,000	5	.413	.003	.422	10.9
	C	1.513	100,000	22	.729	.004		
Mn^{56}+D_2O	$C_{24}H_{50}$	.449	12,000	7	.656	.007	.677	9.6
	C	1.513	1,200	2	.74			
Ga^{72}+Be	$C_{24}H_{50}$	.449	30,000	10	.686	.004	.708	8.7
	$C_{24}H_{50}$	.654	30,000	9	.566	.002	.587	9.1
	C	1.513	41,000	12	.750	.003		
Ga^{72}+D_2O	$C_{24}H_{50}$	.258	42,000	10	.750	.003	.762	11.9
	$C_{24}H_{50}$	.449	50,000	13	.605	.003	.617	12.0
	$C_{24}H_{50}$	.546	23,000	4	.553	.003	.565	11.8
	C	1.513	63,000	14	.731	.004		
Sb^{124}+Be	$C_{24}H_{50}$	.172	110,000	8	.757	.003	.758	18.1
	$C_{24}H_{50}$	.258	110,000	12	.659	.003	.659	18.2
	$C_{24}H_{50}$	.449	100,000	15	.503	.002	.497	17.5
	C	1.513	150,000	10	.710	.004		
	C	2.034	40,000	5	.640	.003		
La^{140}+Be	$C_{24}H_{50}$	.449	14,000	6	.769	.007	.799	5.6
	$C_{24}H_{50}$	.654	20,000	7	.664	.006	.699	6.1
	C	1.513	32,000	8	.779	.007		
La^{140}+D_2O	$C_{24}H_{50}$	.258	15,000	5	.752	.009	.766	11.7
	$C_{24}H_{50}$	.449	30,000	9	.606	.004	.618	12.0
	C	1.513	38,000	10	.732	.007		

assumption is made that the carbon scattering is spherically symmetrical in the laboratory system of coordinates. The transmission of carbon corrected for the scattering-in-effect is given by

$$(T_c)_{\text{corrected}}=\frac{(T_c)_{\text{obs}}-\epsilon_c}{1-\epsilon_c}.$$

ϵ_c is a function of the solid angles subtended by the graphite at the source, by the detector at the source, and by the detector at the graphite. ϵ_c for the standard geometry (Fig. 5) is 0.026.

The scattering-in-effect for paraffin is complicated by the presence of hydrogen and carbon nuclei in the same scatterer. Whereas the carbon scattering is assumed spherically symmetrical in the laboratory system, the hydrogen scattering is spherically symmetrical in the center of gravity system of the hydrogen nucleus and the neutron. With these assumptions it is found convenient to calculate directly the transmission of the hydrogen alone (T_H). The formula used is

$$T_H=\frac{(T_{Pf})_{\text{obs}}-\epsilon_{Pf}}{(1-\epsilon_{Pf})(T_c)^K_{\text{corrected}}}, \qquad (3)$$

where Pf is used to denote paraffin. The exponent K is needed to correct $(T_c)_{\text{obs}}$ for the ratio of carbon atoms present in the paraffin scatterer and the graphite scatterer. Using $C_{24}H_{50}$ for paraffin, we get

$$K=0.851\times\frac{\text{g/cm}^2\text{ of Pf scatterer}}{\text{g/cm}^2\text{ of C scatterer}}.$$

ϵ_{Pf} is a function of the same solid angles as ϵ_c and is also a slowly varying function of the ratio of σ_H and σ_c (the neutron scattering cross section for carbon). ϵ_{Pf} varies from 0.078 to 0.088 when the neutron energy varies from 0.80 to 0.02 Mev.

The values of T_H calculated from Eq. (3) are given in column 7 of Table III.

As a check on the correction for the scattering-in-effect, the area of a paraffin scatterer was doubled and the transmission measured. An appropriate ϵ_{Pf} was calculated for the larger scatterer and Eq. (3) was used. No significant difference in the value of T_H was observed.

Several measurements were made with the source and scatterer separated by distances appreciably different from the standard 50 cm (Fig. 5). The values of T_H found were independent of the distance between the source and the detector.

From the values of T_H and the thicknesses of the scatterers (Table III), σ_H has been calculated using

$$\sigma_H=\frac{11.25\times(-\ln T_H)}{\text{g/cm}^2\text{ of Pf scatterer}}.$$

These values of σ_H are listed in the last column of Table III.

Results

Some of the neutrons suffer collisions within the sources before they escape; these collisions slow down the neutrons. This effect broadens the energy distribution of the neutrons on the low energy side. S. Dancoff has estimated that, on the average, the neutrons are decreased in energy by 20 percent in sources of the size and shape shown in Fig. 3. The amount of broadening can be decreased by using smaller sources; however, there will always be a certain amount of spread in the energy distribution because of the angular dependence term, δ, in Eq. (1).

In passing through a piece of paraffin the neutrons of lower energy are more readily scattered than those of higher energy because of the inverse variation of σ_H with E_n. The mean energy of the transmitted neutrons will therefore be higher than that of the original distribution. This effect is referred to as "hardening." As greater thicknesses of paraffin are used, the amount of hardening increases. The values of σ_H found with the thicker paraffin scatterers should be lower than those found with the thinner scatterers. This manifestation of the hardening seems to be present in the value of σ_H listed in Table III. Unfortunately, the hardening cannot be studied quantitatively because of multiple scattering. The number of neutrons suffering two or more collisions within a scatterer increases with decreasing transmission. Equation (3) assumes single scattering, and it is not valid if there is appreciable multiple scattering. The effect of multiple scattering can probably be neglected for transmissions greater than 0.60.

Because of multiple scattering and hardening, only those cross sections obtained from transmissions greater than 0.60 are used in calculating

TABLE IV. Energy of neutrons and γ-rays.

Source	σ_H $\times(10^{-24}$ cm^2)	E_n (sources of Fig. 3) (Mev)	Av. E_n (sources of Fig. 3) (Mev)	Estimated E_n (very small source) (Mev)	Energy of γ-ray (Mev)
Na+Be	5.1	0.80	0.83	1.00	2.75
	4.9	0.86			
Na+D_2O	10.0	0.200	0.22	0.27	2.72
	9.2	0.245			
Mn+Be	11.4	0.145	(0.15)*	(0.18)	(1.83)
	11.4	0.145			
	11.1	0.157			
Mn+D_2O	9.6	0.220	0.22	0.26	2.7
Ga+Be	8.7	0.270	(0.27)	(0.32)	(1.99)
Ga+D_2O	11.9	0.130	0.13	0.16	2.50
	12.0	0.126			
Sb+Be	18.1	0.024	0.024	0.029	1.67
	18.2	0.024			
La+Be	5.6	0.066	0.62	0.75	2.47
	6.1	0.058			
La+D_2O	11.7	0.135	0.13	0.16	2.50
	12.0	0.126			

* Energies given in parentheses are not correct because of the presence of more than one γ-ray. (See section on these individual sources.)

the energy of the neutrons emitted by the sources. The values of E_n corresponding to the observed values of σ_H are given in column 3 of Table IV. Curve 2 of Fig. 2 (i.e., $\sigma_H(0)=21\times10^{-24}$ cm^2) has been used in calculating these values. The values in column 4 are the averages of the values in column 3. These two columns are characteristic only of the sources shown in Fig. 3. The estimated average energy of the neutrons which would be emitted by extremely small sources is given in column 5 of Table IV. These values are based upon Dancoff's estimate of a 20 percent average energy decrement.

Equation (1) (with $\delta=0$) has been used to calculate the energy of the γ-ray needed to produce the neutrons of the energy listed in column 5. It will be noticed that the γ-ray energies for Mn^{56} (column 6 of Table IV) obtained from Mn+Be and Mn+D_2O disagree. The same thing is true for Ga+Be and Ga+D_2O. These disagreements can be explained if more than one high energy γ-ray is emitted by Mn^{56} and Ga^{72}. If such is the case, then the Ga+Be and Mn+Be sources each emit at least two groups of neutrons of different energies.

Consideration of the Individual Sources

Na^{24}

Previous to these experiments measurements on Na^{24} indicated a single high energy γ-ray. The energy was given as 2.87 Mev by Goldhaber, Klaiber, and Scharff-Goldhaber,[20] as 2.76 Mev by Elliott, Deutsch, and Roberts[21] and as 2.94 by Mandeville.[22] Recently Ogle and Kruger[23] have reported four intense γ-rays of energy 2.56, 2.68, 2.76, and 2.89 Mev and a weak γ-ray of 3.24 Mev.

The γ-ray energy found in this experiment is 2.74 Mev (Table IV); the agreement with Elliott, Deutsch, and Roberts is good. It is possible that the amount of slowing down within the sources has been underestimated; however, this does not seem very likely as the Na+Be and Na+D_2O γ-ray values and the La+Be and La+D_2O γ-ray values agree fairly well.

Confirmative studies have been made by D. Hughes and C. Eggler with a cloud chamber.[24] The proton recoils produced by the neutrons from Na+Be and Na+D_2O were investigated. Only one energy group of neutrons was observed from each of these sources, and the average energies agreed with the values in column 4 (Table IV). The cloud-chamber studies showed that the Na+Be neutron had an energy distribution with a width of about 30 percent (at half maximum). The distribution from Na+D_2O had a width of about 25 percent.

The three curves of Fig. 2 do not visibly differ for the Na+Be source. For the Na+D_2O, the extreme values of E_n differ by about 0.012 Mev from the value of curve No. 2.

The counting rate observed from the Na+Be source was almost the same as that observed from the Na+D_2O source. Both are relatively efficient sources, apparently, of homogeneous neutrons.

Mn^{56}

The previous work on the Mn^{56} high energy γ-rays indicated two γ-rays of 1.81 and 2.13

[20] Goldhaber, Klaiber, and Scharff-Goldhaber, Phys. Rev. 65, 61 (1944).
[21] Elliott, Deutsch, and Roberts, Phys. Rev. 63, 386 (1943).
[22] C. E. Mandeville, Phys. Rev. 63, 387 (1943).
[23] G. Kruger and W. E. Ogle, Phys. Rev. 67, 273 (1945).
[24] D. Hughes (unpublished).

Mev.[25,26] From the energy of the Mn+D_2O neutrons observed in the present work, another γ-ray at roughly 2.7 Mev must exist. The counting rate from the Mn+D_2O source is only one twenty-fifth of that from the Mn+Be source. The 2.7 Mev γ-ray therefore must have a very low intensity.

Studies of the hardening of the neutrons from Mn+Be were made by employing thicker scatterers. It will be noticed (Table III) that no exceptional amount of hardening appeared. This led us to believe that the spectrum from Mn+Be might be composed of mainly one energy group of neutrons. A cloud chamber investigation was undertaken by D. Hughes and C. Eggler.[27] They found that the ratio of the number of neutrons from the 1.8 Mev and from the 2.1 Mev γ-ray was 10:1. Three energy groups of neutrons are emitted by the Mn+Be source, and probably more than 80 percent of the neutrons are in the lowest energy group.

Upon the assumption that 10 percent of the neutrons are in a 0.4 Mev group and 4 percent in a 0.8 Mev group, a calculation was made using $\sigma_H=11.3$ as the effective cross section for all the neutrons from Mn+Be. This leads to a value of 0.14 Mev for E_n for the main group of neutrons. The corresponding γ-ray energy is 1.82 Mev, which is in good agreement with the previous work.[25,26]

The counting rate per curie from the Mn+Be source is one-fourth of that from the Na+Be source. Very little work was done with the Mn+D_2O source because of its poor yield of neutrons.

Ga^{72}

A single high energy γ-ray of 2.65 Mev was reported by Mandeville for Ga^{72}.[28] The results listed in column 6 of Table IV can be explained if there are at least two high energy γ-rays from Ga^{72}. The counting rate observed from Ga+Be was slightly more than double that from Ga +D_2O. By comparison with the counting rates from the La and Na sources, the ratio for the Ga sources indicates γ-rays of approximately equal intensity lie above and below the deuterium threshold energy. That some γ-ray or γ-rays must be below the D threshold is substantiated by the value of the γ-ray energy calculated from the Ga+Be value of E_n. From these considerations and experiments to be reported elsewhere, it is believed that the neutrons emitted by Ga+D_2O are homogeneous. In this case the energy of the γ-ray is 2.5 Mev. The uncertainty in E_n due to the uncertainty in $\sigma_H(0)$ is about 0.010 Mev.

Ga+D_2O is only a moderately efficient source of neutrons; the counting rate per curie from the Ga+D_2O source is one-fourth of that from the Na+D_2O source.

Sb^{124}

The high energy γ-ray from Sb^{124} has been reported as 1.82 Mev[29] and 1.70 Mev.[23] The energy of the γ-ray as determined in this experiment is 1.67 Mev.

Klaiber and Scharff-Goldhaber[30] studied the neutrons emitted by an Sb+Be source. They measured the proton recoils and determined the energy of the neutrons to be 0.115 Mev. The energy of the neutrons found in this experiment (column 5, Table IV) is 0.029 Mev. If one uses curve 3 (i.e., assumes $\sigma_H(0)=22\times10^{-24}$ cm^2) of Fig. 2 instead of curve 2, the value of E_n would be 0.038 Mev. There is thus a serious disagreement between the value of E_n determined in this experiment and the value determined by Klaiber and Scharff-Goldhaber. The percentage spread in energy due to δ of Eq. (2) is greater in the Sb+Be source than in any other Be source employed. The extreme energy variation on either side of the mean is 0.0017 Mev (i.e., $\cos\theta=\pm1$ in Eq. (2)).

D. Hughes and C. Eggler recently studied the recoil protons from Sb+Be neutrons. The cloud chamber was operated at a low pressure.[31] Their results showed a single group of neutrons are emitted with an average energy of 0.035 ± 0.010 Mev, which is in agreement with the energy determined in this experiment.

[25] M. Deutsch and A. Roberts, Phys. Rev. 60, 362 (1941).
[26] L. G. Elliott and M. Deutsch, Phys. Rev. 63, 321 (1943).
[27] D. Hughes (unpublished).
[28] C. E. Mandeville, Phys. Rev. 64, 147 (1943).
[29] Mitchell, Langer, and McDaniel, Phys. Rev. 57, 1107 (1940).
[30] G. S. Klaiber and G. Scharff-Goldhaber, Phys. Rev. 61, 733 (1942).
[31] D. Hughes (unpublished).

TABLE V. Energy of photo-neutrons and the total cross section of carbon.

Source	E_n of sources of this experiment	Cross section of carbon $\times 10^{24}$ cm^2
Sb+Be	0.024±0.015	4.55
Ga+D_2O	0.13 ±0.02	4.3
La+D_2O	0.13 ±0.03	4.3
Mn+Be	0.14 ±0.03*	4.3
Na+D_2O	0.22 ±0.02	4.1
La+Be	0.62 ±0.07	3.4
Na+Be	0.83 ±0.04	2.9

* There are also two less intense groups of neutrons emitted by this source.

The Sb+Be source is a very efficient one; the counting rates per curie observed from the Sb+Be and Na+Be sources were about the same.

La^{140}

All previous measurements of the La^{140} high energy γ-ray indicated an energy of about 2.0 Mev.[32,33] The value of the γ-ray obtained in this experiment is 2.49 Mev. The agreement between the γ-ray energy values obtained from the La+Be and La+D_2O sources indicate that there is only one high energy γ-ray emitted by La^{140}. Therefore, both of these sources emit homogeneous neutrons. The uncertainty in E_n due to the uncertainty in $\sigma_H(0)$ is negligible for the La+Be source. For the La+D_2O source it is about 0.010 Mev.

Unfortunately these sources are relatively inefficient ones. The counting rates per curie from the La+Be source and La+D_2O sources are about one-fiftieth of those observed from the Na+Be and Na+D_2O sources, respectively.

Summary

There are seven sources that probably emit homogeneous groups of neutrons; they are: Na+Be, Na+D_2O, Mn+D_2O, Ga+D_2O, Sb+Be, La+Be, and La+D_2O. Mn+Be emits three groups of neutrons of different energies, but more than 80 percent of the neutrons seem to be in the group at 0.14 Mev.

Table V lists the most useful sources in order of increasing neutron energy. Column 2 gives the values of E_n determined for the particular sized sources employed in this experiment. The author's estimate of the uncertainty in the value of E_n also is given. (In the case of Sb+Be this uncertainty is almost entirely caused by the uncertainty in $\sigma_H(0)$.) These particular sources probably all have energy distributions with widths (at half maxima) of at least 25 percent. From Table V it will be seen that there are sources of neutrons of five distinct energies between 0.024 and 0.83 Mev.

The total neutron cross section of carbon has been calculated for these energies from the data on the graphite scatterers (Table III). The values of σ_c are listed in Table V.

The data on the γ-rays (above 1.63 Mev) are summarized in Table VI.

TABLE VI. Energy of γ-rays.

Isotope	Energy of γ-ray (in Mev)	Remarks
Na^{24}	2.74±0.05*	A single γ-ray
Mn^{56}	1.81±0.05 2.7 ±0.2	There is a third γ-ray present; the 2.7 Mev γ-ray is weak
Ga^{72}	2.50±0.05	There are other γ-rays present with energies below 2.2 Mev
Sb^{124}	1.67±0.02	A single γ-ray
La^{140}	2.49±0.07	A single γ-ray of low intensity

* Author's estimate of the uncertainty.

ACKNOWLEDGMENT

The author is greatly indebted to R. Fields, B. Russell, and D. Sachs for their assistance in the experimental work and to Dr. S. Dancoff for the theoretical work. The author also wishes to express his appreciation to the many members of the Argonne Laboratory staff for their assistance and suggestions; the writer is especially grateful to Dr. D. Hughes for undertaking the cloud-chamber studies and to Dr. W. H. Zinn for his direction of this research.

[32] Mounce, Pool, and Kurbatov, Phys. Rev. 61, 389 (1942); 63, 67 (1943).
[33] C. E. Mandeville, Phys. Rev. 63, 387 (1943).

Total Cross Sections Measured with Photo-Neutrons*

R. FIELDS, B. RUSSELL, D. SACHS, AND A. WATTENBERG**
Argonne Laboratory, University of Chicago, Chicago, Illinois

(Received January 2, 1947)

The total neutron cross sections of twenty-three elements have been measured by use of six photo-neutron sources ranging from 0.024 Mev to 0.83 Mev. The cross sections of the lighter elements behave very anomalously; broad resonances in the scattering are observed in F, Na, Mg, Al, and S. Nickel has the exceptionally high cross section of 23×10^{-24} cm² at 0.024 Mev. The cross sections of elements of atomic weight about 110 show very little variation with energy and are about 7×10^{-24} cm². Three heavy elements have cross sections of about 13×10^{-24} cm² at 0.024 Mev and decrease monotonically to about half that value at 0.83 Mev.

INTRODUCTION

THE determination of the homogeneous nature and the energy of the neutrons emitted by some of the photo-neutron sources made feasible studies of neutron cross sections at known energies. The first study undertaken was the determination of the total cross sections of twenty-four elements by means of simple transmission measurements.

The photo-neutron sources used emit neutrons in the energy range from 0.02 to 0.83 Mev. From other work in this energy region, capture cross sections are thought to be less than 10 percent of the total cross sections except for the case of boron. Therefore, in the experiment reported here, the transmission measurements are really a determination of scattering cross sections.

EXPERIMENTAL

The original experimental data for all the sources are rather lengthy; therefore the data for only one of the sources (Table I) are presented here as a sample.

The source and the detector used in these measurements are the same as those previously described. The energies of the neutrons emitted by these sources are those listed in Table V of the preceding article. The apparatus was mounted six feet above the floor in a large room in the manner shown in Fig. 5 of the preceding article.

The scatterers were machined from pure metal for the elements: Al, Fe, Ni, Cu, Zn, Ag, Cd, Sn, Sb, Pb, and Bi. Magnesium was used in the form of an alloy containing 3 percent aluminum. In the cases of P, I, and W, the pure element as a powder was tightly packed into a cell made of sheet iron with front and back faces 0.065 cm thick. Powdered sulfur was pressed into a briquette of the desired size. The remaining elements were measured as compounds

TABLE I. Data for Sb+Be source (0.024 Mev).

Element	Compound	gms/cm²	Total counts	Corrected average transmission	Std error	Cross section (in 10^{-24} cm²)
Be		1.306	40,000	0.642	0.001	5.1
Be		1.725	20,000	.566	.006	4.9
B	B_4C	2.432	42,000	.490	.003	5.6
B	B_4C	2.574	42,000	.481	.002	5.4
O	BeO	3.081	36,000	.525	.003	3.6
F	BeF_2	3.037	22,000	.625	.005	3.5
Na	NaI	7.35	80,000	.698	.003	5.1
Mg	3% Al Alloy	3.45	75,000	.690	.001	4.4
Al		13.73	94,000	.781	.004	0.80
Al		20.61	45,000	.694	.003	0.79
P		4.85	19,000	.700	.007	3.8
S		9.02	20,000	.843	.008	1.0
K	KI	9.85	69,000	.745	.002	1.2
Fe		9.68	58,000	.798	.004	2.2
Ni		1.326	30,000	.723	.007	24.
Ni		2.710	30,000	.544	.004	22.
Cu		5.60	26,000	.652	.006	8.0
Zn		7.86	60,000	.489	.002	9.9
Ag		13.59	132,000	.545	.002	8.0
Cd		16.64	40,000	.540	.002	6.9
Sn		18.33	65,000	.576	.004	5.9
Sb		10.57	25,000	.718	.004	6.3
I		15.64	36,000	.592	.007	7.0
W		9.33	40,000	.651	.005	13.9
W		17.00	17,000	.475	.005	13.4
Pb		10.81	150,000	.698	.003	11.4
Pb		23.39	40,000	.467	.002	11.3
Bi		12.51	67,000	.645	.004	12.1

* Based on work performed under Contract W-741-eng-37 of the Manhattan District at the Argonne Laboratory, University of Chicago.

** Now a Fellow of the Institute for Nuclear Studies of the University of Chicago.

(column 2 of Table I). Dehydrated powders were put into cells similar to those used with P, I, and W, and the cells were soldered shut. These cans were 8.2×6.6 cm² inside; the dimensions of the other scatterers were 7.6×5.7 cm². The thicknesses used are given in the third column of Table I.

In measuring transmissions of those substances contained in cells, an identical empty cell was used for comparison. Transmission measurements were repeated from four to fifteen times; the total number of counts observed with each scatterer is given in the fourth column (Table I). The average and the standard error of the independent transmission measurement were calculated; the standard errors (column 6) are listed in order to give an idea of the spread in the observed values of the transmissions. The average transmissions listed in column 6 have been corrected for the (small angle) scattering-in-effect by use of the relationship

$$T_{\text{corrected}}=\frac{T_{\text{observed}}-\epsilon}{1-\epsilon}, \qquad (1)$$

where $\epsilon=0.032$ for the scatterers in cells and $\epsilon=0.026$ for the other scatterers. The number of neutrons scattered into the detector from the floor and walls of the room was found to be about 10 percent of the number coming directly from the source. This was determined by interposing a tapered lead plug, 30 cm long, between the source and the detector.

RESULTS

The cross sections (column 8 of Table I) were calculated directly from the transmissions listed. Where a compound was used the cross section of the element of interest was calculated with the aid of the values of the cross section of the other element listed in Table II. The values for carbon included in Table II are from the previous work reported in Table V of the preceding article.

At first both the $La-D_2O$ and $Ga-D_2O$ sources were being used; however, it was found that the first five values obtained with both sources were the same—confirming the previous determination of the energies of these sources as being the same.* When this was observed no further measurements with the $La-D_2O$ source were made because it is a relatively inefficient source of neutrons.

It will be noted in Table I that where several different thicknesses of an element were measured, the cross sections found generally decrease in value for the thicker scatterer (lower transmission). These variations were partly experimental and partly due to two effects which have not been corrected for, namely multiple scattering and hardening of the neutrons. Because of these two effects, the values of the cross sections measured at transmissions less than 0.60 are not considered as reliable as those measured at transmissions between 0.60 and 0.75. This has been taken into consideration in drawing up Table II which is a summary of the cross sections found. The values at 0.83 Mev for Be, C, Al, Pb,

TABLE II. Total cross sections. (All values in units of 10^{-24} cm².)

Element	Atomic weight	0.024 Mev Sb +Be	0.13 Mev Ga +D_2O	0.14 Mev* Mn +Be	0.22 Mev Na +D_2O	0.62 Mev La +Be	0.83 Mev Na +Be
Be	9.0	5.0	4.3	4.3	4.2	3.3	3.1
B	10.8	5.5	4.9	4.7	4.3	—	2.3
C	12.0	4.6	4.3	4.3	4.1	3.3	2.9
O	16.0	3.6	3.5	4.1	3.0	3.5	4.9
F	19.0	3.5	5.7	—	6.9	4.6	4.1
Na	23.0	5.1	3.9	4.2	3.8	5.9	4.6
Mg	24.3	4.4	4.9	5.7	8.7	4.2	3.4
Al	27.0	0.80	5.3	3.2	3.2	4.1	3.5
P	31.0	3.8	3.1	3.1	3.2	3.1	3.5
S	32.1	1.0	4.2	4.5	2.9	—	2.2
K	39.1	1.2	1.6	1.9	1.7	2.3	2.7
Fe	55.9	2.2	4.1	3.9	3.3	—	2.7
Ni	58.7	23.	6.4	4.2	5.8	3.7	3.5
Cu	63.6	8.0	6.2	5.9	5.3	—	3.8
Zn	65.4	9.9	6.6	5.4	5.1	4.7	4.3
Ag	107.9	8.0	8.1	8.1	7.8	7.3	7.2
Cd	112.4	6.9	7.6	7.3	7.3	—	7.1
Sn	118.7	5.9	6.4	6.4	6.3	6.8	6.7
Sb	121.8	6.3	6.9	6.4	6.1	5.7	6.4
I	126.9	7.0	6.6	6.5	6.1	6.8	6.7
W	183.9	13.8	10.0	9.4	8.0	7.8	7.7
Pb	207.2	11.4	10.6	10.6	8.6	6.1	5.8
Bi	209.0	12.1	10.2	9.7	8.0	—	5.9

* The Mn+Be source emits two other groups of neutrons of higher energy that constitute less than 20 percent of the total number emitted.

* In the determination of the energy of the photoneutrons it was not certain that the $Ga+D_2O$ neutrons were homogeneous. The $La+D_2O$ was known to be homogeneous, so the agreement of these cross sections tends to establish the homogeneity of the $Ga+D_2O$ neutrons.

are in agreement with those found by Good and Scharff-Goldhaber[1] for 0.90 Mev neutrons; for Cu there is a disagreement.

CONCLUSIONS

The values of the scattering cross sections for the three heavy elements (atomic weights 183 to 209) seem to vary with energy in a very similar fashion; their cross sections are all about 13×10^{-24} cm^2 at 0.024 Mev and seem to monotonically decrease to about half that value at 0.83 Mev. The five intermediate weight elements (atomic weights 107 to 127) seem to have cross sections that vary very slightly with the neutron energy between 0.024 and 0.83 Mev. We wish to point out that neutrons emitted by the sources used in this work have an appreciable spread in energy, probably at least 25 percent; therefore, one would not observe narrow resonances by the technique employed here. There are also large energy gaps in which we have no neutron sources, and it is possible that broad anomalies might have been missed in the cross section of the heavy and intermediate weight elements. However, from the similar behavior of the elements within each group, it seems more reasonable to believe that there are no broad anomalies in the scattering cross sections of the heavier elements between 0.024 and 0.83 Mev.

The de Broglie wave-length of the neutrons from the higher energy sources is of the same order of magnitude as the nuclear radius of the heavy and intermediate weight elements. Therefore one would expect an appreciable amount of P wave scattering, and it would be of value to study the angular distribution of the scattered neutrons to determine the relative contributions of the P and S wave scattering.

Nickel is exceptional in having a cross section of 23×10^{-24} cm^2 at 0.024 Mev; its scattering cross section at thermal energies is also high, 16×10^{-24} cm^2.

The light elements O, F, Na, Mg, Al, and S all have cross sections that behave very anomalously between 0.024 and 0.83 Mev. These anomalies must extend for at least several hundred electron volts because the sources employed in these experiments have spreads in energy that would not permit observation of the narrow type resonances observed in neutron capture by In and Rh at 1.4 ev. Work of others[2] has shown the existence of broad scattering resonances in He at about 1 Mev in Mg and Al at about 2.5 Mev.[3]

Attempts made to measure the capture cross sections by means of activating foils showed that the capture cross sections of the light elements (with the exception of boron) are a negligible fraction of the total cross sections. This indicates that the observed anomalies are probably "broad resonances" in the scattering of neutrons.

ACKNOWLEDGMENT

The authors wish to express their great appreciation for the aid and advice given by W. H. Zinn. They wish to thank E. Fermi and S. Dancoff for their many helpful discussions and H. Lichtenberger for his aid in the preparation of the sources.

[1] Good and Scharff-Goldhaber, Phys. Rev. **59**, 917 (1941).

[2] H. Staub and H. Tatel, Phys. Rev. **58**, 820 (1940).

[3] MacPhail, Phys. Rev. **57**, 669 (1940).

A Search for the Transmutation Products of Gamma-Meson Reactions Induced by 100-Mev X-Rays

N. A. BONNER,* G. FREIDLANDER, L. P. PEPKOWITZ, AND M. L. PERLMAN
Research Laboratory, General Electric Company, Schenectady, New York

(Received January 2, 1947)

Irradiation with 100 Mev x-rays has been found to produce Zn^{63} from copper and Mg^{27} from aluminum. Experiments involving variations in beam energy and target thickness have shown that these isotopes result from secondary reactions caused by photo-neutrons and photo-protons from the target materials rather than from any primary, x-ray induced processes. No evidence for gamma-meson reactions has been obtained. A search for the transmutation products of gamma-meson reactions is shown to compare favorably in sensitivity with cloud-chamber methods for the detection of meson production, provided mesons are produced singly.

I. INTRODUCTION

IF mesons have masses of less than 195 electron masses, it is energetically possible for mesons to be ejected when nuclei are bombarded with 100-Mev x-rays. Schein, Hartzler, and Klaiber[1] have published cloud-chamber photographs of ionizing particles generated by x-rays from the 100-Mev betatron[2] and have interpreted some of their tracks as possibly being meson tracks.

If a charged meson is ejected from a nucleus after excitation with x-rays or gamma-rays, the resulting nucleus will differ from the original nucleus by one unit in charge, but will have the same mass number. Thus it should be possible to detect such a gamma-meson reaction by means of the radioactivity of the product formed if the target isotope is chosen such that its neighboring isobars are known radioactive species. Baldwin and Klaiber[3] bombarded a number of elements with the x-rays from the 100-Mev betatron at Schenectady; among the reactions observed were the production of a 10-minute magnesium period (probably Mg^{27}) from Al^{27} and a 2.6-hour activity (probably Si^{31}) from P^{31}. Baldwin and Klaiber attribute the formation of Mg^{27} from Al^{27} to the action of quanta rather than stray neutrons and suggest as possible mechanisms positron emission, electron capture, or positive meson emission. The reported production of Si^{31} from P^{31} presumably is an analogous case, although the possibility of an (n,p) reaction was not excluded.

In view of these results it seemed worth while to make a more thorough search for the products of hypothetical gamma-meson reactions[4] in betatron bombardments and, in particular, to develop techniques which would enable one to differentiate between gamma-meson reactions, and other possible reactions leading to the same products.

Target materials for these investigations had to be chosen in such a way that gamma-meson reactions would lead to products of convenient half-lives which could be readily identified chemically. In the case of (γ,μ^+) reactions it was also necessary to use a target element having a single isotope, or one whose heaviest isotope gives rise to the activity of interest by (γ,μ^+) reaction, since (γ,μ^+) reaction on a lighter isotope could not be distinguished radiochemically from a (γ,p), (γ,pn) or similar reaction on a heavier isotope. In case of (γ,μ^-) reactions, no such restriction exists.

II. EXPERIMENTAL PROCEDURE

1. General

The two hypothetical gamma-meson reactions[5] chosen for investigation were $Cu^{63}(\gamma,\mu^-)Zn^{63}$ and $Al^{27}(\gamma,\mu^+)Mg^{27}$.

* Now at Chemistry Department, Washington University, St. Louis, Missouri.

[1] M. Schein, A. J. Hartzler, and G. S. Klaiber, Phys. Rev. **70**, 435 (1946).

[2] W. F. Westendorp and E. E. Charlton, J. App. Phys. **16**, 581 (1945).

[3] G. C. Baldwin and G. S. Klaiber, Phys. Rev. **70**, 259 (1946).

[4] These will be referred to as (γ,μ^+) and (γ,μ^-) reactions, respectively.

[5] A preliminary report of the work on the first of these reactions was presented at the New York meeting of the American Physical Society on Sept. 19, 1946. cf. G. Freidlander, M. Perlman, and L. Pepkowitz, Phys. Rev. **70**, 790 (1946).

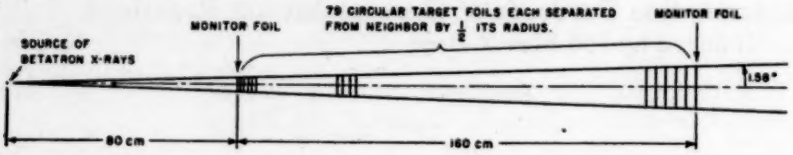

FIG. 1. Schematic diagram of the geometrical arrangement for the bombardment of a thin-foil array.

Briefly, the experiments consisted of exposing the target in the center of the betatron x-ray beam, carrying out rapid chemical separations of the product elements of interest, and following the decay of the samples thus obtained in a standard geometry on a Geiger-Müller counter.

The x-ray intensity in the betatron beam falls off from the central maximum approximately like a Gaussian function;[6] half the total intensity of the 100-Mev beam is contained in a cone of half-angle 2.0 degrees.[2] All the targets used subtended a cone of about 1.6-degree half-angle in the center of the beam, intercepting about 35 percent of the beam.

It proved necessary to use rather thick targets in order to obtain sufficiently active samples for counting. About 2 g/cm^2 of copper and about 0.6 g/cm^2 of aluminum were used. The use of such thick targets introduced the following serious difficulty in interpreting the results: Secondary (p,n) or (n,p) reactions caused by protons or neutrons produced in the thick targets, would give rise to the same products as (γ,μ^-) or (γ,μ^+) reactions, respectively. Assuming an average (p,n) cross section of 10^{-24} cm^2, and a proton range in copper of 0.1 g/cm^2 for the protons produced in copper, one calculates $10^{-24}\times 0.1\times 6\times 10^{23}/63 = 10^{-3}$ (p,n) processes per proton produced. The number of secondary (n,p) processes per neutron produced in aluminum may be even somewhat higher. Since the observed yields of Zn^{63} from copper and of Mg^{27} from aluminum bombardments were of the order of 10^{-3} to 10^{-4} times the yields of observed (γ,n) and (γ,p) processes, it was clear that additional experiments were necessary to differentiate a (γ,μ^-) from a (p,n) reaction, and a (γ,μ^+) from an (n,p) reaction.

Two types of experiments were devised for this purpose. The first was to vary the bombarding energy. Gamma-meson reactions become energetically impossible for bombarding energies lower than the energy necessary to create the meson mass. If the meson mass is near 200 electron masses, this threshold cannot be much below 100 Mev (if, indeed, it is not greater). Bombardments of copper as well as aluminum were therefore carried out not only at 100 Mev, but also at 50 Mev maximum x-ray energy. In these experiments, the targets were disks 4.4 cm in diameter mounted in a cylindrical textolite pillbox with thin Cellophane windows at both ends. The box was clamped in a Bakelite holder located between the magnet coils of the betatron 80 cm from the x-ray source in the doughnut.

In order to be able to compare the results of the various experiments carried out at different energies, and to determine whether the yields of Zn^{63} and Mg^{27} could be correlated with the production by the x-rays of protons and neutrons in the targets, the beam was monitored in each bombardment by observing the amount of (γ,n) reaction induced in a monitor foil. If the observed formation of Zn^{63} from copper and of Mg^{27} from aluminum resulted from the secondary reactions $Cu^{63}(p,n)Zn^{63}$ and $Al^{27}(n,p)Mg^{27}$, then the yields of these two products should vary with bombarding energy in about the same way as the monitor yields. The reactions $Zn^{64}(\gamma,n)Zn^{63}$ and $Cu^{63}(\gamma,n)Cu^{62}$ were chosen to monitor the copper and aluminum irradiations, respectively. The products of these reactions have nearly the same half-lives as the products of the reactions which they monitor.[7] Errors caused by fluctuations in x-ray beam intensity during bombardments are thus minimized. The same monitors were also used to compare x-ray intensities during different bombardments at the same energy.

The second method for distinguishing (γ,μ) reactions from (p,n) or (n,p) reactions made use of variations in target thickness. Since a single thin target would not have resulted in sufficiently active samples, the following technique was

[6] L. I. Schiff, Phys. Rev. 70, 87 (1946).

[7] According to G. T. Seaborg, Rev. Mod. Phys. 16, 1 (1944) the half-lives are: Zn^{63} 38 minutes, Mg^{27} 10.2 minutes, Cu^{62} 10.5 minutes.

employed: The yield from a thick-target bombardment was compared with that from a similar bombardment in which the thick target was split up into many thin foils. These were lined up in the beam and separated from each other sufficiently so that the protons or neutrons produced in the material on the average spent a smaller fraction of their range in the target than they did in the case of the thick target. When protons were the secondary particles of interest, each foil had to be thin compared to the proton range. With a device of this type the yield of a primary (x-ray induced) reaction should remain the same as with a thick target, provided the total thickness of target material traversed by the beam is the same; but the yield of a secondary reaction should be reduced.

The thin-foil experiments were carried out with 79 circular target foils arranged in a conical envelope of 1.6 degree half-angle whose apex was at the x-ray source. The foil nearest the source was 4.4 cm, the most distant foil 13.1 cm in diameter. The distance between each foil and its nearest neighbors was one-half its radius. One monitor foil was located at the front and one at the rear of the target foils. These served to check alignment, as well as to monitor beam intensity. Each foil was supported by two wire hooks from wires stretched on a Bakelite rack; the whole apparatus was constructed with the minimum amount of material in order to avoid complications due to scattered radiation. Figure 1 is a schematic diagram of the foil arrangement, Fig. 2 a photograph of the apparatus in position in front of the betatron.

A rough calculation shows that, with the arrangement described, secondary (p,n) or (n,p) reactions should occur to only about one-third or one-fourth the extent that they do in a single layer of the same total thickness.

2. Copper Bombardments

The known stable and radioactive isotopes in the region of copper and zinc are shown in Fig. 3. It is seen in this chart that the only isotopes which can result from (γ,μ^-) reactions on copper are Zn^{63} of half-life 38 minutes and Zn^{65} of half-life 250 days. The latter half-life is so long that a detectable amount of this isotope could not be produced in the 60 to 90 minute copper bombardments.

Purity Requirements

A preliminary experiment carried out with CP cuprous oxide as target material resulted in the formation of 38-minute zinc activity. Since Zn^{63} could be formed from zinc impurity (by the reactions Zn^{64} (γ,n); Zn^{66} $(\gamma,3n)$; Zn^{67} $(\gamma,4n)$; etc.) and possibly from gallium or germanium impurities (by such reactions as Ga^{69} $(\gamma,p5n)$ or Ge^{70} $(\gamma,2p5n)$), it appeared necessary to investigate whether the observed Zn^{63} activity could be accounted for in this way.

In order to determine the degree of purity required for the copper targets, a weighed zinc foil was bombarded under the same conditions as the copper targets and the amount of 38-minute zinc activity formed was measured. This experiment indicated that, with the beam intensities usually available,[8] 1 mg of zinc impurity in the target would give rise to 100 to 400 counts per minute of Zn^{63} activity at saturation with the particular G-M counters and counting geometry used. For the same range of beam intensities preliminary experiments indicated yields of about 800 to 3500 counts per minute of Zn^{63} activity at saturation from the bombardment of 30 g of copper. Thus, to be sure that no more

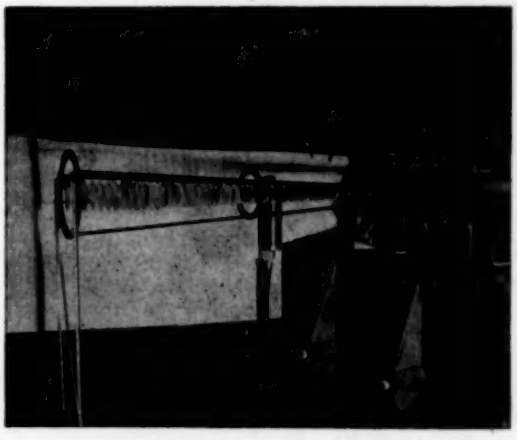

FIG. 2. Apparatus for thin-foil bombardments in position in front of the 100-Mev betatron. A set of copper foils is in place.

[8] 500r to 2000r per minute measured behind ½ inch of lead in the center of the beam one meter from the tungsten target in the betatron.

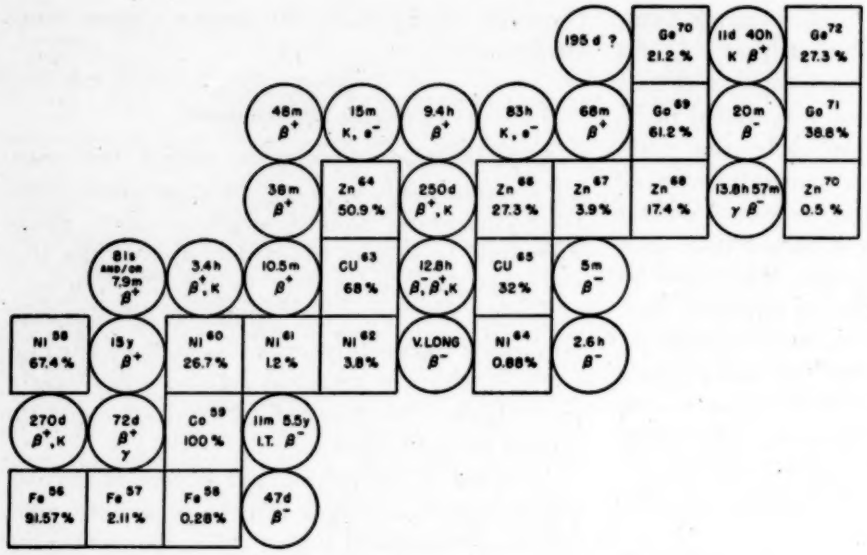

FIG. 3. Known stable and radioactive isotopes in the region of copper. The stable isotopes with their abundances are shown in squares, the radioactive isotopes with their half-lives and modes of decay in circles.

than 1 percent of this effect was attributable to zinc impurity, it was necessary to prove that the copper target contained less than 0.1 mg of zinc per 30 g of copper, less than three parts per million.

No specific determinations of the purity requirements for gallium and germanium were made, but it was felt that these requirements would certainly be much less severe than those for zinc because of the nature of the nuclear reactions which would produce Zn^{63} from these elements.

To be sure that the copper target material could be relied upon to be sufficiently zinc-free, cuprous oxide was prepared from CP cuprous chloride by the following method: The cuprous chloride was dissolved in concentrated hydrochloric acid, reprecipitated by dilution with water, and then washed with distilled water until the washings were neutral to litmus paper; this process was repeated, and the resulting cuprous chloride was converted to cuprous oxide by digesting it with hot 5*N* sodium hydroxide for about 30 minutes. The cuprous oxide was washed with hot water until the washings gave no visible turbidity with silver nitrate solution. To determine the completeness of zinc removal obtained by this method a batch of cuprous oxide was prepared after the addition to the starting material of a known amount of 250-day Zn^{65} tracer; by measuring the chemical yield and the Zn^{65} activity in the cuprous oxide sample obtained, it was found that the zinc content in the copper had been reduced by a factor of at least 4000. The cuprous chloride used as the starting material was known to contain less than 0.1 percent of zinc by weight. Therefore, the tracer experiment showed that the cuprous oxide contained less than 0.35 part per million of zinc. Several other purification procedures tested by the tracer technique described proved much less satisfactory. It should be mentioned that the purification procedure used may also be expected to remove gallium and germanium impurities efficiently. In addition, it seems most unlikely that these elements are present in significant amounts in CP copper salts.

Targets

About 30 g of cuprous oxide prepared by the method described above were used as a target in each of the thick target experiments. Later a supply of copper metal reported by the manufacturers to contain less than one part per million of zinc was obtained from the U. S. Metals Refining Company. This material was rolled[9] to a thickness of about 0.00025 inch (about 5 mg/cm²) and used for the foil bombardments in the apparatus of Figs. 1 and 2. The total thickness of copper traversed by the beam

[9] We are indebted to Messrs. Schermerhorn and Cooley of this laboratory for carrying out this rolling operation.

in the foil experiments was only about 400 mg/cm² while the solid targets were more than four times as thick. The zinc monitor foils had a thickness of 10–14 mg/cm².

Chemical Separations

After each bombardment the zinc activity was isolated chemically from the bombarded copper target and from any radioactive isotopes of other elements which might conceivably have been formed in the bombardment of copper (or cuprous oxide) with the x-ray beam; these other elements are chiefly nickel, cobalt, iron, and manganese.

The following procedure was used for cuprous oxide targets: Cuprous oxide was dissolved in hot concentrated hydrochloric acid containing 250 mg of zinc carrier. The solution was diluted and cuprous iodide precipitated with a small excess of potassium iodide. After centrifugation and neutralization of the supernatant with concentrated ammonia, excess iodine was reduced with hydrazine hydrate. The solution was brought to *p*H 1.0 with hydrochloric acid, and the small amount of copper still in solution was precipitated with hydrogen sulfide. The filtrate from the copper sulfide precipitate was made ammoniacal and then saturated with hydrogen sulfide.[10] The sulfide precipitate was leached with hot 2*N* hydrochloric acid (a small, black residue usually remained), and the hydrogen sulfide was boiled out of the solution. The *p*H was adjusted to 2.5 to 2.7 with 4*M* sodium acetate; 50 mg each of cobalt, nickel, iron, and manganese carriers were added; the solution was heated to boiling; and zinc sulfide was precipitated with hydrogen sulfide. A few milligrams of "Hyflo Supercel" filter aid were added, the precipitate was filtered out and washed, first with 0.1*N* acetic acid saturated with hydrogen sulfide, then with hot acetone. Dry air was then sucked through the precipitate for a short time.

Copper foils were dissolved in an ice-cooled mixture of 12*N* hydrochloric acid and 30 percent hydrogen peroxide (in a volume ratio 2 to 1). Excess peroxide was boiled out, and sufficient potassium iodide was added to reduce all the Cu^{++} to Cu_2^{++} as well as to precipitate cuprous iodide. From this point on the procedure was the same as for cuprous oxide. In either case the entire chemical procedure was performed in 30 to 40 minutes.

The zinc monitor foils were dissolved in hydrochloric acid. A few milligrams of Cu^{++} carrier were added. The H^+ concentration was adjusted to 0.3*N*, and copper sulfide precipitated with hydrogen sulfide. The *p*H of the filtrate was adjusted to 2.5, a few milligrams of Co^{++} and Ni^{++} carriers were added, and hydrogen sulfide was passed in to precipitate zinc sulfide. The precipitate was filtered and dried. In the case of the large monitor of a copper foil bombardment the whole foil was dissolved, but only a 10 to 15 percent aliquot of the solution was processed so that the thickness of the final zinc sulfide precipitate was about the same as that obtained from the small monitor. The chemical yields, both in the target and in the monitor procedures, were determined after the completion of the counting by weighing the dried zinc sulfide precipitates.

Counting

The zinc sulfide samples, obtained from the above procedures, were mounted either on Bakelite cards or, for the weak samples, on $\frac{1}{32}$-inch thick lead squares to increase the counting efficiency by back-scattering. The samples were covered with Cellophane (1 mg/cm²) and placed in a reproducible position under a Geiger-Müller counter. Several different counter tubes were used in the various experiments but they were intercalibrated with Zn^{65} radiation. Decay curves were followed for several half-lives.

3. Aluminum Bombardments

The known stable and radioactive isotopes in the region of aluminum and magnesium are shown in Fig. 4. Aluminum has a single stable isotope and therefore Mg^{27} (half-life 10.2 minutes) is the only product of a (γ,μ^+) reaction to be expected.

Purity Requirements

Mg^{27} could be produced from silicon, phosphorus, or sulfur impurities by the reactions Si^{29} $(\gamma,2p)$; Si^{30} $(\gamma,2pn)$; P^{31} $(\gamma,3pn)$; S^{32} $(\gamma,4pn)$;

[10] This extra step was necessary because the high ionic strength of the solution made the separation of Zn^{++} from Co^{++}, Ni^{++}, Fe^{++}, and Mn^{++} by H_2S precipitation at a controlled *p*H impossible at this point.

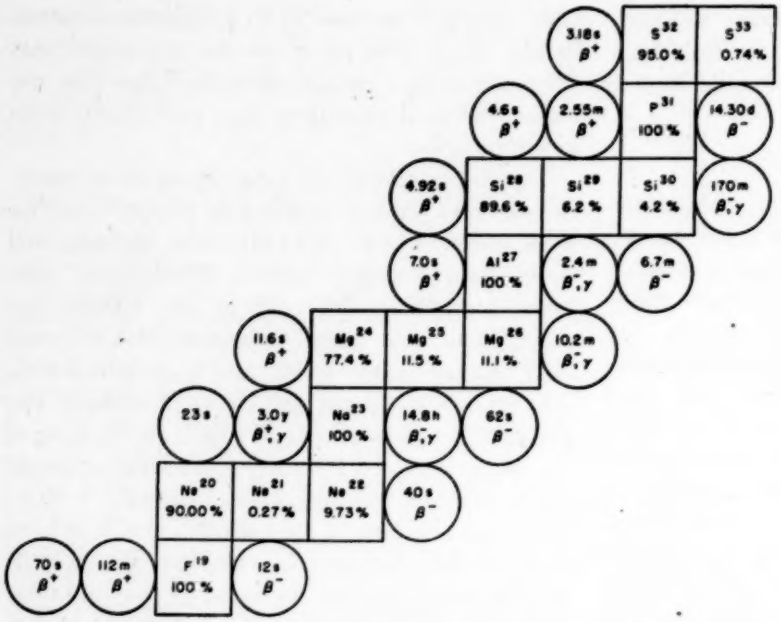

FIG. 4. Known stable and radioactive isotopes in the region of aluminum. The stable isotopes with their abundances are shown in squares, the radioactive isotopes with their half-lives and modes of decay in circles.

S^{33} $(\gamma,4p2n)$; etc. The aluminum used was specially pure metal supplied by the Aluminum Company of America containing less than 0.01 percent of silicon according to the manufacturer's analysis. In view of the low abundance of Si^{29} and Si^{30} this was regarded as a satisfactorily low silicon analysis. No data for the phosphorus and sulfur contents were available; however, these are not common impurities in aluminum, and the reactions resulting in the production of Mg^{27} from these elements by x-rays are probably quite unlikely. Furthermore, the results of the aluminum bombardments described below indicated that most or all of the Mg^{27} formed in thick-target runs resulted from secondary processes rather than from any x-ray induced reactions.

Targets

For the thick-target bombardments stacks of 0.0015-inch aluminum disks were used to facilitate rapid dissolving. The total amount of aluminum used for each bombardment was about 10 g (about 600 mg/cm²). For the foil bombardments the aluminum was rolled to a thickness of about 0.0003 inch (about 2 mg/cm²).[9] Copper monitor foils of about 10 mg/cm² were used.

Chemical Separations

The separation of magnesium from aluminum (and incidentally from sodium and neon) was carried out by the following method: The aluminum was dissolved in hot 12*N* hydrochloric acid containing about 20 mg of magnesium carrier and a small amount of ferrous sulfate as a catalyst. The dissolution was hastened by the gradual addition of 30 percent hydrogen peroxide. The solution was poured into a sufficient excess of 10*N* sodium hydroxide to convert all the aluminum to aluminate ion. The magnesium hydroxide precipitate was centrifuged, the supernatant discarded, and the precipitate dissolved in a small quantity of 6*N* hydrochloric acid. This solution was made ammoniacal (about 0.5*M* in ammonium hydroxide), and magnesium ammonium arsenate was precipitated by the addition of disodium hydrogen arsenate. In the presence of about 0.2*M* tartrate, 1*M* ammonium ion, and 13 percent ethyl alcohol, this precipitation was found to be quite rapid and complete, and aluminum was not carried along. After one minute's stirring the precipitate was filtered, washed successively with ammoniacal tartrate solution, 1*M* ammonia, and acetone, and dried by sucking dry air through it. The entire chemical procedure required 10 to 15 minutes. After the completion of the counting measurements, the chemical yield was found by dissolving the magnesium ammonium arsenate precipitate in hydrochloric acid and determining the magne-

sium content by the 8-hydroxyquinoline method.[11]

The copper activity produced in the copper monitor foils was separated from other possible radioactive products, such as nickel and cobalt, by dissolving the copper in a mixture of 12*N* hydrochloric acid and 30 percent hydrogen peroxide, boiling off excess peroxide, and precipitating cuprous iodide with a slight excess of potassium iodide in the presence of Ni^{++} and Co^{++} carriers. The cuprous iodide precipitate was filtered, washed with water and alcohol, dried, and mounted for counting. The chemical yield was later determined by drying the cuprous iodide at 105°C, and weighing it.

Counting

The counting was done as described above in case of the copper bombardments.

III. RESULTS

Figures 5 and 6 show typical decay curves of the zinc fractions isolated from a thick cuprous oxide target and from a set of copper foils after bombardment with the 100-Mev x-ray beam.

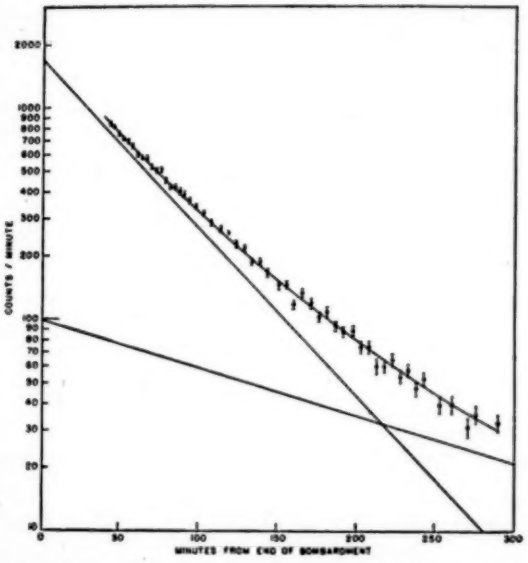

FIG. 5. Decay curve of the zinc fraction isolated from a thick cuprous oxide target bombarded with the 100-Mev x-ray beam.

[11] Kolthoff and Sandell, *Textbook of Quantitative Inorganic Analysis* (The Macmillan Company, New York, 1938), p. 351.

The standard deviations are indicated for all experimental points. Both curves show the presence of an unidentified long-lived (about 2-hour half-life) component. After subtracting this from the experimental decay curve, a 38-minute period is obtained.

Decay curves of the magnesium fractions obtained from typical thick aluminum and aluminum foil bombardments are shown in Figs. 7 and 8, respectively. In this case, no component other than the 10-minute period ascribed to Mg^{27} was found. Again, the counting rates in the foil bombardments were less than 100 counts per minute at the beginning of the counting, and the uncertainty in the position of the decay curve in Fig. 8 is, therefore, relatively large, perhaps ±15 percent.

The results of the six copper bombardments are summarized in Table I. Column 7 gives, for each experiment, the amount of 38-minute zinc activity that would have been obtained if an amount of copper containing one millimole (63 mg) of Cu^{63} per cm^2 had been bombarded to saturation. Similarly, column 11 lists the amount of 38-minute Zn^{63} activity that would have been obtained if an amount of zinc monitor containing one millimole (64 mg) of Zn^{64} per cm^2 had been bombarded to saturation. The values in these columns have all been corrected for counter geometry; they are given for samples mounted in $\frac{7}{8}$-inch diameter circles placed as close as

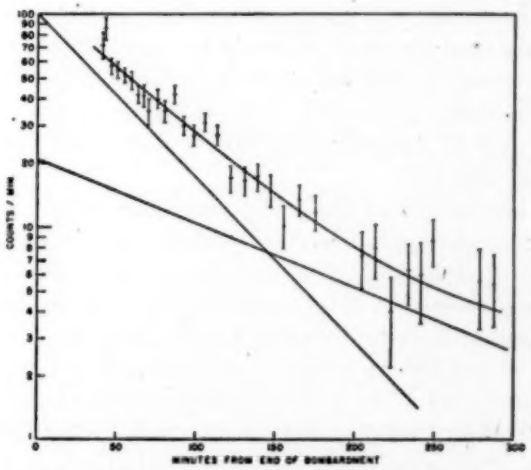

FIG. 6. Decay curve of the zinc fraction isolated from a set of copper foils bombarded with the 100-Mev x-ray beam.

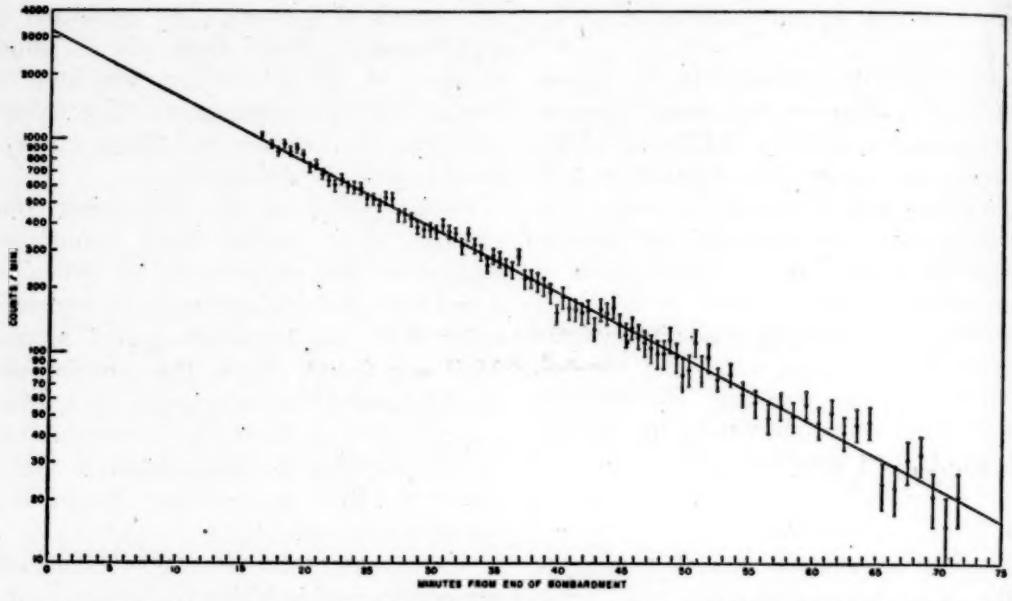

FIG. 7. Decay curve of the magnesium fraction isolated from a thick aluminum target bombarded with the 100-Mev x-ray beam.

possible to the mica window of a conventional bell-type G-M counter and backed by $\frac{1}{32}$ inch of lead. Column 12 lists the ratios of the Zn^{63} activities obtained from target and monitor, and these are the values of interest for deciding on the nature of the reaction leading to the formation of Zn^{63} from copper. For the solid target bombardments this ratio appears to be the same within the experimental errors at 50 and 100-Mev maximum energy. However, a comparison of experiments 1 and 2 with experiments 5 and 6 shows that the production of Zn^{63} from copper is reduced by about a factor of four (relative to the monitor) when a thick target is split up into thin foils. It is estimated that the ratios in column 12 have probable errors of no more than ± 15 percent.

The results of the seven aluminum bombardments are summarized in Table II. This table is arranged in the same way as Table I. Again, the amount of Mg^{27} activity relative to the monitor activity (column 12) is about the same at 50 and 100-Mev maximum bombarding energy (experiments 7 to 11).[12] Splitting the thick target into thin foils (experiments 12 and 13) reduces the Mg^{27} activity by a factor of about 3.5.

[12] The rather large discrepancy between experiment 9 and experiments 10 and 11 is unexplained.

IV. DISCUSSION

The results in Tables I and II indicate clearly that the production of Zn^{63} from thick copper targets and of Mg^{27} from thick aluminum targets in the 100-Mev x-ray beam are not owing to (γ,μ^-) and (γ,μ^+) reactions, respectively, except perhaps to a small extent. In fact, the reduction

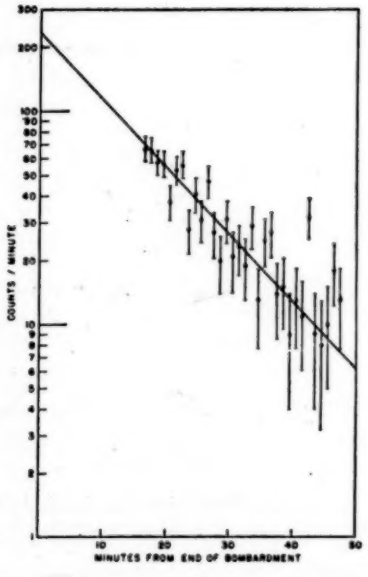

FIG. 8. Decay curve of the magnesium fraction isolated from a set of aluminum foils bombarded with the 100-Mev x-ray beam.

TABLE I. Results of copper bombardments.

1 Exp. No.	2 Max. beam energy Mev	3 Target	4 Millimoles of Cu per cm³ of target	5 Counts/min. of Zn^{63} from target (at end of bombardment)	6 Chemical yield of Zn from target (percent)	7 Counts/min. of Zn^{63} from 1 millimole of Cu^{63} per cm³ of target*		8 Millimoles of Zn monitor per cm³	9 Counts/min. of Zn^{65} from monitor (at end of bombardment)	10 Chemical yield of Zn from monitor (percent)	11 Counts/min. of Zn^{65} from 1 millimole of Zn^{64} per cm³ of monitor*	12 Ratio column 7 / column 11
1	100	Cu_2O	30.7	300	60	65.7		.156	8500	100	3.03×10^5	2.2×10^{-4}
2	100	Cu_2O	27.5	1700	82	161		.199	21,500	93.5	6.40×10^5	2.5×10^{-4}
3	50	Cu_2O	30.5	390	94	45.5		.153	7200	98	2.21×10^5	2.1×10^{-4}
4	50	Cu_2O	28.0	155	63	34.9		.171	4850	99	1.59×10^5	2.2×10^{-4}
5	100	Cu foils	6.24	100	86	39.7	front rear	.198 .211	24,000 3100	90 11.1	7.47×10^5 7.34×10^5	0.54×10^{-4}
6	100	Cu foils	6.24	110	89.5	42.0	front rear	.207 .216	23,000 3400	86 12	7.18×10^5 7.27×10^5	0.58×10^{-4}

* These values are given for saturation bombardment, 100 percent chemical yield, and standard counting geometry on a mica-window counter.

TABLE II. Results of aluminum bombardments.

1 Exp. No.	2 Max. beam energy Mev	3 Target	4 Millimoles of Al per cm³ of target	5 Counts/min. of Mg^{27} from target (at end of bombardment)	6 Chemical yield of Mg percent	7 Counts/min. of Mg^{27} from 1 millimole of Al^{27} per cm³ of target*		8 Millimoles of Cu monitor per cm³	9 Counts/min. of Cu^{62} from monitor (at end of bombardment)	10 Chemical yield of Cu from monitor (percent)	11 Counts/min. of Cu^{62} from 1 millimole of Cu^{62} per cm³ of monitor*	12 Ratio column 7 / column 11
7	100	thick Al	24.6	3200	79.0	220		.181	17,000	43.3	7.81×10^5	2.8×10^{-4}
8	100	thick Al	23.9	3900	85.7	254		.153	15,800	34.6	10.8×10^5	2.4×10^{-4}
9	50	thick Al	24.5	935	83.0	61.3		.177	5400	74.8	1.47×10^5	4.2×10^{-4}
10	50	thick Al	24.9	570	79.0	38.6		.173	5200	79.9	1.36×10^5	2.8×10^{-4}
11	50	thick Al	24.5	770	88.8	47.2		.344	7000	40.8	1.79×10^5	2.6×10^{-4}
12	100	Al foils	5.74	232	80.5	67.0	front rear	.166 .157	25,400 3950	62.6 10.4	7.45×10^5 8.68×10^5	0.83×10^{-4}
13	100	Al foils	5.74	215	85.5	58.5	front rear	.169 .168	36,500 2940	86.4 5.94	9.04×10^5 9.00×10^5	0.65×10^{-4}

* These values are given for saturation bombardment, 100 percent chemical yield, and standard counting geometry on a mica-window counter.

in activity obtained by splitting a thick target into an array of thin foils is consistent with the assumption that the secondary reactions $Cu^{63}(p,n)Zn^{63}$ and $Al^{27}(n,p)Mg^{27}$ are entirely responsible for the production of the two isotopes.[13] If, nevertheless, it is assumed that all the Zn^{63} and Mg^{27} produced in the thin foil bombardments result from (γ,μ) reactions, an upper limit (which is almost certainly set much too high) will be obtained for the ratio of (γ,μ)

[13] In case the secondary bombarding particles are neutrons, as in the aluminum bombardments, the source of the neutrons may not be entirely in the target itself. In an experiment to check this point an aluminum target was bombarded outside the center of the beam in a position where it received only 1/30 as much x-ray intensity as a similar target in the center of the beam. The amount of Mg^{27} produced, however, was reduced only by a factor of two. This indicates that roughly half the Al^{27} (n, p) reactions in the thick-target bombardments were caused by neutrons from sources external to the targets. This does not affect the validity of the conclusion that the Mg^{27} is produced by a secondary rather than a primary reaction.

to (γ,n) cross sections. In both cases this ratio, as taken directly from columns 12 of Tables I and II, is about 5×10^{-5}. If $\sigma_{\gamma,n}$ is assumed to be of the order of magnitude 10^{-25} cm^2 for the betatron x-ray spectrum at 100-Mev maximum energy, this would lead to an upper limit for σ_{γ,μ^+} on Al^{27} and σ_{γ,μ^-} on Cu^{63} of 10^{-29} to 10^{-30} cm^2 for the same spectrum. This, of course, does not mean that the cross sections for (γ,μ) reactions may not be much higher in an energy range where the reactions are possible (if, indeed, they are possible). It does mean that the threshold for (γ,μ) reactions is probably not much below, and may well be above 100 Mev.

It should be pointed out that the radiochemical method described compares very favorably in sensitivity with a cloud-chamber search for meson production processes. If in going from thick to thin targets, the yields of Mg^{27} and Zn^{63} had been reduced by only a small factor such as 1.5, this would be taken as evidence for the occurrence of (γ,μ) reactions. Taking this as a criterion one can calculate a lower limit for the number of gamma-meson processes which could be detected in any x-ray bombardment by the method described. Using this number[14] and comparing the geometrical arrangements and beam intensities used in the present investigation with those used in recent cloud-chamber studies of heavily ionizing particles produced by the 100-Mev betatron,[15] one arrives at a measure of the relative sensitivity of the two methods. This comparison, which involves no assumptions about cross sections, shows that at the limit of sensitivity of the radiochemical method about 15,000 cloud-chamber pictures would be necessary on the average to show one meson track.

It may be, of course, that mesons can be produced by nuclear processes other than simple (γ,μ) reactions. If it should turn out that the production of mesons can occur in pairs only i.e., by $(\gamma,\mu^+\mu^-)$ reactions, the products of such reactions will be indistinguishable from the target nuclei and the radiochemical method will fail. Another possibility is that mesons may be emitted singly but accompanied by heavy particles. The methods described can easily be extended to (γ,μ^-n) and (γ,μ^+p) reactions. However, the product of a (γ,μ^-p) reaction is identical with that of a (γ,n) reaction, and the product of a (γ,μ^+n) reaction is indistinguishable from that of a (γ,p) reaction. These considerations can readily be extended to more complex cases.

ACKNOWLEDGMENTS

It is a pleasure to express our appreciation to Dr. E. E. Charlton and to the operators of the betatron for their kind cooperation. We are grateful to Professor H. A. Bethe for several stimulating discussions.

[14] This turns out to be about 100,000 for Zn^{63} and about 25,000 for Mg^{27} with a 15 percent counting geometry.

[15] G. S. Klaiber, E. Luebke, and G. C. Baldwin, in press.

Absolute Energies of $K\alpha$-Radiation from Thick Targets of Silver

PAUL KIRKPATRICK AND ALBERT V. BAEZ
Stanford University, Stanford University, California

(Received January 2, 1947)

$K\alpha$-radiation from a thick silver target bombarded at 40 kev was isolated by Ross filters of 42 Mo and 45 Rh and the total energy measured with a large air-filled ion chamber and found to be 8.6×10^{-12} erg per electron. This standardizes the curve of intensity *vs.* bombardment voltage measured in arbitrary units up to 180 kv by Webster, Hansen, and Duveneck. A quantitative explanation of the curve is developed upon the basis of the absolute cross section of the silver atom for K-ionization by electron impact, known over a considerable range of bombardment voltages from measurements by Webster, Hansen, and Duveneck and by J. C. Clark. From this cross section and the rate of energy loss of the bombardment electron the absolute energy of Ag $K\alpha$ is calculated and found to agree with the observed values within the limits of the errors of observation. The mass scattering coefficient of air at λ0.56A is found by calculation to be 0.244 cm^2g^{-1}.

1. INTRODUCTION

RELATIVE intensities of the characteristic x-ray lines of a variety of elements were measured by Meyer[1] and by Williams[2] but absolute determinations were not attempted. Webster, Hansen, and Duveneck[3] investigated the manner in which the intensity of the $K\alpha$-lines of silver vary with the energy of the electron bombardment which causes their emission, but again all intensities were recorded in arbitrary units. In WHD I and II both thick and thin target observations were presented, and these experimenters showed that a simple relation connects the thin target line intensity, the retardation rate of electrons in the target material, and the manner in which thick target line intensity increases with bombardment energy. Even without absolute intensity data they were able to exploit this relationship so as to show that the loss of energy per unit distance along the path of an electron up to about $\beta=v/c=0.65$ varies approximately as the -1.4 power of the speed.

The present paper reports a measurement of the absolute energy of the $K\alpha$-radiations of silver as emitted within a thick target bombarded at 40 kv. This is followed by a calculation of this line energy based upon an argument like that of WHD II, absolute thin-target energy from the work of Clark[4] and electron retardation laws regarded as approved by theory and experiment. No attempt is made to predict thick-target characteristic radiation from any pure theory of atomic emission because such theories are not yet sufficiently explicit.[5]

2. EXPERIMENT

Radiation from a commercial x-ray tube passed through an appropriate diaphragm, one of a pair of Ross filters, and into a large ionization chamber filled with dry air at atmospheric pressure. The charge of the ions collected within the chamber was measured with a calibrated Compton electrometer whose indications could be expressed in ergs of received radiation energy.

The $K\alpha$-radiation produced in the target was emitted in all directions with spherical symmetry. The portion which proceeded in the direction of observation first underwent absorption in the target, in the windows of the x-ray tube and ion chamber, in the filter, and in the air both without and within the chamber. All losses of this kind had to be evaluated in the process of determining the energy *as emitted*. The filters, one of molybdenum and one of rhodium,

[1] H. T. Meyer, Wissenschaftliche Veröffentlichungen aus dem Siemens-Konzern **7**, 108 (1929).
[2] J. H. Williams, Phys. Rev. **44**, 146 (1933).
[3] D. L. Webster, W. W. Hansen and F. B. Duveneck, Phys. Rev. **43**, 839 (1933), Phys. Rev. **44**, 258 (1933). These papers will be referred to, respectively, as WHD I and WHD II.
[4] J. C. Clark, Phys. Rev. **48**, 30 (1935).
[5] It has been shown, however, for the special case of the emission of K characteristic x-rays by nickel that the agreement between theory and thin-target observations is rather satisfactory. A report by Pockman, Webster, Kirkpatrick, and Harworth is in press.

embraced between their K absorption discontinuities a wave-length band (pass band) containing the $K\alpha$-lines of the silver target but excluding the other lines of the silver K series. This band also included a substantial proportion of continuous spectrum radiation, which proportion was determined. The thickness of the filters was such that they stopped about 85 percent of the radiation at the long wave side of the pass band. Spectrometer observations showed that for the silver spectrum as observed the errors of filter balance produced an error of less than one percent in the pass-band evaluation.

The filters, balanced in the usual way so as to transmit equally at wave-lengths not in the pass band, were placed in the beam between the tube and the ion chamber, one at a time, and the ionizing power of the filtrate radiation was determined by observation of the charge collected in a measured time t. The charge which would have been produced in the ion chamber by the full strength of the pass-band radiation, unattenuated by filtration, was obtained by dividing the difference between the charges collected when the two filters were used one at a time by a constant T which is characteristic of the filter pair. This constant, the transmission coefficient of the pair, is the difference between the fractions of the silver $K\alpha$-radiation passed by the respective filters. T was determined with the help of a Bragg spectrometer and found to be 0.262 ± 0.004.

The bombardment voltage of 40 kv selected for this measurement is high enough to produce an abundant output of $K\alpha$-radiation without being so high as to introduce undesired second order radiation into certain auxiliary spectrometer measurements to be described below.

We define the following quantities:

B = total Ag $K\alpha$-energy (in ergs) produced at the focal spot of a thick silver target per 40 kv bombarding electron. This quantity includes the line radiation resulting from K ionization produced *directly* by electron bombardment and also that produced *indirectly* by the absorption of continuous x-rays.

W = fraction of the $K\alpha$-radiation emitted in the direction of observation which escapes absorption in the target.

Ω = solid angle embracing the observed radiation.

k_w = fraction of the $K\alpha$-energy which survives absorption by the windows of the x-ray tube and the ion chamber.

k_a = fraction of the $K\alpha$-energy which survives absorption by the air lying between the x-ray tube window and the collecting region of the ion chamber.

k_c = ratio of the $K\alpha$-energy which is expended in ion production in the collecting region of the ion chamber to the $K\alpha$-energy arriving at the entrance end of the collecting region.

δ = ratio of continuous to α line energy in the pass band.

T = transmission coefficient of the filters (defined above).

i = target current in amperes.

t = duration, in seconds, of exposure of the ion chamber to x-rays.

Q_{Rh} = charge, in coulombs, collected in the ion chamber when the rhodium filter is in the beam.

Q_{Mo} = charge, in coulombs, collected in the ion chamber when the molybdenum filter is in the beam.

ϵ = x-ray energy in ergs expended in air per ion pair produced[6] $=5.13\pm0.2\times10^{-11}$ erg/ion pair.

A little thought about these quantities establishes the relation

$$B=\frac{4\pi\epsilon(Q_{Rh}-Q_{Mo})}{\Omega W k_a k_w k_c T(1+\delta)it}. \qquad (1)$$

There follows a discussion of the evaluation of the quantities on the right side of this working equation for the determination of B.

Determination of the collected charges Q_{Rh} and Q_{Mo} required knowledge of the voltage sensitivity of the electrometer and of the capacitance to ground of its associated ion-collecting system. Curves of electrometer deflection *vs.* applied potential were obtained under two conditions; first with the potential applied directly to the collecting system, and second, with a standard condenser of capacitance $C_s=42.88\times10^{-12}$ farad connected in series between the potential source and the collecting system. Since the electrometer was to be used ballistically it was calibrated in the same manner, the applied potential being raised gradually to the final value throughout a time interval t. During x-ray measurements C_s was not connected, and the collected charge producing any given electrometer deflection was calculated by the equation $Q=C_s(V-V_0)$, where V_0 and V are the potentials associated with the observed deflections on the first and second calibration curves, respectively.

The time of exposure t, uniformly 20 seconds, was controlled by a pendulum clock and an electrically operated shutter. The deflections, of

[6] W. Binks, Rep. on Prog. in Phys. 3, 347 (1936).

the order of 20 to 40 centimeters, were quite reproducible. A set of twelve observations with each filter, taken alternately, yielded the values $Q_{Rh}=(23.70\pm0.10)\times10^{-12}$ coulomb and $Q_{Mo}=(8.15\pm0.07)\times10^{-12}$ coulomb, the probable errors indicated being mainly the estimated errors of calibration.

The observed radiation all passed through a reamed hole in a type-metal plate which was mounted 69.7 cm from the center of the small roughened area of the target of the x-ray tube. The hole diameter, according to measurements made with a machinist's hole gauge, was 0.3205 cm. These figures give for the solid angle of observed radiation $\Omega=\pi(5.28\pm0.03)\times10^{-6}$ steradian. The probable error is an estimate which depends principally upon our ignorance of the precise location of the effective center of the focal spot.

The evaluation of the absorption of $K\alpha$-radiation in the silver target was derived from observations by others. It is not possible to deduce the emerging fraction W with precision from WHD II, but their original data, preserved in this laboratory, have afforded the basis for a satisfactory determination. They recorded the intensity, in arbitrary units, of the Ag $K\alpha$-doublet, isolated by a calcite crystal, for the three grazing angles of emergence from the target 5°, 15°, and 25°. For each of these angles they used four different bombardment voltages, respectively, 1.18, 1.5, 2.0, and 3.0 times the K excitation potential at 25.5 kv. None of these data applies exactly to the conditions of the present experiment but fortunately the angles and potentials of Webster, Hansen, and Duveneck bracketed those of this investigation so the required intensities were readily obtained from their data by graphical interpolation.

The treatment of the data for the determination of W follows the method of Kulenkampff.[7] In this method the common logarithms of the intensities for a given bombardment potential are plotted against the cosecant of the grazing angle θ between the emerging radiation and the target face, and the curve (almost straight) is extrapolated to cosecant $\theta=0$. The intensity at this point is taken to be the intensity before target absorption. Used with the data of Webster, Hansen, and Duveneck this process gives $W=0.75\pm0.03$. Wisshak[8] has also recorded intensities of Ag $K\alpha$ emerging at various angles with the target face, and his data provide a check on the W value above. The check is weak in two respects: the original data are unavailable, and the voltage range of his work extended only from 27.5 kv to 31.9 kv. Inferences must be drawn from his Fig. 5 and a drastic extrapolation to 40 kv must be made. Proceeding thus one obtains $W=0.78\pm0.10$. Because of the large indicated uncertainty we shall use the result from Webster, Hansen, and Duveneck, regarding the Wisshak value as confirmatory only.

Air absorption calculations are based upon a mass absorption coefficient of 0.660 $cm^2\ g^{-1}$ at $\lambda=0.560$A, derived from published conclusions of Victoreen[9] and unpublished measurements by David Nicodemus. For air under the conditions of these observations (21°C and 76.3 cm Hg) this gives a linear absorption coefficient $\mu=7.96\times10^{-4}\ cm^{-1}$. The measured air path from the x-ray tube to the collecting region within the ion chamber was 103.3 cm, an absorber passing a fraction $k_a=0.921$.

Window absorptions were directly measured by inserting the absorbing material into the beam entering a Bragg spectrometer adjusted to receive the Ag $K\alpha$-lines. The Cellophane window of the ion chamber absorbed negligibly but the absorption by the wall of the x-ray tube required evaluation. This tube envelope was a reasonably uniform cylinder of Pyrex glass on which one area was rather arbitrarily chosen as the exit port of radiation.

To understand the method by which the absorption at this window was measured without destroying the tube, consider a plane normal to the tube axis and including the chosen window. This plane intersects the tube envelope in a circle, in which an inscribed equilateral triangle may be imagined with one of its vertices coinciding with the center of the window. The x-ray tube was placed before a Bragg spectrometer in such a position that the entering beam of x-rays (from an auxiliary silver-target tube) passed

[7] H. Kulenkampff, Ann. d. Physik 69, 548 (1922).

[8] F. Wisshak, Ann. d. Physik 5, 507 (1930).

[9] J. A. Victoreen, J. App. Phys. 14, 95 (1943).

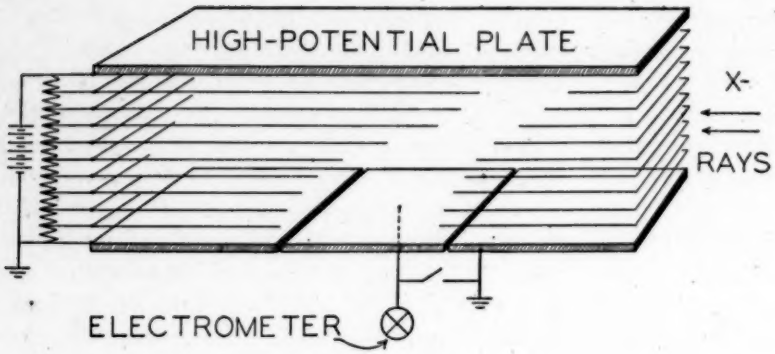

FIG. 1. Internal construction of absolute ion chamber, showing provisions for insuring straightness of field.

along one side of the triangle defined above on its way to the crystal.

The absorption of Ag $K\alpha$ by the tube in this position was measured by making spectrometer observations with the tube in and out of the beam, after which the tube was rotated about its own axis and the measurements repeated with the x-ray beam passing in turn along the other two sides of the triangle. From the three absorption measurements the absorption by the glass tube wall for radial transmission at any of the triangle vertices could readily be calculated. For the area used in the principal measurements of this paper the fraction of Ag $K\alpha$ transmitted was found in this way to be $k_w=0.785\pm0.005$.

The ionization chamber was a steel cylinder 17.5 inches long and 8 inches in internal diameter. The centrally located electrode structure, shown in Fig. 1, consisted of two stiff and parallel aluminum plates 13 inches long, 4 inches wide, and 4 inches apart. One plate was divided into three electrically distinct sections of which the middle one was directly connected to the electrometer, and the others served as guard plates to keep the electrostatic collecting field rectilinear. As further insurance the entire field between the electrodes was surrounded by nine rectangular wire frames of the kind used with success by Taylor and Singer[10] for reducing curvature of their collecting fields. These frames, maintained at properly spaced potentials proportionate to their physical spacings in the electrode gap, together with the guard plates, produced a collecting field straight enough at its entrance and exit boundaries to justify the assumption that the section of the x-ray beam yielding collectible ions was the same in length as the distance ($L=10.25$ cm) between the centers of the gaps separating the collecting plate from the adjacent guard plates. The over-all potential of the chamber was 171 volts, a potential sufficient to produce sensibly complete saturation in air.

[10] L. S. Taylor and G. Singer, Bur. Stand. J. Research 5, 507 (1930).

3. ANALYSIS OF THE DATA

The ions measured were presumed to be those formed within the rectangular collecting volume bounded on one side by the collecting plate and on the opposite side by a portion of the high potential plate. The chamber was open to the atmosphere through a drying tube, so the ionized medium was dry air at the ambient density. Within the collecting region ions must have been produced by: (*a*) cosmic radiation, (*b*) radioactive materials in and near the chamber, (*c*) photo-electrons ejected from air in the collecting region by the primary beam, (*d*) Auger electrons and fluorescence radiation from the excited atoms of *c*, (*e*) recoil electrons ejected from air in the collecting region by the primary beam, (*f*) fluorescence radiation originating in the guard regions and absorbed in the collecting region, (*g*) radiation scattered by air in all regions of the chamber, (*h*) electrons and x-rays evoked from metal surfaces of the chamber by scattered radiation.

Ions from sources *a* and *b* were negligibly few and furthermore were discarded by subtraction in the differential filter process. The energy W_1 expended in ion production in the collecting region by processes *c*, *d*, and *e* is almost exactly $W_1=W_0(1-\exp[-(\tau+\sigma_a)L])$, where W_0 is the Ag $K\alpha$-energy entering the collecting region during the exposure time, τ and σ_a are the linear fluorescence and recoil absorption coefficients of

the air in the chamber for the Ag $K\alpha$-radiation. The inexactitude in the expression for W_1 results from the escape of a portion of the fluorescence radiation emitted within the collecting region.[11] Only the argon K fluorescence, of all the characteristic radiations of air, is hard enough to have a chance of escape, and calculation shows that the amount thus lost is only about one half percent of the total W_1. This loss is in large part compensated by the fluorescence radiation (process f) from the guard regions of the chamber which comes into the collecting region and is there absorbed. Within the accuracy of this experiment W_1 is taken to be the ionizing energy expended in processes c, d, and e.

The coefficient μ covers three processes of removal of energy from the primary beam and may be broken down into the form $\mu=\tau+\sigma_a+\sigma_s$, where σ_s pertains to true scattering, both modified and unmodified. To evaluate the sum $\tau+\sigma_a$ from this equation it is necessary first to determine σ_s.

The linear scattering coefficient σ_s is a combination of the scattering coefficients of the constituent gases. The scattering of x-rays by gases is rather well understood and the present agreement between theory and experiment makes it possible to calculate scattering coefficients with some confidence. For the diatomic gases we have used Woo's[12] equation, which is also conveniently presented by Compton and Allison.[13] This equation, which expresses the intensity of scattering, both modified and unmodified, by a diatomic molecule may be written

$$I_\phi = I(e^4/r^2m^2c^4)(1+\cos^2\phi) \times\{F^2(1+(\sin x)/x)+R(Z-\Sigma f^2)\},$$

where I is the incident intensity, ϕ the scattering angle, r the distance to the point of observation, F the atomic structure factor, Σf^2 the incoherent scattering function, R the Breit-Dirac factor $[1+(h/mc\lambda)\ vs.\ \phi]^{-3}$ and $x=(4\pi s/\lambda)\sin(\phi/2)$ in which s is the distance between the atoms in the molecule. The meaning of the other symbols is obvious. The separation of the oxygen atoms was taken to be 1.22A and that of nitrogen 1.10A, these figures being deduced from Rasetti's[14] spectroscopic determination of the moments of inertia of the molecules. The structure factors of oxygen and nitrogen by Compton and Allison were used as far as possible but they covered only the range of scattering angles from zero to about eighty degrees. The rest of the way as far as 155° was filled out by normalizing Barrett's[15] experimental observations of the scattering by oxygen and nitrogen to fit the calculated angular scattering distribution. From 155° to 180° the curve was drawn in freely, following the known general shape of experimental scattering curves of other scatterers of low atomic number. The calculation is for the wave-length 0.56A whereas Barrett's wave-lengths were 0.48A for oxygen and 0.39A for nitrogen. This discrepancy causes no trouble since the *shape* of the scattering distribution varies quite slowly with wave-length, Barrett's oxygen curves for 0.39A and 0.49A being barely distinguishable.

The linear scattering coefficient may be evaluated by an integration[16] of the angular scattering distribution which must be carried out graphically or numerically in the present case. In this process the ordinates of the distribution curve are multiplied by $\sin\phi$ and since the sine goes to zero at 180° the part of the distribution curve which is most uncertain contributes little to the final result. Graphical integrations yielded the mass scattering coefficients 0.246 for oxygen and 0.242 for nitrogen at λ0.56A. A similar calculation for oxygen was made by Woo and Sun[17] who calculated their own structure factors by the method of Thomas and Fermi. From their curve of atomic absorption coefficient *vs.* wave-length it is possible to deduce for λ0.56A the value $\sigma/\rho=0.246$, in full agreement with the present calculation.

The only other component of air which needs consideration is argon. From the calculations of

[11] Some photo- and recoil electrons will originate in the collecting region but escape into the guard regions, there to expend their energies in the production of uncollectible ions. This loss is almost exactly compensated by the photo and recoil electrons which originate in the guard regions and move into the collecting region to produce ions.

[12] Y. H. Woo, Phys. Rev. **41**, 21 (1932).

[13] A. H. Compton and S. Allison, *X-rays in Theory and Experiment* (D. Van Nostrand Company, Inc., New York, 1935), Eq. (3.58).

[14] F. Rasetti, Phys. Rev. **34**, 367 (1930).

[15] C. S. Barrett, Phys. Rev. **32**, 22 (1928).

[16] After the manner of J. J. Thomson, *Conduction of Electricity through Gases*, second edition, p. 325.

[17] Y. H. Woo and C. P. Sun, Sci. Rep. Nat. Tsing Hua Univ. **3**, 549 (1936).

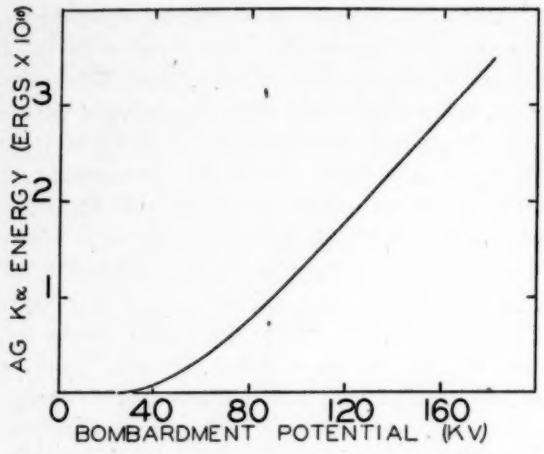

FIG. 2. Total energy of $K\alpha$-radiation produced at the focal spot of a thick silver target per bombarding electron. Observations by the authors and others.

Woo and Sun we deduce $\sigma/\rho=0.374$ for this element at $\lambda 0.56$A. Measurements by Wollan,[18] as interpreted by Woo and Sun, gave 0.395. The value 0.39 is adopted here. From the accepted composition of dry air, the density given above, and the mass scattering coefficients just discussed one obtains directly the mass scattering coefficient 0.244 and the linear scattering coefficient $\sigma_s=2.94\times10^{-4}$ cm^{-1}, which leads to $\tau+\sigma_a=5.02\times10^{-4}$ cm^{-1} and $W_1=0.00514W_0$.

The energy scattered out of the primary beam from the segment of it lying in the collecting region is $W_2=W_0(1-\exp[-\sigma_s L])$. This scattered radiation will traverse the collecting region, having a path length therein of the order of $L/2$, and in so doing will lose by photoelectric and recoil absorption a quantity of energy

$$W_3=W_0(1-\exp[-\sigma_s L])(1-\exp[-\tfrac{1}{2}L(\tau+\sigma_a)]).$$

Scattering takes place also in the guard regions at the ends of the collecting regions. They are approximately the same in size as the collecting region so it may be supposed that each of them sends to the collecting region scattered radiation which expends therein radiation energy W_3. The justification for the roughness of this argument is that $3W_3$ is found by calculation to be a negligibly small quantity. This disposes of ion source g.

Detailed calculations for this chamber show that ions produced by electrons or x-rays from metal parts (source h) cannot exceed a few tenths of one percent of the number formed by primary processes evaluated above so this contribution is neglected. Summarizing these arguments one finds $k_e=W_1/W_0=0.00514$.

When radiation is abundant, air is an excellent gas for use in absolute ionization chambers, since the corrections which cause so much trouble with heavy gases here turn out to be negligible. Furthermore the scattering coefficient may be calculated with a certainty not possible with polyatomic molecules of undetermined structure. It is no disadvantage that the fraction k_e is small.

The ratio δ of continuous to $K\alpha$-line energy in the energy difference between the molybdenum and rhodium filtrates was determined by investigating the pass band region with a spectrometer, using the x-ray tube, tube potential, and ion chamber which were later used in the absolute measurements. Under these conditions δ could be determined by plotting the part of the spectrum lying in the pass band and comparing the line and continuous areas. An error is possible here because of the variation of the calcite spectrometer crystal's reflecting power with wave-length, but this variation is actually slight for good calcite, and the region under consideration has a breadth of only 15 percent of its mean wave-length. No radiations of higher order than the first were included in these spectrometer observations. The observed $\delta=0.920\pm0.02$, where the indicated uncertainty is an estimate taking account of the error just mentioned, the ordinary errors of spectrometer observation, and the uncertainty involved in interpolating a continuous spectrum under a line.

The target current $i=0.0025$ amps., was measured with negligible error with a freshly calibrated milliammeter introduced into the tube circuit so as to measure no corona or other loss currents. Assembling all the numerical quantities we find by applying Eq. (1),

$$B=(8.6\pm0.8)\times10^{-12}\text{ erg}$$

of $K\alpha$-radiation from thick silver per 40-kv electron. This includes all radiation emitted at the focal spot in all directions, the total being taken before absorption. It does not include $K\alpha$-radiation produced at points away from the focal spot by bombardment electrons which

[18] E. O. Wollan, Phys. Rev. **35**, 1019 (1930).

rediffuse from the focal spot by single nuclear scattering and experience radiative collisions elsewhere.

Data on *relative* intensities of $K\alpha$-radiation from thick silver bombarded at potential from 27 to 179 kv were given in WHD II, where curves were presented showing on logarithmic scales the variation of intensity with a stated function of the bombardment energy. Precise relative intensities, however, are not readily extracted from the paper and we have therefore consulted the original data of these authors and have normalized them to the 40-kv value of B given in the preceding paragraph. The result appears in Table I and in Fig. 2.

Argument from Thin-Target Observations

Any theory which would account for the magnitude of B must take account of the K ionization cross section of the silver atom, the relative intensity of the α-lines in the total K spectrum, the intensity of K-radiation from atoms ionized by x-rays rather than by electrons, the silver fluorescence yield, and the rate of loss of bombardment kinetic energy by all processes. Let

$\Phi(\beta)$ = cross section of the silver atom for K ionization by electrons with speed βc.
$-\partial E/\partial x$ = electron energy loss rate in ergs per cm of path in silver.
R = ratio of the number of K ionizations to the number which would have occurred if no electrons had rediffused from the target.
w = silver K fluorescence yield.
P = ratio of directly to indirectly produced $K\alpha$ power.
p = ratio of number of $K\alpha$-quanta to total K quanta emitted.
A = atomic weight of target element.
N = the Avogadro number.
ρ = density of the target substance.

The total number I of K ionizations produced by an electron which enters the target at a speed given by β_0 and slows down therein until it can no longer produce K ionizations is

$$I = -\int_0^{\beta_0} \frac{\partial I}{\partial x}\frac{\partial x}{\partial E}\frac{\partial E}{\partial \beta}d\beta, \qquad (2)$$

in which $\partial I/\partial x = \Phi\rho N/A$, $\partial x/\partial E$ is a function of β to be selected from the theoretical and experimental literature, and the other derivative is obtained from the relativistic kinetic energy expression. All three factors in the integrand are functions of β and the integration must be performed graphically or numerically. The function Φ is known from WHD I and J. C. Clark,[4] and the values obtained by combining the two papers[19] are listed in Table II.

The energy loss rate $-\partial E/\partial x$ has not been measured for electrons in silver with the precision needed here. The nearest thing to an experimental expression which is available comes from Williams'[20] empirical adjustment of Bohr's[21] theory to agree with the observations of White and Millington[22] on the stopping of beta-particles by mica. Williams found the loss rate to be $1.06\,\beta^{-1.4}$kv per milligram/cm^2, which is a rough approximation in that it takes no account of the different stopping properties of the different atoms except as related to the density. The exponent of β was specifically confirmed for silver in WHD II over a range of β applicable here, but the numerical coefficient is supported only by observations on atoms much lighter than silver. For silver Williams' expression may be written

$$\frac{-\partial E/\partial x}{\rho N/A} = 3.04\beta^{-1.4}\times 10^{-28}. \qquad (3)$$

TABLE I. Energy of Ag $K\alpha$ produced in thick targets. Ergs per bombardment electron.

Bombardment potential (kv)	Ag $K\alpha$ energy B (ergs $\times 10^{13}$)
<25.53	0
27.0	0.151
30.1	1.12
38.3	7.14
51.1	23.4
76.6	71.4
102.1	133.
127.6	204.
153.2	272.
178.7	343.

[19] Clark's Φ has been modified by the substitution of more recent values of the silver fluorescence yield and of the ratio p of the number of $K\alpha$-quanta to the total number of K quanta produced.
[20] E. J. Williams, Proc. Roy. Soc. **A130**, 310 (1931).
[21] N. Bohr, Phil. Mag. **25**, 10 (1913).
[22] P. White and G. Millington, Proc. Roy. Soc. **A120**, 701 (1928).

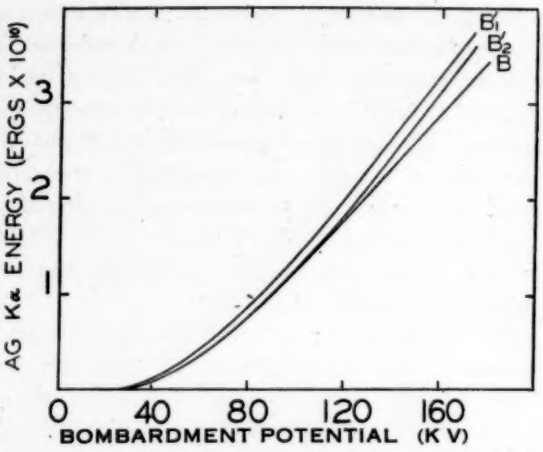

FIG. 3. Total energy of $K\alpha$-radiation produced at the focal spot of a thick silver target per bombarding electron. Curve B, as observed. Curves B_1' and B_2', as calculated from measured K ionization cross sections of the silver atom.

It is possible to use instead of Eq. (3) a formula with a more definite theoretical basis. From the theory of Bethe,[23] based upon Born's approximate collision treatment, one obtains

$$\frac{-\partial E/\partial x}{\rho N/A}=\frac{4\pi e^4 Z}{mc^2\beta^2}\left\{\ln\frac{mc^2\beta^2}{J(1-\beta^2)}-\beta^2\right\}, \qquad (4)$$

where J, the mean excitation energy of the stopping atoms may be taken[24] as $18.4\times10^{-12}Z$ erg. It has been assumed in connection with Eq. (4) that the speed of the incident electron is large compared to the speeds of the atomic electrons. This is certainly not the case with the K electrons of silver but these are of course greatly outnumbered by the slower atomic electrons.

Equation (2) has been used for the graphical evaluation of I, first in combination with Eq. (3) and again with Eq. (4). Each evaluation yields I as a function of β, and it is satisfying to find that the corresponding values of I differ, on the average, by less than ten percent.

The energy of $K\alpha$-radiation resulting from these I ionizations and from the accompanying continuous radiation is

$$B'=h\nu_a pwIR(P+1)/P. \qquad (5)$$

The ratio p of the number of $K\alpha$-quanta to the total number of K quanta is readily evaluated from the known line intensities[25] and is found to be 0.828 ± 0.01. For the K fluorescence yield w Stephenson's[26] value 0.81 ± 0.01 has been adopted. The rediffusion ratio R was estimated by Webster, Hansen, and Duveneck and from Table I of WHD II one obtains by interpolation the values given in Table III below. This table also shows values of $(P+1)/P$ from measurements by Webster.[27] Finally, Table III presents values of B' computed from the tabulated data by the use of Eq. (5). These values of B' are plotted in Fig. 3, together with a curve representing the corresponding directly observed quantity B.

The probable error in the values of B' is estimated to be about ten percent and the probable error for B is estimated at seven percent. In view of these uncertainties, the slight discrepancy between observed and predicted line

TABLE II. Cross sections Φ of the silver atom for K ionization by electrons of speed βc.

β	$\Phi\times10^{23}$ (cm²)
0.306	0
.333	1.60
.367	2.91
.416	3.96
.456	4.37
.493	4.51
.552	4.54
.598	4.45
.640	4.36
.672	4.25

TABLE III. Total energy of $K\alpha$-radiation per incident electron. β_0 is relative speed of an electron at impact with a thick silver target. $B_{1,2}'$ is the number of ergs of resulting $K\alpha$-radiation as predicted from thin target observations. B_1' is calculated by use of Williams' electron-stopping formula, Eq. (3), and B_2' with a formula from Livingston and Bethe, Eq. (4).

β_0	R	$(P+1)/P$	$I_1\times10^3$	$I_2\times10^3$	$B_1'\times10^{10}$	$B_2'\times10^{10}$
0.306			0	0	0	0
0.367	0.863	1.53	0.30	0.24	0.095	0.076
0.416	0.813	1.52	0.90	0.81	0.267	0.241
0.493	0.793	1.51	2.90	2.54	0.834	0.732
0.552	0.781	1.50	5.3	4.89	1.49	1.38
0.598	0.775	1.50	8.1	7.52	2.27	2.10
0.640	0.770	1.49	11.4	10.7	3.13	2.95
0.660	0.768	1.49	13.1	12.6	3.62	3.44

[23] M. S. Livingston and H. A. Bethe, Rev. Mod. Phys. 9, 263 (1937). This article cites many prior references. The factor 2 in their Eq. (749a) does not apply to the stopping of electrons so it is not retained in Eq. (4) above.

[24] R. Wilson, Phys. Rev. 60, 749 (1941).

[25] J. H. Williams, Phys. Rev. 44, 146 (1933).

[26] R. J. Stephenson, Phys. Rev. 51, 637 (1937). See also E. Arends, Ann. d. Physik 22, 281 (1935), I. Backhurst, Phil. Mag. 22, 737 (1936).

[27] D. L. Webster, Proc. Nat. Acad. Sci. 14, 337 (1928).

intensities is without significance; the agreement is as complete as the quality of the observations will permit. Conclusions about the relative merits of the two electron-stopping formulas would scarcely be warranted by these results since all the curves of Fig. 3 are separated by amounts less than their errors.

The present work needs to be extended in two directions: thick and thin target comparisons for other elements should be made, and the thin target characteristics should themselves be explained by fundamental atomic theory. The latter matter is discussed in a report[28] which is in press at this writing. The former will receive attention in a paper now in preparation on the characteristic radiations of copper and nickel.

[28] D. L. Webster, L. Pockman, P. Kirkpatrick, and K. Harworth, Phys. Rev. **71**, 330 (1947).

PHYSICAL REVIEW VOLUME 71, NUMBER 8 APRIL 15, 1947

Range Measurements of Alpha-Particles from 94^{239} and 94^{238}†

O. CHAMBERLAIN*, J. W. GOFMAN,** E. SEGRÈ,** AND A. C. WAHL***
Departments of Chemistry and Physics, University of California, Berkeley, California.
(Received January 3, 1947)

The ranges of alpha-particles from 94^{239} and 94^{238} have been measured by comparison with Po alphas, and are found to be 3.68 and 4.08 cm of air.

INTRODUCTION

TO determine the ranges of alpha-particles from 94^{239} and 94^{238} with greater precision than previously reported,[1,2] a direct comparison of these ranges with the ranges of alpha-particles from Po was carried out.

EXPERIMENTAL METHOD

The samples of 94 were deposited on platinum by evaporation. They were separated from the bombarded uranium with a very small amount of carrier. The uranium sample was electroplated on a copper disk. The thinness of all these samples is borne out by the small values of the straggling coefficient observed, which is reported below.

The range of the alpha-particles were measured by comparison with a thin polonium standard. The samples were put in front of, and at a constant distance from, a shallow (0.23 cm) ionization chamber. The chamber and the sample were enclosed in a vessel, the pressure in which could be varied and the temperature measured. We plotted curves giving the counting rate of the samples, at a constant gain of the amplifier and registering circuit, as a function of the air density in the chamber.

The mean range was computed from the air density at which one obtained half the maximum counting rate according to the formula,

$$R = R_{Po}(\delta/\delta_{Po}), \qquad (1)$$

in which R is the range of the alpha-particles of the substance under investigation, $R_{Po}=3.842$ cm (in air at 15°C and 760 mm of Hg)[3] and δ_{Po}, δ are respectively the densities of the air at which half the maximum counting rate is observed for δ_{Po} and for the substance under investigation. A small correction for varying pressure in the ionization chamber is discussed below. The ranges R obtained in this way are clearly mean ranges in air at 15° and 760 mm Hg.

Various runs for each substance were per-

† This work was done in the Department of Chemistry and Physics, University of California, Berkeley, California, in June, 1943.
* Institute of Nuclear Studies, University of Chicago, Chicago, Illinois.
** University of California, Radiation Laboratory; Department of Physics, Berkeley, California.
*** Department of Chemistry, Washington University, St. Louis, Missouri.
[1] J. W. Kennedy, G. T. Seaborg, E. Segrè, and A. C. Wahl, Phys. Rev. **70**, 555 (1946).
[2] G. T. Seaborg, A. C. Wahl, and J. W. Kennedy, Phys. Rev. **69**, 367 (1946).

TABLE I.

Element	Mean range	α
Po	3.842 cm	0.09 cm
94^{239}	3.68	0.11
94^{238}	4.08	0.12

formed in order to check the reproducibility of the positions in changing samples, and additional runs were made for studying the influence of the minute amounts of carrier contained in the samples of 94.

STRAGGLING

The total experimental straggling parameter,[3] α, obtained by taking $\alpha=2s/\pi^{\frac{1}{2}}$ in which s is the difference between the extrapolated and mean range is reported in Table I together with the mean ranges.

Our straggling figures are higher than the ones obtained under the best possible conditions;[3] this is due to several factors, including the comparatively low specific activity of the substances studied which requires some sacrifice in the geometrical conditions to keep the counting time within reasonable limits.

[3] M. G. Holloway and M. S. Livingston, Phys. Rev. **54**, 18 (1938).

CORRECTION FOR DEPTH OF DETECTOR

Equation (1) is nearly exact if R is close to R_{Po}, otherwise it needs some small corrections because of the fact that varying the density of the air also produces a change in the residual range that the alpha-particle must spend in the shallow ionization chamber in order to trip the counter. If we call ϵ the minimum residual range at 760 mm of Hg and 15°C that an alpha-particle must spend in the chamber in order to produce enough ions to trip the counter, Eq. (1) must be replaced by

$$(R-\epsilon)/(R_{Po}-\epsilon)=\delta/\delta_{Po}. \qquad (2)$$

In order to determine ϵ we reduced the air density in the chamber until only half of the polonium particles were counted. This occurred at a density of 0.20 of the density of air at 760 mm of Hg and 15°C. Under these conditions the alpha-particles reaching the chamber had a residual range of 2.8 cm and would produce approximately 3000 ion pairs per millimeter in air at 760 mm of Hg and 15°C or 1350 in our chamber with the air at $\frac{1}{5}$ the density. This number of ions corresponds to a residual range of 0.08 cm in air at 760 mm of Hg and 15°C. This was obtained from the curve of specific ionization *versus* range for a single alpha-particle as given by Holloway and Livingston.[3]

Infra-Red Absorption in Formaldehyde beyond 10μ

WILLARD E. SINGER*
Department of Physics, The Ohio State University, Columbus, Ohio
(Received January 8, 1947)

The infra-red absorption of formaldehyde in the region between 10μ and 20μ was studied with a KBr prism spectrometer. Two methods of preparing the gas were used. No appreciable absorption was observed.

I. INTRODUCTION

IT has been suggested by Sponer and Teller[1] that certain experimental results in the band spectra of formaldehyde are more readily explained if a vibrational frequency exists near 600–700 cm^{-1}. If this were so, that band would have to be the bending frequency ν_6. The work of Ebers and Nielsen[2] suggested that this bending frequency ν_6 is centered at 1165 cm^{-1} and partly overlaps the frequency ν_5 which is believed to lie at 1278 cm^{-1}. On the basis of the discussion by Sponer and Teller, the band at either 1165 cm^{-1} or 1278 cm^{-1} would have to be interpreted as $2\nu_6$. There are certain definite objections to this kind of assignment.

First: Both of the bands, 1165 cm^{-1} and 1278 cm^{-1}, appear to be of the perpendicular type. If, however, ν_6 lies at 600–700 cm^{-1}, as Sponer and Teller suggest, then $2\nu_6$ should be a band of the parallel type. If either of the bands is to be considered as an overtone band and have perpendicular characteristics, it would have to be $3\nu_6$, and the intensities observed appear much too great to be considered as those of a second overtone.

Second: Both of these bands at 1165 cm^{-1} and 1278 cm^{-1} have an anomalous spacing between the rotation lines, i.e., the spacing is considerably larger than that of the 3.6μ perpendicular bands. This anomalous spacing can be understood on the basis of the theory, discussed in a paper by Nielsen,[3] which supposes the existence of Coriolis resonance interaction between the frequencies ν_5 and ν_6 which are mutually perpendicular to each other. This interaction would be small if ν_5 and ν_6 were very different in frequency. It may, moreover, be shown that no Coriolis resonance can exist in first order between a fundamental and and an overtone.

It has, therefore, seemed worth while to investigate the region from 10μ, the limit to which Ebers and Nielsen explored, to approximately 25μ, where KBr begins to lose transparency, in order to determine if any further absorption bands exist in this region.

II. EXPERIMENTAL

Two entirely different methods were followed in the preparation of the absorbing gas. For the first method an absorption cell was constructed of a glass tube 5 cm in diameter and 7 cm long with flat ground ends. Windows of polished KBr plates approximately one centimeter thick were clamped in place by means of two brass plates connected by two threaded brass rods. Suitable openings were provided in the brass plates for the passage of the light beam. The junction of glass and KBr was sealed with four successive thin layers of clear Glyptol (No. 1202) applied with a brush, with an 18–24 hour drying period between the successive applications. This method apparently eliminated the difficulty of cracked windows on cooling, encountered by Ebers and Nielsen. An 8 mm side tube on the cell permitted evacuation. The entire cell was then placed inside a small electric furnace so constructed as not only to heat the cell but also keep the windows at such a temperature as to obviate the polymerization of the formaldehyde vapor onto the windows. The cell was first evacuated at the elevated temperature and tested for leaks. A small amount of the paraformaldehyde was then introduced, the cell evacuated and sealed off,

* On leave from Bowling Green State University, Bowling Green, Ohio.
[1] H. Sponer and E. Teller, Rev. Mod. Phys. **13**, 76 (1941).
[2] E. S. Ebers and H. H. Nielsen, J. Chem. Phys. **5**, 822 (1937).
[3] H. H. Nielsen, J. Chem. Phys. **5**, 818 (1937).

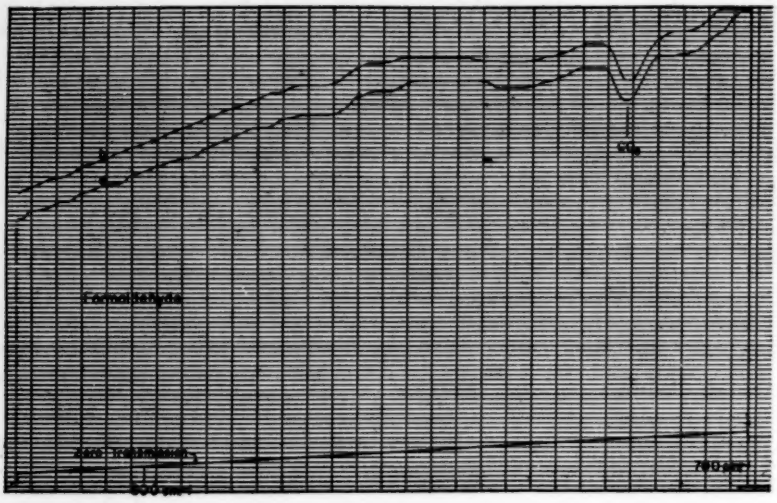

FIG. 1. Infra-red absorption on formaldehyde between 600 cm^{-1} and 700 cm^{-1}. Curve *b* was made without the cell, and curve *a* with the cell in the light beam.

and the heated cell placed in the optical path of a KBr prism spectrometer of the Wadsworth-Littrow type with attached automatic recorder.

For the second method a cell 9 cm in length was prepared similar to the cell described above, except that there was connected to the side tube a trap 15 cm long and 1.2 cm in diameter. This trap was connected through a stopcock to a special apparatus for the preparation of monomeric formaldehyde as described by Spence and Wild.[4] After 2–3 cc of the liquid monomer had collected in the cell trap, the cell and this trap were sealed off from the remainder of the system and the entire unit consisting of cell, trap, and trap refrigerant placed in the spectrometer. Since it was deemed wise to measure the absorption at several pressures, it was necessary to find means to maintain the trap at certain low temperatures. This was finally accomplished by filling almost full of acetone the quart-size Dewar flask and adding small chunks of solid CO_2 until the temperature was lowered to the desired value. It was found that this temperature could readily be maintained within a half degree centigrade during the course of a given run of 30 to 45 minutes. Temperatures were measured with a pentane thermometer which was checked at three points, *viz.* 0°C, −78°C, −183°C.

[4] R. Spence and W. Wild, J. Chem. Soc. 507 (1935); R. Spence and W. Wild, J. Chem. Soc. 338–340 (1935).

III. EXPERIMENTAL RESULTS

Following the first procedure, experimental runs were made at temperatures of 73°C, 100°C, 120°C, and 134°C with corresponding vapor pressures of 220 mm, 370 mm, 580 mm, and 750 mm of mercury, respectively, over the range from 14μ to 20μ (700–500 cm^{-1}). Within this region no absorption bands were observed. In order to confirm the presence of an absorbing gas, a run was made at a pressure of 580 mm of Hg over a portion of the region covered by the work by Ebers and Nielsen, and absorption bands reported by them were observed with somewhat greater detail than that shown in their prism curve. An additional absorption maximum at 10.7μ was noted which is probably part of the 7μ–10μ region reported by them.

Following the second procedure, an experimental run was made over the region 7μ–20μ (1430–500 cm^{-1}) with the trap maintained at a temperature of −35°C, and a corresponding vapor pressure of 360 mm of Hg. Additional observations were made over the range 575 cm^{-1} to 725 cm^{-1} at temperatures of −50°C and −25°C with corresponding pressures of 155 mm and 585 mm of Hg, respectively. Again, no absorption was observed in the 600–700 cm^{-1} region and the maximum at 10.7μ also occurred. Figure 1 shows one record made over the range 600–700 cm^{-1} with a vapor pressure of 155 mm of Hg. The upper trace *b* was made without the cell in

the light path while the lower trace a was made with the cell containing the formaldehyde vapor placed in the light path.

No evidence has been uncovered by these observations that any appreciable absorption exists beyond the region studied by Ebers and Nielsen. This supports their assignment of the regions 1165 cm^{-1} and 1278cm^{-1} as due to the frequencies ν_5 and ν_6.

The writer wishes to express his sincere appreciation for help and encouragement to Dr. H. H. Nielsen, Chairman of the Department, who suggested the project and made available the facilities of the Infra-Red Laboratory.

PHYSICAL REVIEW VOLUME 71, NUMBER 8 APRIL 15, 1947

Experimental Evidence of the Viscous Behavior of Grain Boundaries in Metals*

T'ING-SUI KÊ
Institute for the Study of Metals, The University of Chicago, Chicago, Illinois

(Received November 12, 1946)

The mechanical behavior of grain boundaries in metals has been a subject of constant controversy. The present research is designed to examine thoroughly the mechanical behavior of grain boundaries in metals in a quantitative manner. A simple torsional apparatus has been devised for measuring four types of anelastic effects at very low stress levels, namely: internal friction at low frequencies; variation of dynamic rigidity with temperature; creep under constant stress; and stress relaxation at constant strain. All four types of anelastic effects have been studied in 99.991 percent polycrystalline aluminum as well as in single crystal aluminum; these effects are practically absent in single crystal aluminum. The four types of anelastic effects observed in polycrystalline aluminum are completely recoverable and are linear with respect to the applied stress and prior strain. They satisfy the interrelations derived by Zener from Boltzmann's superposition principle within experimental error. These are consistent with the viewpoint that the grain boundaries behave in a viscous manner. The maximum amount of shear stress relaxation in polycrystalline aluminum determined by the four types of anelastic measurements is about 33 percent. This is in good agreement with the theoretical value of 36 percent calculated by assuming the grain boundary to be viscous. The heat of activation associated with the viscous slip along the grain boundaries has been found to be 34,500 calories per mole. The coefficient of viscosity of the grain boundaries in aluminum estimated using this heat of activation, is consistent with that of molten aluminum at the same temperature. Similar anelastic effects have been also observed in polycrystalline magnesium, indicating that the viscous behavior is common to all metals.

INTRODUCTION

IN a polycrystalline material, it is reasonable to think that there is merely a transition layer at the grain boundary, where the atom positions represent a compromise between the crystalline arrangements in the two adjoining grains. However, for the purpose of understanding the mechanisms of deformation and fracture in polycrystalline metals, it is convenient to consider the grain boundary as an entity and to study its mechanical behavior without inquiring into its true nature.

Back in 1912, or earlier, Rosenhain[1] and others suggested that the grain boundaries in metals may be conceived as an intergranular amorphous cement. This assumption is based primarily on the facts that grain boundaries in a metal behave as if they are regions of strength at low temperature and high deformation rate but are regions of weakness at high temperature and low deformation rate. This is precisely the behavior of amorphous or viscous materials. The existence of an actual intergranular cement has been the subject of constant controversy. However, whether this is true or not, it is only necessary

* This research has been supported by the Office of Research and Inventions, U.S.N. (Contract No. N6ori-20-IV) since May 1, 1946.

[1] W. Rosenhain and D. Ewen, J. Inst. Metals 8, 149 (1912). Or see Jeffries and Archer, *The Science of Metals* (McGraw-Hill Book Company, New York, 1924), Chap. IV.

to consider that the grain boundaries behave as if they were viscous, having a coefficient of viscosity decreasing with an increase of temperature. Guided by such a picture, one may explain qualitatively many observed phenomena. A review of such explanations has been made recently by Zener.[2]

It can be easily seen that if the grain boundaries in metals behave in a viscous manner, the so-called anelastic effects, which are effects arising from the strain not being uniquely determined by the stress in the pre-plastic region, should be observed under proper experimental conditions. The measurement of anelastic effects offers, therefore, a powerful tool for the study of the mechanical behavior of grain boundaries in metals. Zener and his collaborators[3] have made a preliminary study of the viscous behavior of grain boundaries in zinc, alpha brass and alpha iron by measurements of internal friction and elastic after-effect. However, only qualitative information has thus far been obtained. The purpose of the present research program is to examine quantitatively the viscous behavior of the grain boundaries in metals and to make a systematic study of the effect of standard metallurgical variables upon this behavior with four types of anelastic measurements in torsion. They are: internal friction at low frequencies (a few cycles per second); variation of dynamic rigidity with temperature; creep under constant stress; and stress relaxation at constant strain.

EXPERIMENTAL METHODS OF MEASURING ANELASTIC EFFECTS

In the measurement of anelastic effects, the applied stress should be so small that the following conditions are fulfilled: (1) There should be no permanent set after the stress is removed and all the effects should be recoverable after a sufficiently long period of time; (2) The observed anelastic effects should be linear with the applied stress or prior strain. Thus the internal friction and the dynamic rigidity should be independent of the amplitude of vibration; the creep per unit elastic strain (or instantaneous strain) should be independent of the magnitude of the elastic strain; and the stress relaxation per unit initial stress should be independent of the magnitude of the initial stress. Such a linearity is necessary for a simple interpretation of the observed anelastic effects. Thus, if the grain boundaries in metals behave in a viscous manner, one can consider that a polycrystalline metal consists of a two-component system. One component behaves in a viscous manner, obeying the relation

$$\dot{e}=as+b\dot{s}, \tag{1}$$

where s is the shear stress component, e the shear strain, and a and b are constants independent of s, e, and $\dot{s}$. The other component is of a true elastic nature, obeying the relation

$$e=s/M, \tag{2}$$

where M is the elastic modulus. These two microscopic relations are linear in stress, strain, and their time derivatives. Therefore, according to the superposition principle, the macroscopic behavior of the metal specimen as a whole must also be linear in these variables.

The torsional method was chosen in the present investigation for the following reasons. (1) The torsional method can be conveniently used for the measurement of all the anelastic effects mentioned before. This renders an easier comparison and correlation between these effects. (2) The torsional method is much simpler experimentally than the other methods when the strain to be measured or the stress applied is very small. One objection to the torsional method is that the strain in the specimen is inhomogeneous. But this will have no consequence in the present problem if the effects observed can be shown to be linear with strain and stress. In all the following measurements, the experimental conditions were so regulated that this linearity has been checked and the discrepancy, if any, lies within the experimental error.

I. Measurement of Internal Friction and Rigidity

The internal friction and rigidity were determined by measuring, respectively, the logarithmic decrement and the frequency of the free torsional vibration of a wire specimen carrying a small

[2] C. Zener, Metals Technology (August, 1946).
[3] A. Barnes and C. Zener, Phys. Rev. 58, 87L (1940); C. Zener, D. Van Winkle, and H. Nielson, Trans. A.I.M.E. 147, 98 (1942); W. A. West, Metals Technology (August, 1946).

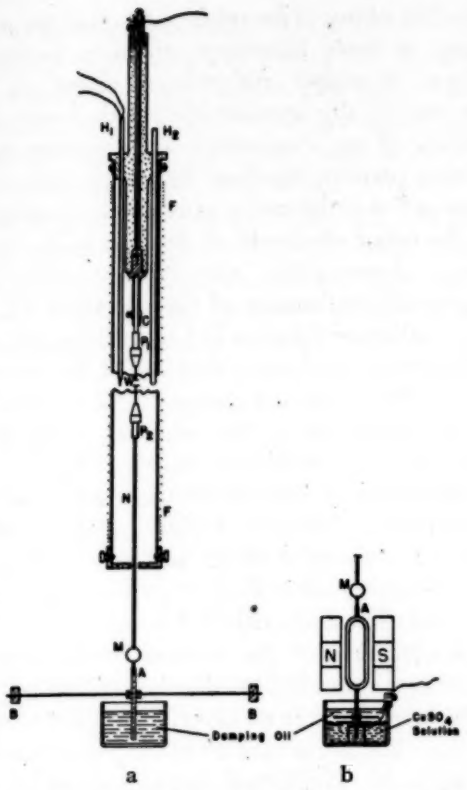

FIG. 1a. Apparatus for measuring internal friction and dynamic rigidity of wire specimen. 1b. Moving coil arrangement for measuring creep under constant stress and stress relaxation at constant strain of wire specimen.

torsional bar. The measure of internal friction herein adopted is the logarithmic decrement divided by π, (Q^{-1}). When the logarithmic decrement is small, the rigidity modulus G of the wire is proportional to the square of the frequency of vibration provided the length and radius of the wire are kept constant.

The arrangement for the measurement is diagrammatically shown in Fig. 1a. W is the test wire of 0.033″ diameter and 12″ length. P_1 and P_2 are two small steel pin vises, to which both ends of the wire are firmly clamped. The handle of the upper pin vise P_1 is clamped tightly inside a steel tubular chuck C. The top of the steel chuck is screwed into a cylindrical transite rod and cemented there rigidly with Insalute adhesive cement. This transite rod minimizes the loss of heat in the test wire outward through conduction. The top of the transite rod is enlarged to rest on the fringed top of the steel wall of an electric furnace as shown in the figure. It can be clamped to prevent rotation by a set of three screws in the furnace wall.

The lower pin vise P_2 is welded to a thick nichrome wire N (B & S gauge No. 12) which is a poor conductor of heat but has a much higher rigidity than the test wire at various temperatures. M is a concave mirror mounted on the nichrome wire. By means of this mirror, a beam of light passing through a narrow slit forms a sharp image on a translucent scale 3 meters away from the mirror. BB is a torsional bar about 8 inches long carrying at each end a cylindrical piece of iron. The total longitudinal load on the test wire, including the lower pin vise, nichrome rod, the mirror, and the torsional bar is about 30 g. An electromagnet is placed at a suitable distance from the iron weight, so that the torsional vibration can be started by tapping a key beside the scale while watching the deflection of the light on the scale. The lower end of the rod is attached to a thicker brass tube and this is dipped into a beaker containing thick machine oil, the depth of immersion being so adjusted that the lateral motion is critically damped. With such an arrangement, measurements can be taken immediately after the torsional vibration is started.

FF is an electrical resistance furnace. It consists of a thin seamless steel tube 1½″ in diameter and 28 inches long, wound with B & S gauge No. 18 nichrome wire. The turns were spaced more closely near both ends of the tube to obtain a uniform temperature along the axis of the furnace. The temperature does not vary more than 2°C over a length of 15 inches at 350°C and the test wire was always placed in this region of uniform temperature. Furthermore, since the ends of the test wire were effectively thermally insulated from outside, the temperature of the wire is uniform throughout its length. The lower end of the furnace was closed by a split transite cap having a central hole just large enough to permit the nichrome rod N to emerge from the furnace without contact.

The temperature was measured by means of a chromel p-alumel thermocouple inserted into the furnace through the hole H_1. The hole H_2 was used to insert short pieces of test wire inside a Pyrex glass tube to be taken out at desired times

for microscopic examination and other purposes. It was also occasionally used to lead a jet of nitrogen or inert gas into the furnace to prevent excessive oxidation of the test wire at high temperatures.

The usual method of timing was followed in measuring the period of vibration. The period of torsional vibration of the test wire was raised to about 1.2 seconds at room temperature by attaching the torsional bar *BB* as described above. Visual observations could therefore be easily made. The logarithmic decrement was determined by observing the consecutive amplitudes of vibration for a suitable length of time. In all the measurements at all temperatures, the maximum amplitude of vibration (on a scale 3 meters away from the mirror) used was less than 8 cm. With a test wire of 0.033″ diameter and 12″ long, this amplitude corresponds to a maximum shearing strain on the surface of the test wire of 2×10^{-5}. When the consecutive amplitudes were plotted on a semi-logarithmic paper against the ordinal number of vibrations, a straight line has always been obtained indicating that, under the experimental conditions used, the logarithmic decrement is independent of the amplitude of oscillation.

II. Measurement of Creep under Constant Stress and Stress Relaxation at Constant Strain

A simple technique has been devised for both kinds of measurements by utilizing the principle of a moving coil galvanometer. The test wire to be examined forms the suspension of a moving coil galvanometer. Since experiments are only conducted at a low stress level, the current passing through the galvanometer is a measure of the shear stress acting on the test wire, the deflection of the galvanometer is a measure of the shear strain. The apparatus used is the same as that used for the measurement of internal friction and rigidity, except that the torsional bar is unscrewed at *A* and a moving coil with appropriate damping arrangement is substituted. This is schematically shown in Fig. 1b. The moving coil was made by winding about 700 turns of B & S gauge No. 38 copper wire on an oval copper frame having average dimensions of $\frac{3}{4}\times2\frac{3}{8}$ inches. The total resistance of the coil is about 150 ohms. The permanent magnet used consists of three horseshoe magnets mounted together. A copper rod was attached to the lower end of the moving coil. This forms one electrode of an electrolytic coil serving as a rotatable current junction. The electrolyte used for the cell is saturated copper sulphate solution and the other electrode of the cell is a copper cylinder surrounding the copper rod. The damping to the torsion of the specimen by the copper sulphate solution is negligibly small and the change of internal resistance of the electrolytic cell due to the expansion of the test wire at high temperatures is also small in comparison with the total resistance in the circuit. The measurements at different temperatures can thus be compared without worrying about the effect due to the expansion of the test wire. A layer of heavy machine oil is floated on the copper sulphate solution and critical damping of the torsional vibration of the system is obtained by attaching a cross bar to the copper rod so that it is immersed in the oil layer. The orientation of the cross bar is parallel to the plane of the observing scale. The lateral motion parallel to the scale is also critically damped by such an arrangement. The total longitudinal load on the wire, including the moving coil and the damping arrangement, is about 30 g.

In the measurement of creep under constant stress, a constant torque was applied and the creep was recorded visually. Measurements can be started one second after the torque is applied. In the measurement of stress relaxation at constant strain, the current through the galvanometer coil was reduced by increasing the resistance in the circuit so as to maintain a constant deflection.

ANELASTIC EFFECTS IN POLYCRYSTALLINE ALUMINUM

In the study of the mechanical behavior of grain boundaries in metals by measurement of anelastic effects, it is of paramount importance that the measurement is done under controlled conditions so that the effects attributable to the grain boundaries can be observed and can be separated from those attributable to other reasons. It is thus desirable to start the investigation with pure metals to avoid possible

effects due to impurities. Aluminum was chosen as the principal working metal for the present investigation for the following reasons: (1) The so-called temperature of recrystallization of aluminum is relatively low, and controllable grain size can be obtained by annealing at moderately low temperatures. (2) Aluminum possesses a high elastic isotropy and thus the mechanical behavior will not change appreciably even if there is a change of crystal orientation during measurement.

I. Internal Friction

The 99.991 percent aluminum was kindly supplied by the Aluminum Company of America in the form of ingots. A piece of about one cubic inch was cut from the ingot without remelting and this was swaged into rods in the Metallurgy Section of this Institute. The rod having a diameter of about 0.15 inch was annealed at 500°C for one hour. This annealed rod was then cold-worked by drawing successively through the holes of a drawing plate always along the same direction to a final size of about 0.033″ diameter without intermediate annealing. This corresponds to a cold work of about 95 percent reduction in area (95 percent RA). After being straightened by pulling, the wire was mounted between the two pin vises shown in Fig. 1a, so that the portion between the two pin vises was exactly 12 inches long. The whole suspension system (except the inertia bar) was fed into the furnace through the top of the furnace, the axis of which was adjusted to be exactly vertical. The inertia bar was then slipped underneath and screwed tight to the damping pin. The wire was annealed in the furnace at 450°C for five hours for stress relief and to give a comparatively stable grain size. The logarithmic decrement and rigidity were determined at and below 450°C down to room temperature and then again from room temperature up to 450°C. The wire was examined microscopically (etched with 0.2 percent hydrofluoric acid) after the measurement and was found to be recrystallized into rather uniform grains having an average grain diameter of about 0.03 cm. A short piece of aluminum wire was placed in a Pyrex glass tube fed into the furnace through the hole H_2 to receive the same heat treatment as the test specimen except that no longitudinal load was applied during annealing. It gave recrystallized grains having the same size as the test specimen.

The variation of internal friction in polycrystalline aluminum with temperature is shown in Fig. 2. The frequency of vibration used is about 0.8 cycle per second at room temperature. It is seen that the internal friction reaches a maximum at a temperature of about 285°C and has a maximum value of about 0.09. The existence of a maximum is just what was expected, accepting the concept of a viscous grain boundary. The internal friction is determined by the product of the distance slipped and the resistance to slip along the grain boundaries. At low temperatures, the viscous slip along the grain boundaries is small and therefore the internal friction is small. At high temperatures, the resistance to slip along the grain boundaries is small, so again the internal friction is small. Only in an intermediate temperature range, when both the slip distance and the resistance to slip are appreciable, will the internal friction be appreciable.

In order to show that this effect observed in thoroughly annealed polycrystalline aluminum has its origin at the grain boundaries rather than in the interior of the grains, the internal friction of a "single-crystal" wire of commercially pure aluminum, consisting at most of a few grains in a wire one foot long, was measured at temperatures up to 450°C. This is also shown in Fig. 2. It is small over the whole temperature range but increases slightly at higher temperatures. However, there is definitely no maximum at around 285°C as in the case of polycrystalline aluminum. Further experiments have shown that the slow increase in internal friction in "single-crystal" aluminum may be due to the handling of the "single-crystal" wire. As the wire was first prepared in an annealing furnace and then mounted between the two pin vises, it is unavoidable that a certain amount of cold work was introduced during the manipulation.

If the internal friction observed in polycrystalline aluminum is entirely due to the viscous slip along the grain boundaries, the internal friction should decrease continuously at high

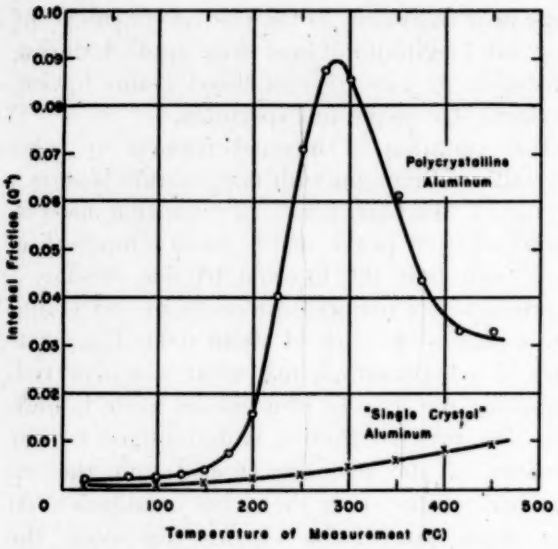

FIG. 2. Variation of internal friction with temperature in polycrystalline and "single crystal" aluminum (frequency of vibration = 0.8 cycles per second at room temperature).

temperatures once the maximum is over. However, as can be seen in Fig. 2, the internal friction did not decrease as rapidly as expected at high temperatures. It has been found that the high temperature side of the internal friction curve is quite sensitive to the amount of pre-anneal cold work, indicating that some other effects connected with the cold work come in at very high temperatures.

Another factor to be considered is the possible effect of the longitudinal load on the wire, which is about 30 g. Since the diameter of the wire is 0.033 inch, this corresponds to a stress of about 94 pounds per square inch. It has been found that the internal friction shown in Fig. 2 remains approximately the same when a longitudinal load three times as large was used, as long as the applied stress is sufficiently low so that the internal friction is independent of the stress levels. The frequency of vibration was, of course, kept the same in both cases.

In summary, it is obvious that the internal friction observed in polycrystalline aluminum as described above cannot be ascribed to thermoelastic origin, because it is very much larger than the internal friction attributable to thermal diffusion.[4] It cannot be ascribed to the self-diffusion in aluminum, as this internal friction observed does not occur in single crystal aluminum. It cannot be due to the diffusion of impurities along the grain boundaries, since the internal friction in less pure (99.2 percent) aluminum has been found to be smaller under similar conditions. Also it is unlikely to be due to the effect of crystal growth, because reasonable stable grains have been obtained by annealing the wires 5 hours at 450°C, and no grain growth can be detected during the time of a single measurement which takes only about ½ minute. It seems thus to be justifiable to say that the internal friction observed in thoroughly annealed polycrystalline, but not in single-crystal aluminum, has its origin at the grain boundaries.

II. Modulus of Rigidity

The rigidity of a thoroughly annealed aluminum wire (95 percent RA, 450°C anneal for 5 hours) was determined simultaneously with the measurement of internal friction. As before, the frequency of vibration is about 0.8 cycle per second at room temperature. The variation of rigidity is shown in Fig. 3,* as has been briefly reported before.[5] It is seen from Fig. 3 that the rigidity curve is essentially a straight line at low temperatures, and there is a rapid change in curvature around 200°C. This rapid change was not observed in single-crystal aluminum wire, indicating that the observed rapid decrease of rigidity of thoroughly annealed metals at high temperatures is due to viscous slip along grain boundaries.

Since there is no grain boundary in a single crystal, the rigidity curve of single-crystal aluminum can be considered as the unrelaxed rigidity G_U. Let $G(T)$ be the rigidity in polycrystalline aluminum at the temperature T, then we have

$$G(T)/G_U = (f_p/f_s)^2, \tag{3}$$

[4] C. Zener, Phys. Rev. **53**, 90 (1938).

* Actually, the curves shown in Fig. 3 are f^2-temperature curves, where f is the frequency of vibration. These curves are somewhat different from the G-temperature curves because the length and diameter of the wire change somewhat with temperature and therefore G is not strictly proportional to f^2. However, the error thus introduced will not affect the general shape of the curves and thus the f^2-temperature curve can be taken as G-temperature curve in qualitative discussions.

[5] T. S. Kê, Phys. Rev. **70**, 105A (1946).

where f_p and f_s are, respectively, the frequency of vibration in polycrystalline and single-crystal aluminum at the temperature T. The ratio $G(T)/G_U$ is plotted as a function of the temperature of measurement in Fig. 4. It is seen that the ratio is about unity at temperatures below 200°C, drops suddenly therafter, and approaches a constant value of about 0.67, or less, at high temperatures. As a first approximation, we have $G_R/G_U=0.67$, where G_R is the relaxed rigidity. The fractional amount of the total shearing stress that can be relaxed across the grain boundaries can thus be taken as $1-0.67$, or 0.33.

"If the individual grains are essentially equiaxed, and the grain size distribution is uniform, it is anticipated that only a fraction of the overall stress can be relaxed by grain boundary slip. The situation is analogous to the case of a jig saw puzzle where the over-all configuration possesses rigidity in spite of the fact that no shearing stress exists between adjacent pieces." With such a picture in mind, a formula has been arrived at theoretically by Zener by strain energy consideration for the case of equiaxed grains of uniform size, that[6]

$$E_R/E_U=\tfrac{1}{2}(7+5\sigma)/(7+\sigma-5\sigma^2), \qquad (4)$$

where E_R is the Young's modulus of a polycrystalline specimen in the case where the grain boundaries are slippery and the relaxation of shearing stress across the grain boundaries has been complete, E_U is the Young's modulus where no slip occurs across the grain boundaries, and σ

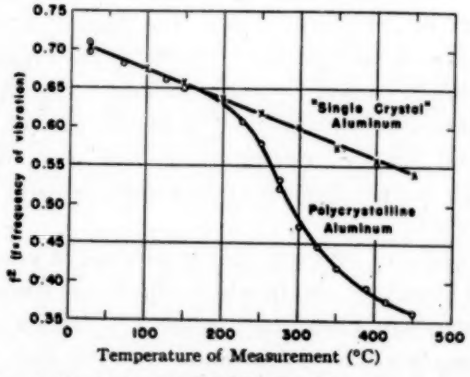

FIG. 3. Variation of "rigidity" with temperature in polycrystalline and "single-crystal" aluminum.

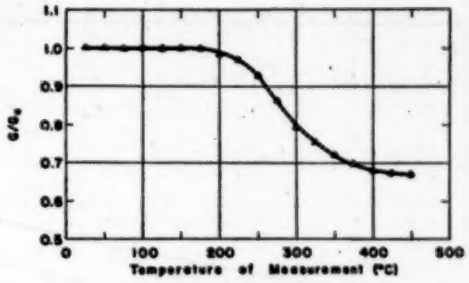

FIG. 4. Relaxation of rigidity in polycrystalline aluminum.

is the Poisson's ratio. The corresponding ratio in rigidity moduli, G_R/G_U, can be shown to be

$$G_R/G_U=2(7+5\sigma)/5(7-4\sigma). \qquad (5)$$

According to Birch,[7] the Poisson's ratio for aluminum (commercial) is 0.355 at 30°C, thus we have

$$G_R/G_U=0.636.$$

This is in good agreement with the experimental value which is about 0.67 as indicated in Fig. 4.

III. Creep at Constant Stress

The viscous grain boundary slip in metals will lead to the relaxation of shearing stress across the grain boundaries and this relaxation will cause an over-all slow yielding or creep of the metal when the applied stress is kept constant. The creep measurement at low stress levels will thus give direct information as to the viscous behavior of the grain boundaries.

The aluminum wire to be examined forms the suspension of a moving coil galvanometer as has been described above. The deflection of the specimen has been found to be proportional to the current passing through the coil when the deflection is small. In all measurements, the maximum deflection used was kept less than 8 cm on a scale 3 meters away from the mirror. This corresponds to a maximum shearing strain on the surface of the test wire of 2×10^{-3}, as has been mentioned above. The creep at the time t is measured by the ratio d_t/d_0 where d_t is the deflection at time t and d_0 the "instantaneous" deflection at $t=0$ when the constant torque was suddenly applied. In the case of single-crystal aluminum wire (99.2 percent pure), there is no

[6] C. Zener, Phys. Rev. 60, 906 (1941).

[7] F. Birch, J. App. Phys. 8, 129 (1937).

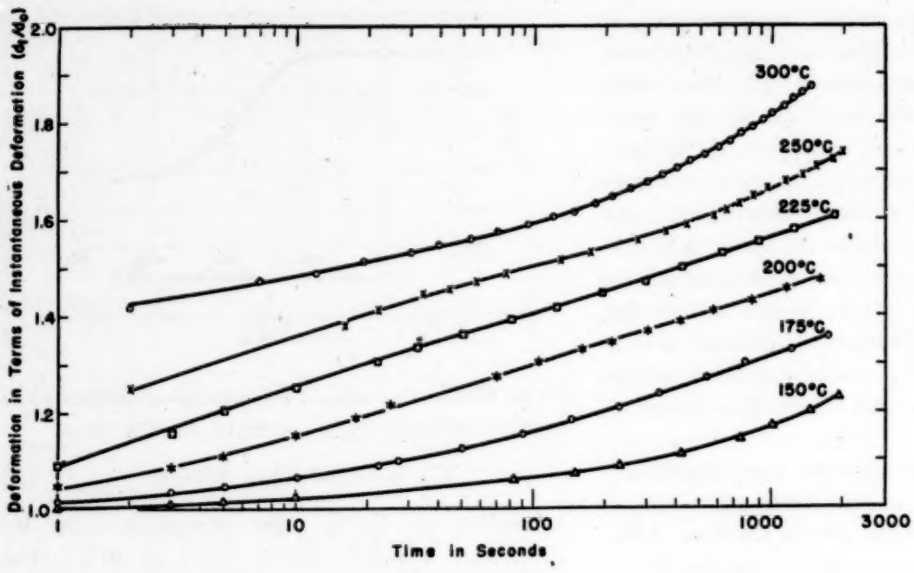

FIG. 5. Creep under constant stress at various temperatures in polycrystalline aluminum.

appreciable creep up to a temperature of about 350°C. This corroborates the viewpoint that the creep observed in polycrystalline aluminum is due to the viscous slip along the grain boundaries.

The creep curves of a 99.991 percent aluminum wire (95 percent RA, 450°C anneal for 5 hours) measured at various temperatures are shown in Fig. 5, in which d_t/d_0 is plotted against logarithm of time. The constant current used to furnish the torque was 1.5 ma in all the measurements. It can be seen that d_t/d_0 increases as a rule with both temperature and time of observation. In order to find if there is a time-temperature relation for the observed creep, let us assume that there is a heat of activation associated with this creep. Then we can express the creep as a function of time and temperature through the heat of activation H:

$$(d_t/d_0) = Af[t \exp(-H/RT)], \qquad (6)$$

where R is the gas constant, T the absolute temperature, and A a constant independent of t and T. If, now, we observe the time required to reach the same d_t/d_0 at different temperatures, then the derivative of d_t/d_0 with respect to $1/T$ is zero, whence we get

$$\frac{d \log_{10} t}{d(1/T)} = \frac{H}{2.3R}. \qquad (7)$$

If such a relationship holds true for all values of d_t/d_0, then the straight lines corresponding to different d_t/d_0 should be all parallel. This has been found to be the case and the average slope is 7400. This gives a heat of activation of 34,000 calories per mole. A composite curve is thus obtained as shown in Fig. 6. It is seen from Figs. 5 and 6 that the creep has a tendency to flatten out when the value of d_t/d_0 is about 1.5, indicating that this is about the limiting value of the over-all creep caused by the viscous slip along the grain boundaries. Further slip along the grain boundaries is probably hindered by the interlocking of the corners between adjacent grains.

The creep curves in Fig. 5 indicate that another effect comes in at higher temperatures. The creep curves at 250°C and higher do not remain constant as they should if the creep is completely caused by grain boundary slip. With the same kind of reasoning as for the case of the internal friction measurement, this new effect at high temperatures may be connected with the cold work.

In order to corroborate the concept of viscous grain boundary slip in which all the microscopic relations are linear with respect to strain and stress, tests have been made showing that the observed creep attributed to grain boundary slip is recoverable (Fig. 7) and d_t/d_0 is independent of the applied stress and prior strain.

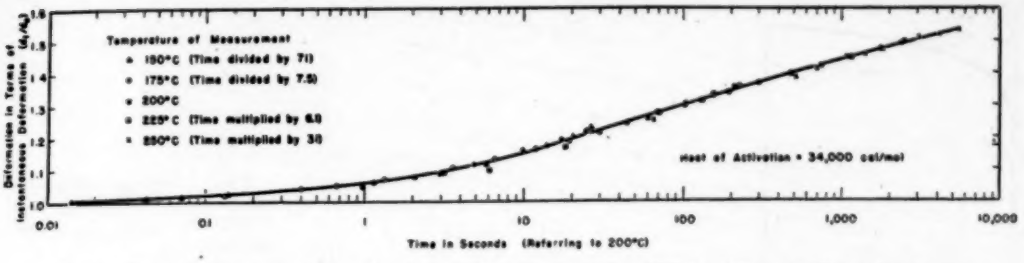
Temperature of Measurement
• 150°C (Time divided by 71)
• 175°C (Time divided by 7.5)
• 200°C
• 225°C (Time multiplied by 6.8
• 250°C (Time multiplied by 36
Heat of Activation = 34,000 cal/mol
Deformation in Terms of Instantaneous Deformation
Time in Seconds (Referring to 200°C)

FIG. 6. Composite curve of creep under constant stress at 200°C in polycrystalline aluminum.

IV. Stress Relaxation at Constant Strain

As the torque applied to the specimen is proportional to the current passing through the moving coil, the stress (in terms of the initial stress) at the time t required to keep the specimen at a constant strain is measured by the ratio i_t/i_0, where i_t is the current at time t and i_0 is the initial current at $t=0$. As expected, no appreciable stress relaxation occurs in single-crystal aluminum. The stress relaxation curves of a 99.991 percent aluminum wire (95 percent RA, 450°C anneal for 5 hours) measured at various temperatures are shown in Fig. 8, in which i_t/i_0 is plotted against logarithm of time. The constant deflection maintained in all the measurements was 4 cm. This corresponds to a maximum shearing strain of 10^{-5}.

The heat of activation associated with the observed stress relaxation was determined in a similar manner as has been done in the creep measurements. This is done by finding from the curves in Fig. 8, the time required to reach a given i_t/i_0 at different temperatures and then plotting $\log_{10}t$ against $1/T$. Several d_t/d_0's were picked out and a curve was plotted for each d_t/d_0. These lines have been found to be all parallel. The average slope of these lines is found to be 7500, giving a heat of activation of 34,500 calories/mole, which is very close to that obtained in creep measurements.

It can be seen from Fig. 8 that the stress relaxation has almost been completed after one hour at 225°C, giving an asymptotic value of $i_t/i_0=0.67$. However, at still higher temperatures, the stress starts to relax again, indicating that a new effect enters. This may be connected with the cold work. The composite stress relaxation curve, taking the time at 200°C as unity, is shown in Fig. 9. This common curve tells the complete story of the stress relaxation associated with the grain boundary slip.

BOLTZMANN'S SUPERPOSITION PRINCIPLE AND THE INTER-RELATION BETWEEN VARIOUS ANELASTIC EFFECTS[8]

In order to generalize Hooke's law so that the elastic after-effect can be interpreted, Boltzmann[9] assumed that the fundamental relations between stress and strain are linear in stress and strain and in their time derivatives. The solutions then satisfy the superposition principle. This allowed Boltzmann to consider that the strain is a function also of the past history of the stress. The deformation at any instant can be considered thus as the result of a continuous series of constant forces previously applied. Using the superposition principle as a tool, Boltzmann was able to fit into a precise mathematical formulation all previously observed elastic after-effects and related phenomena. However, the relations derived are valid only when the elastic after-effect and related effects are small. A set of relations was recently derived by Zener[10] which holds independent of the magnitude of the observed effects. The relations correlating the four anelastic effects observed in the present research are as follows:

(1) Between stress relaxation at constant strain and creep under constant stress:

$$\delta(t)f(t)=1+\int_0^t\{\delta(t)-\delta(t-t')\}f(t')dt', \quad (8)$$

where $\delta(t)$ is the creep function and is defined as

[8] T. S. Kê, Phys. Rev. **71**, 142A (1947).
[9] L. Boltzmann, Ann. d. Physik **7**, 624 (1876).
[10] C. Zener, private communication. The detailed derivation of these relations will occur in "Elasticity and Anelasticity of Metals," Institute for the Study of Metals Monograph Series, The University of Chicago Press. In preparation.

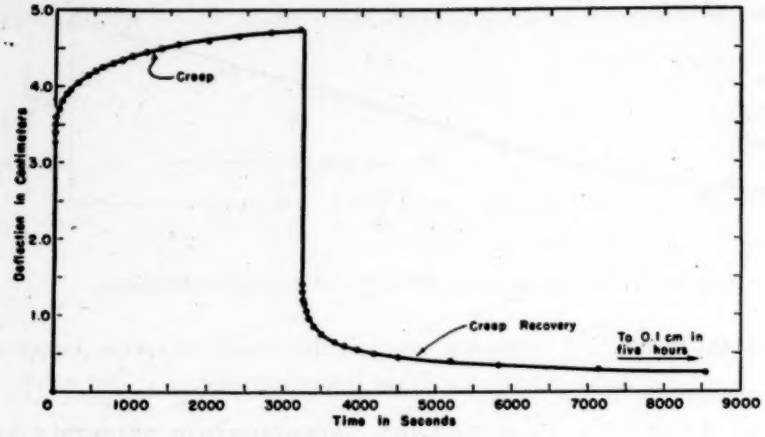

FIG. 7. Creep under constant stress and creep recovery at 175°C in polycrystalline aluminum.

the deformation at the time t when a constant force of magnitude unity was suddenly applied at $t=0$; $f(t)$ is the stress function and is defined as the force which must be applied at the time t in order to keep the deformation at a constant value of unity suddenly applied at $t=0$.

(2) Between dynamic modulus and stress function:

$$M(\omega)=f(t)_{t\cong P/8}, \tag{9}$$

where ω is the angular frequency and P the period of oscillation.

(3) Between internal friction Q^{-1} and stress function:

$$Q^{-1}(\omega)=-(\pi/2)(d\ \ln f/d\ \ln t)_{t\cong P/8}. \tag{10}$$

Now, these relations are derived on the basis of Boltzmann's superposition principle. If they can be experimentally verified and if we can demonstrate that all the effects observed are linear with respect to stress and strain and their time derivatives, then the microscopic relations stated in Eqs. (1) and (2) are adequate. Let us now proceed to compare Eqs. (8), (9), and (10) with experimental data.

I. Dynamic Rigidity and Stress Relaxation at Constant Strain

The relation between dynamic rigidity and stress function is given by

$$G(\omega)=f(t)_{t\cong P/8}.$$

Now, at a constant deformation D, the stress function is

$$f(t)=F(t)/D,$$

where $F(t)$ is the force applied at the time t. In terms of the quantities actually measured in the experiment, we have

$$f(t)=G_U(i_t/i_0),$$

and thus

$$G(P)/G_U=(i_t/i_0)_{t\cong P/8} \tag{11}$$

at a given temperature.

Now consider the case at 200°C. G/G_U at 200°C is, from Fig. 4, 0.985. The period of oscillation at 200°C is 1.26 sec.* Thus from Eq. (11), we obtain $i_t/i_0=0.985$ when $t=\frac{1}{8}(1.26)=0.16$ sec.

Let the conversion factor for converting the time scale at a temperature T to that of 200°C be τ_T, then it can be shown that

$$\log_{10}\tau_T=7500(1/473-1/T). \tag{12}$$

The conversion factors so calculated are summarized in the third column of Table I, from which we can calculate the value of t when $i_t/i_0=G/G_U$. The calculated values of i_t/i_0 in Table I are plotted against the corresponding value of t in the fifth column. These are shown by circles in Fig. 10, where the observed stress relaxation curve, the solid curve, is included for comparison.

II. Internal Friction and Stress Relaxation at Constant Strain

The relation between internal friction and stress relaxation at constant strain is shown in

* This is obtained from the f^2 curve for polycrystalline aluminum in Fig. 3.

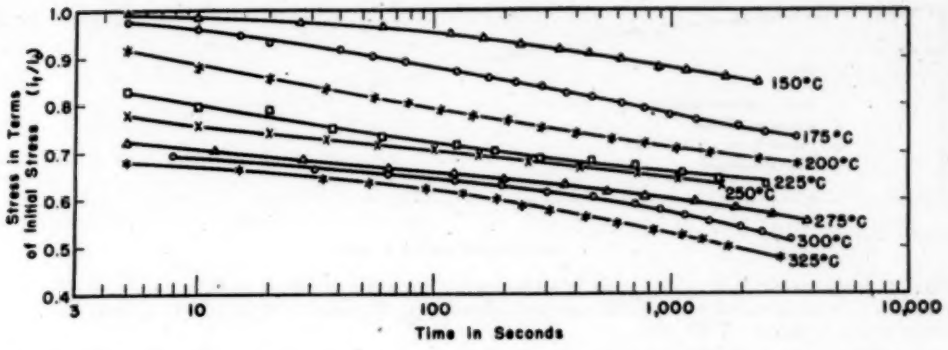

FIG. 8. Stress relaxation at constant strain at various temperatures in polycrystalline aluminum.

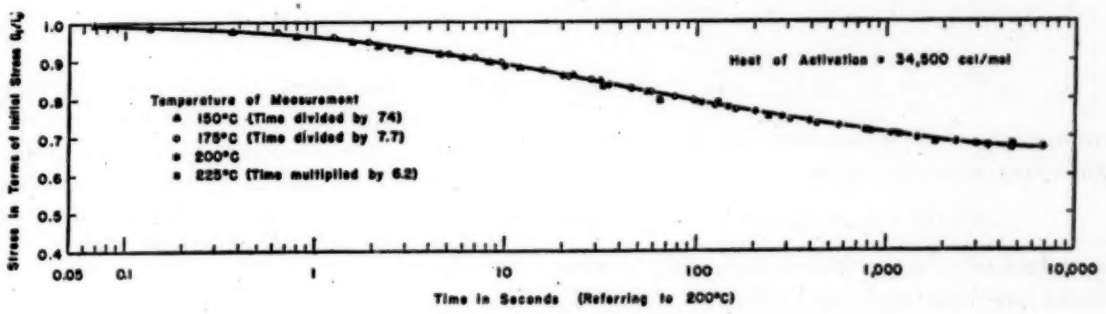

FIG. 9. Composite curve of stress relaxation at constant strain at 200°C in polycrystalline aluminum.

Eq. (10). We have as before,

$$f(t) = G_U(i_t/i_0).$$

Now

$$d\ln f(t) = d\ln G_U(i_t/i_0),$$

hence at a given temperature, we have

$$Q^{-1}(P) = -(\pi/2)\{d\ln(i_t/i_0)/d\ln t\}_{t\cong P/8},$$

because G_U is independent of t at a given temperature. Making use of the time-temperature relation

$$d\ln t/d(1/T) = H/R,$$

we have on integrating and taking the lower temperature limit $T_1 = 200°C$, at which $i_t/i_0 = 0.985$ which is very close to unity,

$$\ln(i_t/i_0) = -0.0092 - 11{,}000\int_{200°C}^{T} Q^{-1}(T)d(1/T). \tag{13}$$

In order to evaluate the integral on the right-hand side, the internal friction is plotted against $1/T$. The values of i_t/i_0 calculated are shown in Table II.

The calculated values of i_t/i_0 in Table II are plotted against the corresponding values of t in the fourth column (from Table I). These are shown by crosses in Fig. 10. The observed values of i_t/i_0 listed in Table II are obtained from the composite stress relaxation curve shown in Fig. 9.

III. Creep Under Constant Stress and Stress Relaxation at Constant Strain

The relation between stress relaxation at constant strain and creep under constant stress is shown by Eq. (8). Now $\delta(t) - \delta(t-t')$ is always positive and $f(t')$ is always negative, therefore the integral at the right-hand side is always negative and we have

$$\delta(t)f(t) \leqq 1. \tag{14}$$

It can be shown that the value of the integral is usually much smaller than unity unless the relaxation is complete within a short interval of time as in the case when there is only one single

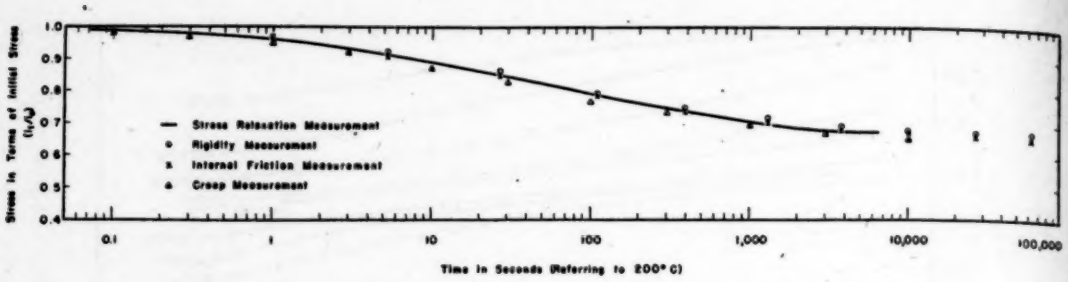

FIG. 10. Stress relaxation across grain boundaries in aluminum at 200°C as determined by four types of anelastic effect measurements (99.991 percent aluminum, 95 percent RA, 450°C anneal for 5 hours; average grain diameter = 0.03 cm).

time of relaxation. In our present case, therefore, we can consider that $\delta(t)f(t)=1$. Now, we have

$$\delta(t)=D(t)/F=D(t)/MD(0),$$
$$f(t)=F(t)/D=MF(t)/F(0). \quad (15)$$

Thus in terms of the quantities actually observed in the experiment, we have

$$\delta(t)f(t)=d_t/d_0\cdot i_t/i_0=1. \quad (16)$$

The values of i_t/i_0 calculated according to this formula are tabulated in Table III. The calculated values of i_t/i_0 in Table III are plotted against the corresponding values of t. These are shown by triangles in Fig. 10.

COEFFICIENT OF VISCOSITY OF GRAIN BOUNDARIES IN ALUMINUM

Having obtained a self-consistent picture that the grain boundaries in polycrystalline aluminum behave in a viscous manner, we are now in a position to compute or, at least, to estimate this coefficient of viscosity and its variation with temperature. Consider a grain boundary with an effective thickness d. Then the coefficient of viscosity may be defined by

$$\eta=s/(v/d), \quad (17)$$

where s is the shearing stress and v is the rate of relative displacement of the two sides of the boundary. Take the case of equiaxed grains as shown in Fig. 11. Let Δx be the distance slipped along the grain boundary during the time τ where τ is the time of relaxation, then

$$v\cong\Delta x/\tau.$$

TABLE I. Conversion table from rigidity relaxation to stress relaxation at 200°C

T (°C)	T (°K)	τ_T	P_T (sec.)	$t=\tau_T P_T/8$ (sec.)	i_t/i_0 (calc.)	i_t/i_0 (obs.)
175	448	1.23×10^{-1}	1.25	1.9×10^{-2}	1.00	——
200	473	1.00	1.26	1.6×10^{-1}	0.985	0.99
225	498	6.25	1.28	1.0	0.97	0.96
250	523	3.23×10	1.32	5.3	0.925	0.915
275	548	1.48×10^{2}	1.38	2.6×10	0.865	0.85
300	573	5.82×10^{2}	1.45	1.1×10^{2}	0.795	0.79
325	598	2.06×10^{3}	1.50	3.9×10^{2}	0.75	0.735
350	623	6.55×10^{3}	1.55	1.3×10^{3}	0.72	0.70
375	648	1.91×10^{4}	1.59	3.8×10^{3}	0.70	0.69
400	673	5.10×10^{4}	1.62	1.0×10^{4}	0.68	——
425	698	1.32×10^{5}	1.65	2.7×10^{4}	0.675	——
450	723	3.02×10^{5}	1.67	6.3×10^{4}	0.67	——

TABLE II. Conversion table from internal friction to stress relaxation at 200°C

T(°C)	Q^{-1}	$\int_{200°C}^{T} Q^{-1}(T)d(1/T)$	t (sec.)	i_t/i_0 (calc.)	i_t/i_0 (obs.)
225	0.040	249×10^{-8}	1.0	0.965	0.96
250	0.071	758×10^{-8}	5.3	0.91	0.915
275	0.088	1368×10^{-8}	2.6×10	0.85	0.85
300	0.086	2053×10^{-8}	1.1×10^{2}	0.79	0.79
325	0.071	2647×10^{-8}	3.9×10^{2}	0.74	0.735
350	0.057	3004×10^{-8}	1.3×10^{3}	0.71	0.70
375	0.044	3327×10^{-8}	3.8×10^{3}	0.685	0.69
400	0.036	3508×10^{-8}	1.0×10^{4}	0.675	——
425	0.032	3697×10^{-8}	2.7×10^{4}	0.66	——
450	0.032	3842×10^{-8}	6.3×10^{4}	0.65	——

TABLE III. Conversion table from creep under constant stress at 200°C to stress relaxation at constant strain at 200°C.

t (sec.)	d_t/d_0	i_t/i_0 (calc.)	i_t/i_0 (obs.)
0.1	1.02	0.98	0.99
0.3	1.03	0.97	0.98
1	1.06	0.95	0.96
3	1.09	0.92	0.93
10	1.15	0.87	0.89
30	1.22	0.82	0.84
100	1.30	0.77	0.79
300	1.36	0.74	0.76
1000	1.44	0.70	0.71
3000	1.50	0.67	0.68

The strain is given by

$$e \cong \Delta x/AB,$$

where AB is the length of one side of the grain and is approximately equal to the average grain diameter ($G.S.$). Consider the region in the immediate vicinity of the boundary, we have

$$e = s/G_U,$$

where G_U is the unrelaxed rigidity. As these two strains must be equal, we get

$$\Delta x/(G.S.) = s/G_U,$$

and thus

$$v \cong s(G.S.)/G_U\tau,$$

whence we may estimate η from the following formula,

$$\eta = G_U\tau d/(G.S.). \quad (18)$$

We shall now estimate the coefficient of viscosity at 285°C where the internal friction is a maximum. The rigidity G_U of aluminum at room temperature is about 2.4×10^{11} dynes/cm². From Fig. 3 it can be shown that the rigidity G_U at 285°C is about 2.0×10^{11} dynes/cm². The average grain diameter of the aluminum wire used in the present study is about 0.03 cm. The thickness of the grain boundary is not known from experimental work. However, it is known that the forces between atoms in solids are of short range type, extending with appreciable intensity only over a few atomic distances.[11] In our present estimation, it is reasonable to consider d as of the order of magnitude of one atomic distance; thus for aluminum, we can take $d \cong 4$A. Thus we have

TABLE IV. Estimated coefficient of viscosity of grain boundaries in aluminum as a function of temperature.

T (°C)	T (°K)	G_U (dynes/cm²)	η (poise)
25	298	2.4×10^{11}	2.2×10^{16}
100	373	2.3×10^{11}	2.1×10^{11}
200	473	2.1×10^{11}	1.3×10^{7}
285	558	2.0×10^{11}	4.8×10^{4}
350	623	1.9×10^{11}	2.0×10^{3}
450	723	1.8×10^{11}	43.0
550	823	1.7×10^{11}	2.2
660	933	1.5×10^{11}	0.18
670	943	1.5×10^{11}	0.14

[11] See F. Seitz, *The Physics of Metals* (McGraw-Hill Book Co., New York, 1943), p. 108.

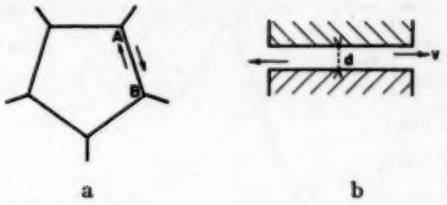

a b

FIG. 11a. Equiaxed grains. 11b. Viscous slip along grain boundary.

have

$$\eta_{285°C} = 2.7\times10^{5}\tau_{285°C}. \quad (19)$$

The natural period of oscillation at 285°C is 1.4 second. This is the period at which the internal friction is a maximum, when the time of relaxation τ associated with the grain boundary slip is comparable with the period of oscillation. Now we may consider that

$$\tau_{285°C} = P/8 = 0.18 \text{ sec.}, \quad (20)$$

thus

$$\eta_{285°C} = 4.8\times10^{4} \text{ poise}. \quad (21)$$

The temperature dependence of τ can be determined through the heat of activation H. Thus we have

$$\tau_T \exp(-H/RT) = k, \quad (22)$$

where $H = 34{,}500$ calories/mole, and k is a constant which can be determined by the condition that at 285°C, $\tau = 0.18$ sec., thus

$$\tau_T = 9.2\times10^{-15}\exp(H/RT) \quad (23)$$

and

$$\eta_T = 1.2\times10^{-20}G_U \exp(17{,}250/T). \quad (24)$$

The values of η at different temperatures calculated according to this formula are shown in Table IV. It is seen that the coefficient of viscosity at the melting point of aluminum, 659.7°C, is 0.18 poise. And at 670°C, the coefficient of viscosity is 0.14 poise. This is of the same order of magnitude as the coefficient of viscosity of molten aluminum determined experimentally by Polyak and Sergee,[12] which has a value of 0.065 poise at 670°C.

CONCLUDING REMARKS

It is shown above that the four types of anelastic effects observed in polycrystalline

[12] E. V. Polyak and S. V. Sergee, Comptes rendus Acad. Sci. U.S.S.R. **30**, 137 (1941).

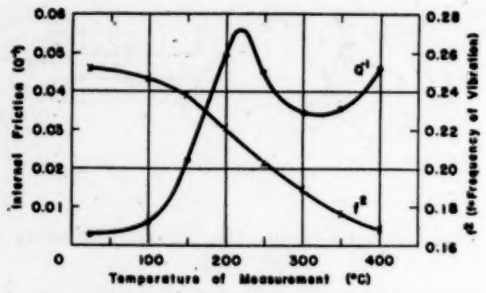

FIG. 12. Variation of internal friction and rigidity in polycrystalline magnesium (frequency of vibration = 0.5 cycles per second at room temperature).

aluminum have their origin at the grain boundaries. These effects are linear with respect to stress and strain and satisfy the inter-relations derived on the basis of the superposition principle within experimental error. We can infer that the microscopic mechanism causing these effects should obey relations which are linear in stress and strain components. The proposed microscopic mechanism is that the grain boundaries in metals behave in a viscous manner. The microscopic relations concerned with such a microscopic mechanism are linear in stress, strain, and their time derivatives.

The concept of a viscous grain boundary is quantitatively substantiated by the following findings:

(1) The maximum amount of shearing stress relaxation is polycrystalline determined by the four types of anelastic measurements is about 33 percent. This is in good agreement with the theoretical value of 36 percent calculated by assuming the grain boundary to be viscous.

(2) The estimated value of the coefficient of viscosity for the grain boundary is of the same order of magnitude as the experimentally determined value of the molten metal at the same temperature.

In order to show that the anelastic effects reported above are not peculiar to polycrystalline aluminum, similar measurements have been done for polycrystalline magnesium. The 99.97 percent magnesium used in the investigation was kindly supplied by the Dow Chemical Company in $\frac{1}{8}$"-rod, extruded at a die temperature of 260°-282°C at a speed of 5 ft/min. The rod was annealed at 450°C for one hour. An average grain diameter of about 0.02 cm was obtained by such a heat treatment. The internal friction and dynamic rigidity of this rod were measured at and below 400°C down to room temperature. The apparatus used for measurement is similar to that shown in Fig. 1a, except that the clamps used for holding the specimen are more rigid and the rotational inertia of the torsional bar is much larger. The frequency of torsional vibration is, in the present case, about 0.5 cycle per second at room temperature. The variation of internal friction and rigidity with temperature is shown in Fig. 12. It is seen that these curves vary in a similar manner as in the corresponding case of aluminum, indicating that the viscous behavior of grain boundaries is common to all metals.

ACKNOWLEDGMENT

The author wishes to express his deep appreciation of the active interest taken in this problem by Dr. Clarence M. Zener, without whose stimulating suggestions and discussions this investigation could not have been carried out. Thanks are also due to Dr. Cyril S. Smith, Director of the Institute, for discussions on metallurgical problems and suggestions especially during the preparation of the manuscript. Acknowledgment for help is here made to almost every member of the Institute.

On the Momentum Operator in Wave Mechanics

AUREL WINTNER
Department of Mathematics, Johns Hopkins University, Baltimore, Maryland
(Received December 30, 1946)

A simple example shows that a standard tacit hypothesis concerning quadratic integrability in momentum space is not in general legitimate, if only quadratic integrability in configuration space is assumed. Inasmuch as only the latter assumption is justified, there arises the need for criteria which prevent the occurrence of this difficulty. Such a criterion is developed in terms of the qualitative behavior of the potential. The conditions on the potential are of such a nature as to be satisfied in all cases which seem to be reasonable.

1.

An eigenfunction, belonging to a "discrete" characteristic energy level, must be defined merely by the property that the square of the function has a finite integral over the configuration space. In fact, this, and nothing more than this, is needed for the normalization which makes the total probability involved equal to unity. On the other hand, certain considerations[1] belonging to the very foundations of wave mechanics imply that the gradient of the eigenfunction has the same property of quadratic integrability as the eigenfunction itself. In particular, there is a step in the foundations which depends on partial integrations,[2] and the latter assume that the momentum operator is of integrable square *because* the configuration operator has this property.

That this assumption, though indeed usually made tacitly, actually is hypothetical, is seen from the following counter-example: The one-dimensional wave equation

$$\phi''+(e^{2x}-\tfrac{1}{4})\phi=0, \quad (\phi'=d\phi/dx)$$

is readily verified to have the general solution

$$\phi(x)=c\exp[-\tfrac{1}{2}x+ie^{x}], \quad (c=a+ib).$$

This makes it clear that

$$\int_0^\infty |\phi(x)|^2dx<\infty,$$

(for every $a+ib=$const., so that the eigenvalue is multiple; this, however, is immaterial). But it is also clear that

$$\int_0^\infty |\phi'(x)|^2dx=\infty,$$

(unless $c=0$, i.e., $\phi(x)\equiv 0$). Naturally, the choice of a potential which, as the above $V(x)=-e^{2x}$, leads to this phenomenon of "high frequency," should be excluded for physical reasons. It remains, however, to prove that such a high frequency case is the *only* possibility contradicting the tacit assumption referred to above.

The purpose of this note is to prove[3] that there is no other exception to the standard hypothesis. In other words, the tacit assumption concerning the momentum operator is automatically satisfied if the potential is bounded away from infinity in *one* direction, namely, in the direction of the *hyperbolic* range, of the spectrum. This is the content of (III) below.

2.

Let f, g, ϕ be real-valued, continuous functions of position on the whole (x, y, z)-space. By solutions of the partial differential equation

$$\phi_{xx}+\phi_{yy}+\phi_{zz}+f(x, y, z)\phi=g(x, y, z)$$

will be meant only solutions $\phi(x, y, z)$ having continuous partial derivatives of the second order (including the derivatives ϕ_{xy}, ϕ_{yz}, ϕ_{zx}). Any of these functions will be called of class (L^2) if its square has a finite volume integral over the whole (x, y, z)-space.

[1] W. Pauli, *Handbuch der Physik*, 24_1 (Verlagsbuchhandlung Springer, Berlin, 1933), second edition, pp. 97 and 99.

[2] Reference 1, pp. 99–101 or, in a more involved context, E. Schrödinger, Ann. d. Physik [4], 79, 734–756 (1926).

[3] The proofs depend on appropriate adaptations of arguments used, in a paper to appear elsewhere, in the one-dimensional case, in which more complete, but of course less general, results can be obtained.

(I) *If f is a (continuous) bounded function of position on the (x, y, z)-space, a solution,*

$$\phi=\phi(x, y, z),$$

of the wave equation

$$\Delta\phi+f(x, y, z)\phi=0 \tag{1}$$

cannot be of class (L^2) unless $\nabla\phi$ also is of class (L^2).

It is understood that

$$\Delta\equiv\text{div grad}, \quad \nabla\equiv\text{grad}, \tag{2}$$

and that the vector $\nabla\phi$ is said to be of class (L^2) if $(\nabla\phi)^2$ is of class (L). Here $(\nabla\phi)^2$ denotes the square of the length of $\nabla\phi$. Thus, from (2),

$$\tfrac{1}{2}\Delta(\phi^2)=\phi\Delta\phi+(\nabla\phi)^2. \tag{3}$$

Since the assumptions of (I) imply that both ϕ and $\Delta\phi$ are of class (L^2), the assertion of (I) is contained in the following lemma, which has nothing to do with differential equations:

(II) *If a function, $\phi=\phi(x, y, z)$, has continuous derivatives of the second order, and if both ϕ and $\Delta\phi$ are of class (L^2), then $\nabla\phi$ also is of class (L^2).*

Remark. Since the functions of class (L^2) form a linear space, (II) implies that (I) remains true if Eq. (1) is replaced by

$$\Delta\phi+f(x, y, z)\phi=g(x, y, z), \tag{4}$$

where $g(x, y, z)$ is any (continuous), not necessarily bounded, function of class (L^2).

In order to prove (II), let $R=R_r$ denote the interior, and $S=S_r$ the boundary, of the sphere of radius r about $(x, y, z)=(0, 0, 0)$. Then if $\alpha(x, y, z)$ and $\beta(x, y, z)$ have continuous second derivatives, Green's formula gives

$$\int_R(\alpha\Delta\beta-\beta\Delta\alpha)dR=\int_S(\alpha\beta_r-\beta\alpha_r)dS, \tag{5}$$

since the direction of an exterior normal of S is that of increasing radius. If Eq. (5) is applied to

$$\alpha=\tfrac{1}{2}\phi^2, \quad \beta=1,$$

it follows from Eq. (3) that

$$\int_R\phi\Delta\phi dR+\int_R(\nabla\phi)^2dR=\int_S\phi\phi_r dS. \tag{6}$$

Let $r\to\infty$ in Eq. (6), where $R=R_r$, $S=S_r$. Then the assumptions of (II) and Schwarz's inequality imply that the first integral on the left tends to a finite limit. On the other hand, the assertion of (II) is that the same is true of the second integral on the left of Eq. (6). Hence, it is sufficient to prove that the same is true of the integral on the right of Eq. (6). Actually, it is sufficient to prove that the latter integral is a bounded function of r, since the second integral on the left, being the integral of a square, must tend to a finite limit if it is bounded.

Put

$$\lambda(r)=\int_R\phi^2dR \quad (R=R_r).$$

Then, since ϕ is of class (L^2), there exists a finite limit, $\lambda(\infty)$. It is also clear that, if λ' denotes $d\lambda/dr$,

$$\lambda'(r)=\int_S\phi^2dS \quad (S=S_r).$$

One more differentiation gives

$$\tfrac{1}{2}\lambda''(r)=\lambda'(r)/r+\int_S\phi\phi_r dS,$$

where the subscript of ϕ denotes partial differentiation in the direction of increasing r. But the last integral is precisely the one on the right of Eq. (6), that is, the integral the boundedness of which was seen to imply (II). It follows therefore from the last formula line that (II) will be proved if it is shown that

$$\tfrac{1}{2}\lambda''(r)-\lambda'(r)/r\to\infty \quad \text{as} \quad r\to\infty$$

is impossible.

Suppose that it is possible. Then a quadrature gives

$$\tfrac{1}{2}\lambda'(r)-\int^r d\lambda(s)/s\to\infty.$$

A partial integration transforms this into

$$\tfrac{1}{2}\lambda'(r)-\lambda(r)/r-\int^r\lambda(s)ds/s^2\to\infty.$$

But $0\leqq\lambda(r)\leqq\lambda(\infty)<\infty$, hence $|\int^r\lambda(s)ds/s^2|<\text{const.}$ Consequently, $\frac{1}{2}\lambda'(r)\to\infty$. Hence, one more quadrature leads to $\frac{1}{2}\lambda(r)\to\infty$, that is, to $\lambda(\infty)=\infty$. Since this contradicts the assumption $\lambda(\infty)<\infty$, the proof of (II) is complete.

3.

What is essential in the above proof of (II), an elementary lemma of standard type, is that the proof can be adjusted to lead to the following refinement of the corollary, (I), of (II):

(III) *The assumption of* (I) *concerning f, viz., the assumption $|f| <$ const., can be relaxed to the unilateral restriction $f <$ const.*

Incidentally, (III) can be generalized in the direction of the Remark following (I):

(III*) *The assertions of* (I), (III) *remain true if Eq. (1) is generalized to Eq. (4), where g is any (continuous) function of class (L^2).*

First, if g and ϕ are of class (L^2), then, according to Schwarz's inequality, $g\phi$ is of class (L). Hence, if Eq. (4) is multiplied by ϕ, it follows that the sum $(\phi\Delta\phi+f\phi^2)$ is of class (L). On the other hand, the assumption made in (III), (III*) with regard to f means that there exists a (continuous) *negative* function, say $f^*=f^*(x, y, z)$, for which $f-f^*$ becomes a bounded function. But then, since ϕ is of class (L^2), the function $(f-f^*)\phi^2$ is of class (L). It follows, therefore, by subtraction, that the sum $(\phi\Delta\phi+f^*\phi^2)$ is of class (L), that is, it is absolutely integrable (over the (x, y, z)-space).

In particular, this sum has a convergent improper integral, that is, its integral over the sphere $R=R_r$ tends to a finite limit as $r\to\infty$. It turns out that the same is true of the integral of the first term, $\phi\Delta\phi$, of the sum. For otherwise the second term, $f^*\phi^2$, ought to have an integral (over $R=R_r$) which tends to $-\infty$ as $r\to\infty$, since $f^*\phi^2\leqq 0$. Inasmuch as the integral of the sum tends to a finite limit, this means that the integral of the first term, $\phi\Delta\phi$, tends to ∞. In view of Eq. (6), this is equivalent to

$$\int_S \phi\phi_r dS-\int_R (\nabla\phi)^2 dR\to\infty.$$

Consequently, since the function beneath the second integral sign is non-negative,

$$\int_S \phi\phi_r dS\to\infty.$$

But this limit relation is precisely the one which, in the proof of (II), has led to the contradiction $\infty=\lambda(\infty)<\infty$.

Accordingly, the integral over $R=R_r$ of the second term of the sum $\phi\Delta\phi+f^*\phi^2$ cannot tend to $-\infty$ as $r\to\infty$. Since this sum is of class (L), and since $f^*\phi^2\leqq 0$, it follows that $\phi\Delta\phi$ *is of class* (L) (this by-product of the proof of the assertions (III), (III*) is not contained in their wording).

In particular, the first integral on the left of Eq. (6) must tend to a finite limit, as $r\to\infty$. Hence, if the second integral on the left of Eq. (6) did not tend to a finite limit, there would follow, *via* the last two formula lines, the same contradiction as before. But the fact that the second integral on the left of Eq. (6) must tend to a finite limit proves that $\nabla\phi$ is of class (L^2).

Letters to the Editor

PUBLICATION of brief reports of important discoveries in physics may be secured by addressing them to this department. The closing date for this department is, for the issue of the 1st of the month, the 8th of the preceding month and for the issue of the 15th, the 23rd of the preceding month. No proof will be sent to the authors. The Board of Editors does not hold itself responsible for the opinions expressed by the correspondents. Communications should not exceed 600 words in length.

Notes on the Wheeler-Feynman Theory

CARLTON W. BERENDA
The University of Oklahoma, Norman, Oklahoma
March 13, 1947

THE present writer has suggested[1] that there is a qualitative relation between Mach's principle of the relativity of inertia as employed in Einstein's general theory, and the Wheeler-Feynman principle that the radiative damping reaction is dependent upon absorbers *via* advanced potentials.[2] Professor Wheeler[3] believes this suggestion may be significant. In relativity, there would be no inertial reaction of mass particles if there were no gravitational bodies in the universe; and the retarded gravitational fields of the material universe provide these inertial reactions.[4] In the Wheeler-Feynman theory, there would be no radiative reaction of electrical particles if there were no absorbing bodies in the universe; and the half-advanced electromagnetic fields of the absorbers provide the radiative reaction of the charged particle. It may be advisable to "symmetrize" the gravitational potentials by introducing both the half-advanced and half-retarded fields. Taking the interior gravitational law for macroscopic matter under certain specified coordinate conditions and for weak fields:[5]

$$2R_\mu{}^\nu - g_\mu{}^\nu R = -\frac{16\pi G}{c^4}\cdot T_\mu{}^\nu,$$

we obtain

$$\nabla^2 f_\mu{}^\nu - \partial^2 f_\mu{}^\nu/c^2\partial t^2 = -4\pi\left(-\frac{4\pi G}{c^4}\cdot T_\mu{}^\nu\right),$$

which could be solved symmetrically over the volume v:

$$f_\mu{}^\nu = \frac{1}{2}\cdot\frac{1}{4\pi}\int\frac{\left[-\frac{16\pi G}{c^4}\cdot T_\mu{}^\nu\right]}{r}dv + \frac{1}{2}\cdot\frac{1}{4\pi}\int\frac{\left\{-\frac{16\pi G}{c^4}T_\mu{}^\nu\right\}}{r}dv,$$

where the square brackets refer to retarded time $t-r/c$, and the curly brackets refer to advanced time $t+r/c$; and where

$f_\mu{}^\nu = h_\mu{}^\nu - \frac{1}{2}\delta_\mu{}^\nu h$, and $h_\mu{}^\lambda = \delta^{\lambda\alpha}h_{\mu\alpha}$, $h = h_\alpha{}^\alpha$ and $g_{\mu\nu} = \delta_{\mu\nu} + h_{\mu\nu}$,

where $\delta_{\mu\nu}$ are the Galilean values and $h_{\mu\nu}$ are the higher order deviations of the gravitational field from these values.

It also seems of considerable importance to direct attention to the fact that Wheeler and Feynman employ Frenkel's solution for a *point* charge which gives a *finite* self-energy or self-mass. In this way we can define a *point* mass for the subatomic "particles." Some years ago, L. Silberstein[6] obtained an axially symmetric line element for a gravitational field:

$$ds^2 = e^\nu dt^2 - e^{\lambda-\nu}\cdot(dx^2+dy^2) - x^2e^{-\nu}dz^2.$$

He pointed out that λ and ν cannot be functions of the time t if this line element is to remain in agreement with the gravitational law:

$$R_{\mu\nu} = 0.$$

His solution would therefore represent two resting gravitational bodies that would have to remain at fixed distances with respect to each other. For macroscopic gravitational bodies, this would be absurd. This absurdity arises from the fact that Silberstein treated these finite bodies as *point* singularities of the field, the problem thereby having axial symmetry. But if we are willing to take over the theory of Frenkel into the domain of *all* subatomic "particles," then Silberstein's solution may be most significant. Thus the proton-neutron combination could be represented by Silberstein's solution, and could give rise to fixed energy levels between these particles, i.e., with point masses in the subatomic equations, general relativity, for the first time, opens up the possibility of deriving quantization.

There are two further facts that are relevant: the laws of motion are obtainable[7] for two bodies from $R_{\mu\nu}=0$, hence quantized motion may also emerge in this case. Finally, it may be possible to obtain the nuclear forces from gravitation.[8]

[1] C. W. Berenda, Phil. Sci. 14, No. 1, p. 19.
[2] J. Wheeler and R. Feynman, Rev. Mod. Phys. 17, 157 (1945).
[3] Private communication.
[4] H. Thirring, Physik. Zeits. 19, 33, 156 (1918); 22, 29 (1921).
[5] R. Tolman, *Relativity, Thermodynamics, and Cosmology* (Oxford Press, New York, 1934), pp. 236–238.
[6] L. Silberstein, Phil. Mag. 24, 814 (1937).
[7] Einstein, Hoffmann, Infeld, and Robertson, Annals Math. 39, 65, 101 (1938); 41, 455 (1940).
[8] M. Wang, K. Wang, and H. Tsao, Phys. Rev. 66, 103, 155 (1944); 68, 163 (1945).

Probability of Nuclear Meson-Absorption

GEORGE GAMOW
The George Washington University, Washington, D. C.
March 20, 1947

THE experimental studies of the decay of negative mesons stopped in various materials[1] leads to the conclusion[2] that the probability for a K-orbit meson to be absorbed by the nucleus is of the order of magnitude of 10^6 sec.$^{-1}$, i.e., about 10^{12} times smaller than would be expected on the basis of conventional meson field theory.[3] It is significant that a discrepancy of the same factor of 10^{12} was encountered in the early attempts to explain nuclear forces (and magnetic momenta) on the basis of electron-neutrino exchange theory.[4] In connection with this earlier discrepancy it was suggested by Gamow and Teller[5] that the probabilities of the three possible processes, (1) electron-pair emission, (2) electron-neutrino emission, and (3) neutrino-pair emission, may represent a geometrical progression with a ratio equal to 10^{12}, the first being the most probable and the last the least probable. Under such an assumption, nuclear forces must be due exclusively to

electron-pair exchange, the processes involving β-transformations to the electron-neutrino creation or annihilation, whereas the emission of neutrino-pairs could be associated with the gravitational radiation. Since in the meson-language the process (1) should be described as the emission of a neutral meson, whereas the process (2) corresponds to charged (positive or negative) mesons, the former "*three-processes-hypothesis*" can be now reformulated in the following way. *The exchange forces between nucleons (and also their magnetic momenta) are due exclusively to the exchange of neutral mesons, whereas all the processes connected with charged mesons* (such as ordinary β-decay, K-capture, urca-processes, emission or absorption of charged mesons by various nuclei, etc.) *possess probabilities which are smaller by a factor of the order of magnitude* 10^{12}. The above-mentioned discrepancy between the observed and calculated probabilities of nuclear meson-absorption seems to represent a strong argument in favor of this point of view.

[1] M. Conversi, E. Pancini, and O. Piccioni, Phys. Rev. 71, 209 (1947); T. Sigurgeirsson and A. Yamakawa, Phys. Rev. 71, 319 (1947).
[2] E. Fermi, E. Teller, and V. Weisskopf, Phys. Rev. 71, 314 (1947); J. A. Wheeler, Phys. Rev. 71, 320 (1947).
[3] Kobayasi and Okayama, Proc. Phys. Math. Soc. Japan 21, 1 (1939); Sakata and Tanikawa, Proc. Phys. Math. Soc. Japan 21, 58 (1939).
[4] H. Bethe, Rev. Mod. Phys. 8, 203 (1936).
[5] G. Gamow and E. Teller, Phys. Rev. 51, 289 (1937).

Relative Moments of H_1 and H_3

F. Bloch, A. C. Graves, M. Packard, and R. W. Spence*
Los Alamos Scientific Laboratory, Santa Fe, New Mexico
March 14, 1947

We have recently[1] established the fact that the triton has the spin $\frac{1}{2}$ and a positive magnetic moment about 1.067 times larger than that of the proton. In view of the interest in the result it seemed desirable to improve the accuracy of the ratio of the two moments.[2]

In order to facilitate comparison a new sample was prepared, which, according to a density determination, contained approximately equal amounts of H_1 and H_3 in the form of a 0.1 molar solution of $MnSO_4$ in water. Confirming our previous results for the spin of the triton and the sign of its moment, signals of equal sign and about equal size and shape were obtained from the two isotopes under identical radiofrequency conditions and with those values of the d.c. field at which their respective resonances were expected to occur.

A highly accurate value for the relative moments of H_1 and H_3 was obtained by superimposing in the transmitter coil two r.f. fields of different frequencies ν_1 and ν_3, delivered from independent oscillators. The receiver coil could be tuned to simultaneous response for both frequencies by two coupled resonant circuits, so that a single diode was able to detect the peak voltage of both frequencies and hence the instantaneous sum of the two signals, received from both isotopes. The original method of field modulation and representation[3] gave thus two separate signals on the screen as long as the resonance fields for the two isotopes had still different values but were already within the sweep of the modulating field. A slight variation of ν_1 resulted in the merging of the two separate signals into one of about twice the size and was continued until maximum height of this signal was observed. This indicated, within a fraction of the line width, that a common value of the resonance field for the two isotopes had been reached, so that independent of this value, their gyromagnetic ratios γ_P and γ_T had to stand in the proportion of the two frequencies ν_1 and ν_3.

A considerable improvement of the accuracy was obtained by using larger pole pieces than before so as to obtain a more homogeneous field over the region in which the sample was located. We were thus able to obtain lines with a half-width of somewhat less than 0.5 gauss.[4]

By proper setting of ν_1 we were able to ascertain equality of the resonance fields for the two isotopes within 0.1 gauss; since the d.c. field had a value of about 10,000 gauss, an accuracy of about 1 in 10^5 was thus obtained.

In the actual measurements, ν_3 and the beat frequency $\Delta\nu=\nu_3-\nu_1$ were obtained from a Navy type LM-18 crystal calibrated frequency-indicating meter so that for the gyromagnetic ratios γ_T and γ_P of the triton and the proton we had the relation:

$$\gamma_T/\gamma_P=[1-\Delta\nu/\nu_3]^{-1}.$$

Calibration of the frequency-indicating meter showed that frequency readings were accurate to about one part in ten thousand. An uncertainty of 1 in 10,000 in $\Delta\nu$ and ν_3 introduces an uncertainty of 1 in 10^8 in γ_T/γ_P as calculated from the above formula.

TABLE I. Results for the gyromagnetic ratio γ_T of the triton in terms of γ_P of the proton obtained from two sets of runs with different values of the d.c. field B_0.

B_0 (Gauss)	No. of Runs	γ_T/γ_P
9300	17	1.066638 ± 0.000007
9900	21	1.066635 ± 0.000011

Table I gives the results of 17 runs in which the d.c. field had a value of about $B_0=9300$ G and 21 more runs where $B_0=9900$ G. The indicated probable errors for each set of runs are obtained in the usual way from mean square deviation of individual runs from the average, and it is seen that the two sets agree well within their individual errors. Taking both together, and in view of our earlier result for the spin of the triton and the sign of its moment, we obtain

$$\mu_T=(1.066636\pm0.00001)\mu_P$$

for the moment μ_T of the triton in terms of μ_P, that of the proton.

* Work done at Stanford University and at the Los Alamos Scientific Laboratory operated by the University of California under U. S. Government contract.
[1] F. Bloch, A. C. Graves, M. Packard, and R. W. Spence, Phys. Rev. 71, 373 (1947).
[2] While this work was in progress we were informed that H. Anderson and A. Novick had found the gyromagnetic ratio of tritium to be 1.06666 ± 0.0001 times that of the proton; the more accurate result, reported here, lies within their error.
[3] F. Bloch, W. W. Hansen, and M. Packard, Phys. Rev. 69, 127 (1946); 70, 460 (1946).
[4] This confirms the recent interesting result of N. Bloembergen, R. V. Pound, and E. M. Purcell, Phys. Rev. 70, 986 (1946), that the line width in liquids is far less than originally expected. We were not able, however, to reach their limit of 0.15 gauss, probably because of insufficient homogeneity of our field.

Artificial Radioactive Isotopes of Polonium, Bismuth and Lead*

J. J. HOWLAND, D. H. TEMPLETON, AND I. PERLMAN
Radiation Laboratory, University of California, Berkeley, California
March 8, 1947

THROUGH use of cyclotron beams of 20-Mev deuterons and 40-Mev helium ions and of an intense neutron source, new artificial radioactive isotopes have been produced and identified to varying degrees of certainty as shown in Table I.

As a result of the new experiments, definite mass numbers have been assigned to some previously known radioactive isotopes as shown in Table II.

The mass assignments of the polonium isotopes were made on the basis of their relative yields when lead of different isotopic composition was bombarded with 40-Mev helium ions.[1]

The 9-day Po^{206} was found to decay into the 6.4-day bismuth activity assigned to Bi^{206} or Bi^{207} by Fajans and Voigt.[2] The assignment to Bi^{206} is in agreement with the observation of Corson, MacKenzie, and Segrè[3] that this activity is not produced by the alpha-decay of $_{85}At^{211}$.

The 5.7-hour Po^{207} cannot be Po^{208} because it was not made by bombardment of Bi^{209} with 20-Mev deuterons, for which a high $(d, 3n)$ cross section is expected.

The alpha-activity attributed to Po^{208} may be a mixture of Po^{208} and Po^{209} with similar α-particle ranges, but on the basis of yield arguments most of this activity must be Po^{208}.

The high yield of the 12-hour bismuth from deuterons on Pb^{206} limits the assignment to Bi^{203} or Bi^{204}, and the high yield from helium ions on thallium sets 204 as the lowest possible mass. Therefore the isotope is Bi^{204}. It decays into the 68-minute lead[2,4] which assigns this lead to an excited state of Pb^{204}. Only 4 percent as many counts of 68-minute Pb are observed as of 12-hr. Bi^{204}. Unless the counting efficiencies are different by 25-fold, some of the Bi^{204} decays directly to stable Pb^{204}.

A long-lived activity (negative electrons and γ-rays) was found in bismuth which had been subjected to a very high neutron flux for several months. The long-lived activity followed the bismuth through several chemical separations from added Ag, Sb, Sn, Tl, Hg, and Pb. It is assumed to be Bi^{208}, which may decay either by β^- emission or by electron capture, since both Pb^{208} and Po^{208} appear to be stable with respect to such decay.

The 52-hr. lead isotope has been produced previously by deuterons on thallium[2,5] and by fast neutrons on lead[4] and was assigned to either 203 or 205. Since it failed to appear as a result of the reaction $Pb^{204}(d, p)Pb^{205}$, it is now assigned as Pb^{203}. Maurer and Ramm[4] made the same assignment on the basis of experiments which seemed to show that the activity was produced from Pb^{204} but not from Pb^{206} by fast neutrons. We have confirmed this result by bombarding Pb^{204} and Pb^{206} in the Argonne pile.

Detailed accounts of the experiments leading to these results will appear in forthcoming papers.

TABLE I.

Isotope	Mode of Decay	Half-life	Method of Production
Po^{208}	K (~90%), α (~10%, 5.2 Mev), γ	9 day	$Pb^{204}(\alpha, 2n)$
Po^{207}	K (~100%), α (~0.01%, 5.1 Mev), γ	5.7 hr.	$Pb^{206}(\alpha, 3n)$
Po^{208}	α (5.14 Mev)	~3 yr.	$Pb^{207}(\alpha, 3n)$
Bi^{204}	K (e^-, γ)	12 hr.	$Pb^{204}(d, 2n)$ $Tl(\alpha, 3n)$
Bi^{203}?	? (e^-, γ)	long-lived	$Bi(n, 2n)$?

TABLE II.

Isotope	Mode of Decay	Half-life
Bi^{196}	K, e^-, γ	6.4 day
Pb^{204g}	$I.T., e^-, \gamma$	68 min.
Pb^{203}	K, e^-, γ	52 hr.

* This report is based on work performed under Contract No. W-7405-eng-48 with the Manhattan Project at the Radiation Laboratory, University of California.
[1] We are indebted to Dr. B. J. Moyer, Dr. C. M. Van Atta and members of the isotope separation staff for making available the separated lead isotopes, to Dr. E. H. Huffman, Mr. R. C. Lilly, and Miss Dorothy Bockhop for their purification, and to Mr. T. J. Vale for his mass spectrometric assay. The bombardments were made possible through the cooperation of Dr. J. G. Hamilton, Mr. T. Putnam and other members of the group that operates the 60-inch cyclotron.
[2] K. Fajans and A. F. Voigt, Phys. Rev. 60, 619, 626 (1941).
[3] D. R. Corson, K. R. MacKenzie, and E. Segrè, Phys. Rev. 58, 672 (1940).
[4] W. Maurer and W. Ramm, Zeits. f. Physik 119, 602 (1942).
[5] R. S. Krishnan and E. A. Nahun, Proc. Camb. Phil. Soc. 36, 490 (1940).

Auger Showers and the Comets

V. ROJANSKY
Union College, Schenectady, New York
March 20, 1947

KLEIN has conjectured that the Auger extensive cosmic-ray showers are produced by fragments of hypothetical matter having negative atomic nuclei.[1] The writer has conjectured that the comets consist of this type of matter.[2] Now, if both these conjectures should be correct, then, in the absence of adverse variations of barometric pressure, the frequency of Auger showers in any locality would be expected to increase during a cometary meteor shower overhead. Therefore, even at the risk of engaging in what might perhaps be loosely described as a wild-goose chase, it should be of interest to schedule experiments on Auger showers so as to determine whether or not such increases actually occur. By combining these experiments with visual observations—or with radio-echo or radar observations, so as not to be dependent on darkness and a clear sky—one could also attempt to determine whether or not the passage of an individual cometary meteor near the zenith is accompanied by Auger showers.

One of the meteor showers to which a parent comet has been assigned is the Perseid shower in August.

I am indebted to Professor Niels Arley for calling my attention to Klein's paper.

[1] O. Klein, Arkiv f. mat. astr. och fysik 31A, No. 14 (1944–45).
[2] V. Rojansky, Astrophys. J. 91, 257 (1940); Phys. Rev. 58, 1010 (1940).

Validity of the Franck-Condon Principle in Collisions of the Second Kind

ROLAND E. MEYEROTT
Sloane Physics Laboratory, Yale University, New Haven, Connecticut
March 17, 1947

THE application of the principle of resonance to collisions of the second kind between an atom and a molecule or between two molecules is generally uncertain, because of the lack of any rule for deciding how much energy can be absorbed as vibrational energy of the molecule or molecules. For example, the probability of the following transfer reactions in the upper atmosphere[1]

$$O^+ + O_2 \rightarrow O + O_2^+ + 1.3 \text{ ev},$$
$$N_2^+ + O \rightarrow N_2 + O^+ + 2.0 \text{ ev},$$
$$N_2^+ + O_2 \rightarrow N_2 + O_2^+ + 3.3 \text{ ev},$$

depends upon whether such a large amount of energy can be absorbed as vibrational energy. In collisions involving He_2 or He_2^+, failure to take into account the vibrational energy led to confusion as to the carrier of the excitation energy in He.[2]

In considering the latter problem, it was suggested by the present writer that the Franck-Condon (F-C) principle also applied to collisions of the second kind. Ideally, one could consider the transfer of energy as an induced emission and absorption process. In this case the F-C principle would hold for each of the colliding molecules. For very close collisions this ideal situation would need modification. However, close collisions are not likely to affect the cross sections appreciably, since to have a large cross section means a large collision radius and hence a long range transfer of excitation. In the limit, this would be essentially a radiation problem.

Experimentally, excitation of N_2 by the metastable states or ions of Xe, Kr, A, Ne, and He afford a good check of the above hypothesis. Here the metastable state or ion is atomic so that the only dependence of cross section on the F-C principle is that involving N_2. A list and a discussion of most of the states excited in N_2 is given by Bernard.[3] It is significant that all these states can also be excited by electron impact in which the F-C principle is known to hold. (The possible exception, that of the $C\,^2\Sigma$ state of N_2^+ excited by He^+, has now been removed, as will be shown in a paper to follow.) No new states appear (many more might be expected on theoretical grounds), and no evidence exists for excessive dissociation of N_2 although all of the metastable states involved have energies greater than the dissociation energy of N_2. Hence, it would appear that those collisions in which the transfer of energy can obey the F-C principle in the molecule are most probable.

Collisions of the second kind between two molecules are more restricted because of the fact that the F-C principle must hold for each of the colliding molecules. An examination of the molecular states excited in active nitrogen shows that in all cases (except where molecular formation takes place as the β-bands of NO), the excitation can be accounted for in detail by an application of the F-C principle to the forbidden transitions $A\,^2\Sigma_u \rightarrow X\,^1\Sigma_g$, $a\,^1\Pi_g \rightarrow X\,^1\Sigma_g$, and $a\,^1\Pi_g \rightarrow A\,^2\Sigma_u$ transitions in N_2.

Application of the F-C principle to the reactions listed in the first section of this letter indicates that the transfer of charge as indicated would likely be very improbable, since the potential curves of N_2^+ and O_2^+ lie directly above those of N_2 and O_2, respectively, in their ground states. Hence, no mechanism exists for converting an excess energy of the order of volts into vibrational or translational energy of the colliding molecules.

[1] D. R. Bates and H. S. W. Massey, Proc. Roy. Soc. **A187**, 261 (1946).
[2] R. E. Meyerott, Phys. Rev. **70**, 671 (1946).
[3] R. Bernard, Ann. de physique **13**, 1 (1940).

The Elastic Constants of Sodium Chlorate

S. BHAGAVANTAM AND D. SURYANARAYAN
Department of Physics, Andhra University, Waltair, India
March 19, 1947

SODIUM chlorate ($NaClO_3$) crystallizes in the cubic tetratohedral class. It has three elastic constants and Voigt[1] reported that one of them is negative, making the crystal possess a negative value of Poisson's ratio. Recently Mason[2] remeasured these constants and found all of them to be positive in contrast to Voigt's results. A new dynamical method based on the use of a piezoelectric wedge has been developed in this laboratory[3] for measuring the elastic constants of crystals, and, in view of the importance of the above results in the case of sodium chlorate, it is considered desirable to provide independent confirmation. Fairly large sized crystals of this substance have been grown from aqueous solution and the results in Table I are obtained by working with suitable sections. The values of the c's in the last row are obtained by direct measurement and the s's are derived therefrom. The values of the s's as measured by Voigt and by Mason, and those of c's, which are deduced therefrom, are given for comparison in the first and the second rows. The symbol K in the last column stands for the bulk modulus and is equal to $(c_{11}+2c_{12})/3$.

TABLE I. Elastic constants of sodium chlorate.

Unit / Constant	(10^{-13} cm²/dyne) s_{11}	s_{12}	s_{44}	(10^{11} dynes/cm²) c_{11}	c_{12}	c_{44}	K
Voigt	24.6	12.52	83.6	6.19	−2.087	1.196	0.67
Mason	23.35	−5.15	85.4	4.90	1.386	1.17	2.56
Authors	22.9	−5.35	84.7	5.09	1.55	1.18	2.73

Our results are in agreement with those of Mason and it is to be concluded that this crystal has a positive value of Poisson's ratio like most other substances. Bridgman[4] obtained 1.99×10^{11} dynes/cm² for the bulk modulus of this substance. This measured value is in qualitative agreement with that derived from the results of Mason and the authors but differs greatly from that based on Voigt's values.

[1] W. Voigt, *Lehrbuch der Kristallphysik* (Teubner, Leipzig, 1910).
[2] W. P. Mason, Phys. Rev. **70**, 529 (1946).
[3] S. Bhagavantam and J. Bhimasenachar, Proc. Ind. Acad. Sci. **20** 298 (1944).
[4] P. W. Bridgman, Proc. Am. Acad. **64**, 51 (1929).

Analysis of High Energy X-Ray Spectra

G. C. BALDWIN AND G. S. KLAIBER
Research Laboratory, General Electric Company, Schenectady, New York
March 8, 1947

AN impediment to studies of nuclear phenomena induced by high energy quanta is the fact that artificial sources necessarily give continuous spectra of quanta. Since one must know the x-ray spectrum before one can calculate accurate cross sections from excitation curves,[1] experimental determination of the spectrum is essential to quantitative use of betatrons and synchrotrons. To obtain this, one must employ a process whose cross section as a function of quantum energy is known. The most satisfactory process available is pair production. Several methods for analyzing high energy x-ray spectra have been considered in which the total energies of a large number of positron-electron pairs generated in a suitable target by the x-ray beam are measured, and the resulting number-*vs.*-energy distribution divided by the theoretical total cross section for pair formation. This involves either laborious analysis of thousands of cloud-chamber photographs or elaborate coincidence methods which are difficult when dealing with pulsed radiation with the distribution in time typical of betatron radiation.

This note is to point out that x-ray spectra can be determined without observing both members of each pair. Although the energy of one member of a pair does not determine the energy of the quantum which produced that particular pair, it is possible to calculate statistically the energy distribution of quanta which will produce an observed distribution of positrons. With the need for coincidence or cloud-chamber technique eliminated, more convenient methods can be employed.

The differential cross section for pair production is ordinarily expressed in the form $\psi(u, W)du$ where $u=U/W$, W being the quantum energy and U being the total energy of the positron.[2] The distribution in u for any given W is roughly independent of u. If one considers the production of positrons with fixed values of U, for example of 20 Mev and of 25 Mev, respectively, it is found that the values of u corresponding to these two positron energies become more and more nearly equal as W increases, hence for W well above the thresholds the respective values of $\psi(u, W)du$ tend toward equality. This is seen more readily by transforming the differential cross section into the form $\psi'(W, U)dW$, when it is found that the curves characterized by different values of the parameter U rise rapidly at first from their respective thresholds, then merge into a slowly varying envelope which is nearly independent of U. The total number of positrons of a given energy U produced by a spectrum whose distribution function is $n(W, E)$, E being the maximum energy, is

$$\pi(U, E)=\int_0^{\infty} n(W, E)\psi'(W, U)dW.$$

The excess of the number of 20-Mev over 25-Mev positrons, for example, will be almost exactly proportional to the number of quanta lying between about 21 and 26 Mev, because of the peculiar behavior of $\psi'(W, U)$.

If, therefore, one measures the number-energy distribution of positrons, $\pi(U, E)$, produced by x-rays of maximum energy E in a thin target of low atomic number, one can calculate the x-ray spectrum by first differentiating $\pi(U, E)$ with respect to U and then dividing by the envelope of the $\psi'(W, U)$ curves. Having an approximate spectrum (probably correct to within 10 percent except at the high energy tip) one should be able by further analysis to obtain a more accurate spectrum. Calculations to test this point are now being carried out by Drs. R. H. Vought and Leo Seren of this Laboratory, to whom we are grateful for discussions of this method.

We intend to carry out the indicated experiment first in an exploratory way with a cloud chamber and later by an integral method, registering the magnetically analyzed positrons either in a photographic emulsion or by means of counters.

[1] G. C. Baldwin and G. S. Klaiber, Phys. Rev. 71, 3 (1947).
[2] Bruno Rossi and Kenneth Greisen, Rev. Mod. Phys. 13, 258-261 (1941); H. Bethe and W. Heitler, Proc. Roy. Soc. 146, 83 (1934).

Absorption of Methyl Alcohol and Methylamine for 1.25-Cm Waves

W. D. HERSHBERGER
RCA Laboratories, Princeton, New Jersey
AND
JOHN TURKEVICH
Frick Chemical Laboratory, Princeton, New Jersey
March 20, 1947

FIVE sharp lines in the microwave absorption spectrum of methyl alcohol have been observed and the frequencies in megacycles are given quite accurately by the formula:

$$\nu=\nu_0+20m^2,$$

where m is integral and takes on all values from 0 to 4, while ν_0 is 24,930 Mc.

Ten lines in the spectrum of methylamine have been found. Six of these fit the curve

$$\nu=\nu_0-32m-50m^2,$$

but the four remaining lines appear to belong to some other sequence. ν_0 is 25,436 Mc and only the lines for m from 2 to 7 have been observed owing to the limits of operation of the klystron used.

Molecules of this type have been treated as slightly asymmetrical tops with free internal rotation by Nielsen[1] with energy levels given by $F(J, K, K_1, K_2)=BJ(J+1)-K^2B+A_1K_1^2+A_2K_2^2$ where $K=K_1+K_2$.

The transition $\Delta J=\pm 1$ gives us frequencies twice as high as those observed; the transition $K=0\leftrightarrow K=1$ with all other quantum numbers unchanged gives us approximately the observed frequency. For this transition, K, K_1, and K_2 could not be co-linear.

The rotational constant B of CH_3F lies in the same range as that of the two other molecules named but no absorption lines for this material have been found. The above hypothesis has the advantage of simplicity over one involving the tunnel effect as in ammonia or one involving hindered rotation about a C−N or C−O bond.

[1] H. H. Nielsen, Phys. Rev. 40, 445 (1932).

Grain Growth in High Purity Aluminum

PAUL A. BECK, JOSEPH C. KREMER, AND L. DEMER
Department of Metallurgy, University of Notre Dame, Notre Dame, Indiana
March 8, 1947

MEASUREMENT of the average grain size in a set of high purity aluminum specimens heated for various periods of time, ranging from 20 seconds to 11 days at a series of constant temperatures from 350°C to 650°C gave the following results:

(A) For isothermal grain growth the average grain size D at time t can be expressed as

$$D=D_0t^n. \tag{1}$$

The exponent n increases linearly with temperature from $n=0.06$ at 350°C to $n=0.16$ at 500°C.

(B) The $D=D_0t^n$ relation holds true only until the grain size is well below the thickness of the specimen. When D (measured in the plane of the sheet specimen) is somewhat larger than the specimen thickness, grain growth completely stops; the grains extend through the thickness of the specimen, and their boundary surfaces are approximately perpendicular to the specimen surface. At 650°C this condition was fully reached in 20 seconds, and up to 11 days no further change occurred in the average grain size. At lower annealing temperatures the same maximum grain size was approximated in longer periods of time. The maximum grain size obtainable in a specimen through grain growth was found to increase linearly with the specimen thickness over a wide range.

As a result of the variation of n with temperature, it is not possible, strictly speaking, to derive a heat of activation from grain growth data. The Q value derived from plotting $\log t$ *vs.* the reciprocal absolute temperature, for a certain grain size, varies with both the grain size and the temperature. The values thus obtained, however, are in the approximate range of 55 to 65 kcal./g atom. It is interesting to note that this range is in agreement with the Q values obtained by Anderson and Mehl[1] for growth during recrystallization of high purity aluminum. These values are considerably higher than the heat of activation for self-diffusion in aluminum, estimated to 37.5±4 kcal./g atom.[2] Perhaps this may be interpreted to mean that the energy for the activation of an aluminum atom to jump across a grain boundary is higher than that required to produce an exchange of position within the same lattice, as in diffusion.

Attempting to check the relative magnitude of the heat of activation derived from grain growth data and that for self-diffusion with other materials than high purity aluminum, we were unable to find satisfactory grain growth data in the literature. However, the data available for brass could be used if certain idealizing assumptions were made.

Let us assume the validity of the $D=D_0t^n$ relation, the independence of n on temperature, and the existence of a heat of activation Q for the process. Under such idealized conditions the following general formula can be derived

$$D=D_0(te^{-Q/RT})^n, \tag{2}$$

and for constant time

$$D=D_0e^{-nQ/RT}. \tag{3}$$

The grain growth data by R. S. French[3] on brass satisfy the isothermal relation Eq. (1), if a correction of 10 min. is made in order to allow for the heating-up period. The corrected data for both 575°C and 640°C give $n=0.16$. By using the grain size *vs.* temperature data given in Fig. 1 of French's paper, in connection with relation (3), the value of nQ can be computed. From this, with $n=0.16$, one can obtain $Q=73.5$ kcal./g atom for 70–30 cartridge brass. The heat of activation for self-diffusion in brasses, as determined by Rhines and Mehl, is 32 to 40 kcal./g atom. Although the heat of activation from grain growth data for brass, as given above, is merely a crude approximation, and the value of a comparison is further diminished by a difference in the zinc contents between the alloys used by French and by Rhines and Mehl, it is at least probable that, for brass too, the activation energy from grain growth data is considerably higher than that for self-diffusion.

This work is part of a research project on grain growth in metals sponsored by the Office of Naval Research, U. S. Navy.

[1] Anderson and Mehl, Trans. A.I.M.E. 161, 140 (1945).
[2] Private communication from Dr. Wm. A. Johnson.
[3] R. S. French, Trans. A.I.M.E. 156, 195 (1944). Correction for heating-up period is based on private communication from Mr. R. S. French.

Separation by Diffusion in Fields of Ultrasonic Waves

H. FREI AND M. SCHIFFER
Department of Physics, Hebrew University, Jerusalem
March 21, 1947

IN a discussion of a paper of Willard,[1] Herzfeld[2] mentions the possibility of separation by ultrasonic waves, but finds the effect too weak for observation in a field of plane waves.

We have found that in a field of standing waves, or in an inhomogeneous field of ultrasonic waves, separation of homogeneous substances does occur. It has long been known that such a separation of inhomogeneous substances is easily attainable (dust tube method of Kundt[3] and others[4–6]).

Solutions of glycerin with water and of hexane with heavier paraffins have been subjected to a field of ultrasonic waves of approximately 2 watt/cm² and 1 Mc/sec. With the "Schlieren method" flaws (Schlieren) can be seen to remain in the nodes of the field after the ultrasonic waves are switched off, fading out only after 24 hours or more. Provision against convection which always occurs in a field of ultrasonic waves has been made by placing cover glasses parallel to the plane of the waves. It is considered that this method can be used for separation in a manner similar to thermodiffusion or ultra-centrifugation. Quantitative measurements as well as experiments with a view to develop a countercurrent method in order to obtain separation of appreciable amounts are being undertaken.

[1] G. W. Willard, Phys. Rev. 57, 1057 (1940).
[2] K. F. Herzfeld, J. Chem. Phys. 9, 513 (1941).
[3] A. Kundt, Pogg. Ann. 127, 497 (1866).
[4] K. Buecks and H. Mueller, Zeits. f. Physik 84, 75 (1933).
[5] O. Brandt and H. Freund, Zeits. f. Physik 92, 385 (1934); 95, 415 (1935).
[6] E. B. Pearson, Proc. Phys. Soc. London 47, 136 (1945).

The Total Neutron Cross Section of Dysprosium and Neodymium

WILLIAM J. STURM AND GEORGE P. ARNOLD
Argonne National Laboratory, Chicago, Illinois
March 19, 1947

STUDIES by Fermi and Marshall[1] of the order intensities of Bragg-reflected neutron beams for many substances show that the (111) plane of lithium fluoride is particularly well suited for neutron monochromator work since the reflectivity for high orders is relatively very small. Their measurements show that the second order contributes only about 0.1 percent of the first order intensity, and the third order about 4 percent for a neutron energy of ~0.04 ev. In addition, the first order reflectivity is greater than that of the LiF(100) planes previously used[2,3] for energy dependent cross section measurements.

Such LiF(111) crystals have recently been used with the crystal spectrometer at the Argonne National Laboratory. Figure 1 shows the spectrum obtained from the heavy water pile with the (111) crystals as compared with that of the LiF(100) crystals formerly used. Neither of the spectra has been corrected for the effect of varying resolution, which is to shift the maximum of the distribution to higher energy. The resolution of the (100) crystals is slightly better, but the superiority of the reflectivity of the (111) crystals is obvious. The decreased high order reflectivity in the case of the LiF(111) crystals is evidenced by the sharper intensity decrease in spectrum measurements at large glancing angles for this crystal.

The cross sections of dysprosium and neodymium have been examined briefly in the region of low neutron energies with the new crystals. For dysprosium (Fig. 2) $\sigma\sqrt{E}$ is plotted against E; this would show a $1/v$ cross section as a horizontal line. In addition to the two resonance levels at 1.74 and 5.5 ev, there is evidence of a level at negative energy and of one at an energy higher than 20 ev. The sample was a pressed pellet of Dy_2O_3 of surface density 0.89 g/cm². No correction has been made for the small oxygen scattering cross section or for resolution of the instrument.

Neodymium was measured in the form of pressed pellets of Nd_2O_3 powder with surface densities between 5 and 18 g/cm². It was necessary to subtract 6.2×10^{-24} cm²/atom, $\frac{3}{5}$ the atomic oxygen scattering cross section, in the calculation of the total cross section of the neodymium atom. The

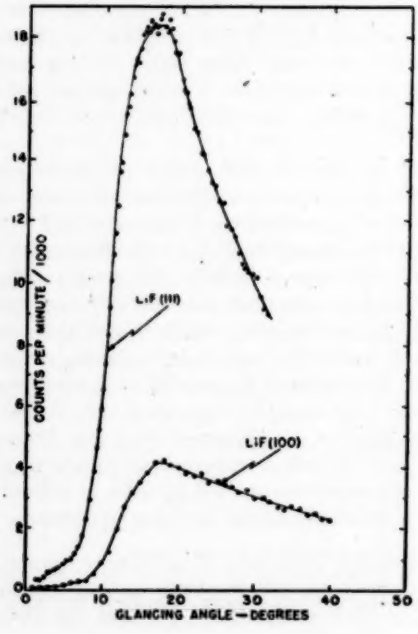

FIG. 1. Neutron spectrum.

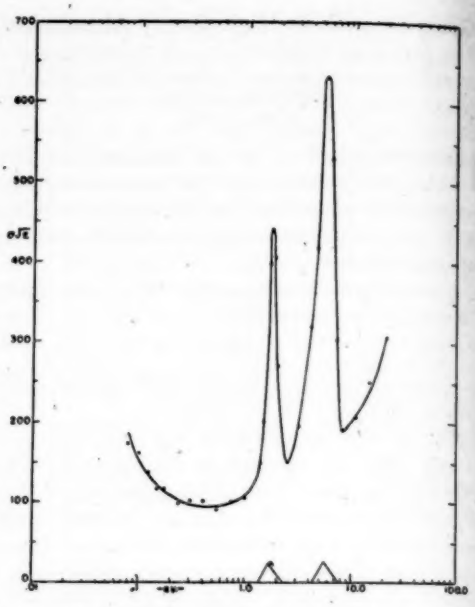

FIG. 2. Total cross section of dysprosium.

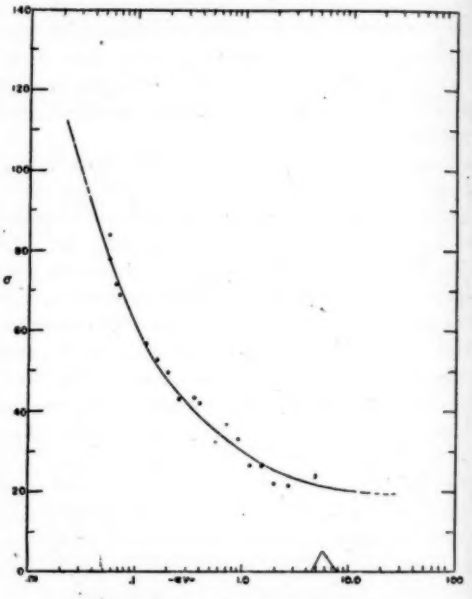

FIG. 3. Total cross section of neodymium.

results are shown in Fig. 3. A plot of σv (cross section $\times$neutron velocity) against E shows a marked rise with energy, indicating a large scattering cross section or a strong resonance level at higher energy. The curve becomes nearly horizontal if a constant value of 15×10^{-24} cm²/atom is attributed to scattering, thus making the absorption cross section at 0.025 ev about 92×10^{-24} cm²/atom. In the present measurement, however, much significance cannot be attributed to the value of the scattering cross section evaluated in this manner. Earlier measurements[4,5] at a single energy gave the absorption cross section for kT neutrons at about 75×10^{-24} cm²/atom.

This document is based on work performed under Contract No. W-31-109-eng-38 for the Manhattan Project at the Argonne National Laboratory.

[1] E. Fermi and L. Marshall, Phys. Rev. 70, 103A (1946).
[2] W. H. Zinn, Phys. Rev. 70, 102A (1946).
[3] W. J. Sturm and S. H. Turkel, Phys. Rev. 70, 103A (1946).
[4] H. Bomke and H. Reddemann, Zeits. f. Physik 120, 56 (1942).
[5] W. Riezler, Ann. d. Physik 41, 476 (1942).

Temperature of the Upper Atmosphere

S. L. Seaton
Little Silver, New Jersey
March 21, 1947

ACCORDING to Appleton[1] the penetration frequency, f, of a radio wave through an ionospheric layer at normal incidence is related to the maximum electron density of the layer thus, for the ordinary ray

$$N=kf^2. \tag{1}$$

Experimental values of f are determined through systematic observation at many places. From such experimental determinations N is readily found, and hence throughout the day dN/dt is available. From the well-known relationship

$$dN/dt=q-\alpha N^2 \tag{2}$$

between time rate of change of ionization, rate of electron production, q, and recombination coefficient, α, Appleton has argued that at night α may be found at once, since $q=0$. He has also suggested that across sunrise or sunset times, for equal values of N, both q and α may be determined on assumption of equal values of α. Such evaluations have been carried out by Mohler[2] and by Appleton[1] over limited time intervals. Furthermore, Appleton[3] has proposed that for times equally spaced either side of noon, q and α at these times may be considered approximately equal, and hence q and α may be found in the daytime.

In extending the earlier calculations I have evaluated q and α throughout the 24 hours for three typical latitudes during an equinoctial interval at sunspot minimum. The variations in α were quite interesting, and it appeared possible to get at the absolute temperature in the upper atmosphere by means of these values and use of J. J. Thompson's[4] relationship involving the recombination coefficient and absolute temperature at low pressures, i.e.,

$$\alpha=\alpha_0(T_0/T)^{\frac{1}{2}}. \tag{3}$$

Reference values of α_0 and T_0 were decided upon after examination of the work of Vegard and Tönsberg[6] who evaluated T_0 at about 230°K on the basis of studies of auroral spectra at Tromsø, Norway. This value for T_0 was used with the night value of α set equal to α_0 for each location. The assumption was made that $T_0=230$°K everywhere above 100 km in the early morning hours.

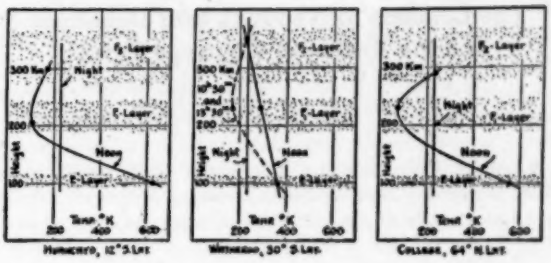

FIG. 1. Calculated relation between temperature and ionospheric height. The vertical line at 230°K represents the assumed night temperature, according to Vegard and Tönsberg.

Noon values of T were found for Huancayo, Peru (12° S.Lat.), Watheroo, Western Australia (30° S.Lat.), and College, Alaska (64° N.Lat.), from CRPL published data[7] of f for these locations and the foregoing argument.

From Fig. 1 it appears that at E-layer heights of 100 km, high temperatures are to be expected, and that F_1- and F_2-layers (around 200 km and 350 km, respectively) may be at considerably lower temperatures. Apparently there is a remarkable variation in temperature in these regions of the atmosphere from night to day.

The Watheroo, Western Australia, temperatures in the F_1-layer go through a reversal in trend around 10^h30^m and again around 13^h30^m local mean time and so an additional calculation at these times has been made and indicated in the central group of the figure by a dotted line. Other detailed fluctuations in temperature around sunrise and sunset were found.

[1] E. V. Appleton, Proc. Phys. Soc., London 45, 673 (1933).
[2] F. L. Mohler, Bur. Stand. J. Research 25, 507 (1940).
[3] E. V. Appleton, Proc. Roy. Soc. [A] 162, 451 (1937).
[4] J. J. Thomson, *Conduction of Electricity Through Gases* (The Cambridge Univerity Press, 1928), Vol. 1, p. 38.
[5] L. Vegard and E. Tönsberg, Geofys. Pub. Oslo (Norway) 11, No. 2; 12, No. 3, 1935.
[6] CRPL-*F* Series, Ionospheric Data, Nat. Bur. Stand., Washington, D. C.

Erratum: On the Disintegration of Negative Mesons

[Phys. Rev. 71, 209 (1947)]

M. Conversi, E. Pancini, and O. Piccioni
Centro di Fisica, Nucleare del C. N. R. Istituto di Fisica dell'Università di Roma, Italia

IN the letter to the Editor with the above title, Fig. 1, the block diagram of the registering set, shows the "delay" in a wrong place, that is between counters "C" and "coincidences III." Actually the "delay" must be understood to be between counters "A" and "coincidences III" and between counters "B" and "coincidences III." No delay is inserted between counters "C" and "coincidences III." For more details, see M. Conversi and O. Piccioni, Phys. Rev. 70, 859 (1946).

The Collision of Neutrons with Deuterons and the Reality of Exchange Forces

H. S. W. MASSEY AND R. A. BUCKINGHAM
University College, London, England
March 20, 1947

A DECISION regarding the reality of exchange forces between a neutron and a proton is not easily arrived at from a study of the collisions of neutrons with protons. The reason for this is the short range of the forces. For a marked difference between exchange and ordinary forces to show up, collisions in which the relative angular momentum is greater than zero must take place with appreciable probability. With a short range force this will be the case only if the neutron energy is high. On the other hand, owing to the relatively diffuse structure of the deuteron, its interaction with a neutron has a much longer range than that of a proton. As a result, collisions of neutrons with deuterons, in which the neutrons possess a relative angular momentum greater than zero, occur with appreciable probability at much lower energies than with protons. A study of these collisions should therefore assist in establishing the reality or otherwise of exchange forces. In 1941 we published a detailed theoretical study of the scattering of neutrons,[1] with energies ranging from 0.1 to 11.5 Mev, by deuterons. The fundamental interaction energy V between nucleons was taken of the form

$$V(r)=A(mM+hH+bMH+\omega)e^{-r/a},$$

where M is the Majorana operator interchanging position but not spin coordinates, and H the Heisenberg operator interchanging all coordinates. The constants A and a were taken to be those derived by Present and Rarita[2] from a study of the binding energies of the light nuclei. Calculations were carried out for three separate sets of assumptions regarding the constants m, h, b, ω:

I. Ordinary type forces
$m=h=0, \quad \omega=\frac{1}{2}(1+x), \quad b=\frac{1}{2}(1-x)$

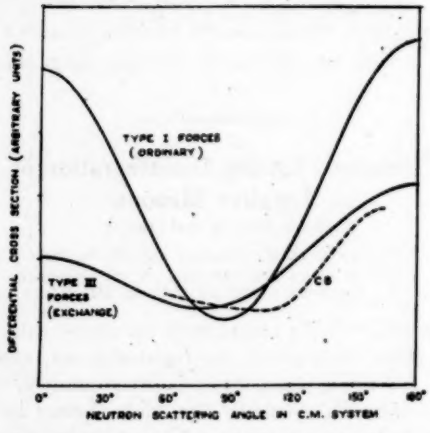

FIG. 1. Comparison of observed and calculated angular distributions, in the center of mass system, of 2.53-Mev neutrons scattered by deuterons.
The full line curves are according to the theory on the respective assumption of ordinary and exchange forces. The dashed curve gives observations of Coon and Barschall. The scale is adjusted to give agreement between theory and experiment near 90°.

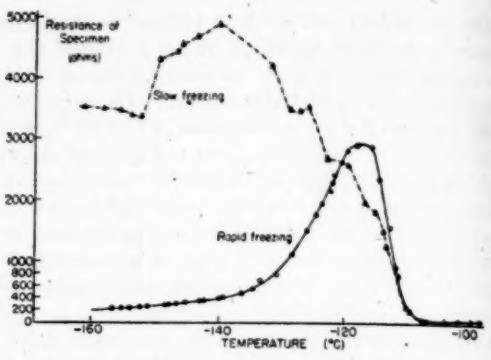

FIG. 2. Comparison of the observed and calculated total cross sections for collisions of neutrons with deuterons. The upper and lower curves are derived theoretically on the respective assumption of ordinary and of exchange forces. The vertical lines indicate values observed by Ageno, Amaldi, Bocciarelli, and Trabacchi, including range of error.

II. Exchange type forces
$\omega=b=0, \quad m=\frac{1}{2}(1+x), \quad h=\frac{1}{2}(1-x)$

III. Exchange type forces
$m=2b=\frac{1}{2}(1+3x), \quad h=2\omega=\frac{1}{2}(1-3x).$

All three of these are consistent with the binding energy of the ^1S as well as ^3S state of the deuteron, if x is taken to be 0.6.

It was found that, whereas the two exchange type forces II and III did not give substantially different results, they gave quite markedly different results from the ordinary type forces I for neutrons with energies greater than 2 Mev. At the time of writing of the paper there was little experimental information available to decide which assumption gave the best results. Recently two sets of measurements have been published, those of Coon and Barschall[3] on the angular distribution of 2.53-Mev neutrons scattered by deuterons, and those of Ageno, Amaldi, Bocciarelli, and Trabacchi[4] of the cross sections for elastic collisions of 4.1, 12.5, and 14-Mev neutrons with deuterons. Comparison of the theoretical predictions with these observations, as illustrated in Figs. 1 and 2, is interesting. On the whole, the evidence is decidedly in favor of exchange (Type III) forces. It is true that the observed cross sections for the higher energy neutrons are somewhat larger than predicted on the assumption of these forces, but this is to be expected as the additional contribution to the cross section from neutrons with two units of relative angular momentum has been ignored in the theory and it must be appreciable at these energies. The theory is being extended to allow for these contributions.

In our previously published theoretical work,[1] two forms of wave function for the doublet state of the three particle systems were used, referred to as doublet (a) and doublet (b) respectively. The second only of these has the correct form for a true doublet wave function, and it has been used in obtaining the theoretical results illustrated in Figs. 1 and 2.

[1] R. A. Buckingham and H. S. W. Massey, Proc. Roy. Soc. [A] 179, 123 (1941).
[2] R. Present and W. Rarita, Phys. Rev. 51, 788 (1937).
[3] J. H. Coon and H. H. Barschall, Phys. Rev. 70, 592 (1946).
[4] M. Ageno, E. Amaldi, D. Bocciarelli, and G. C. Trabacchi, Il. Nuov. Cimento 9, 1 1943; Phys. Rev. 71, 20 (1947).

The deHaas-van Alphen Effect in a Single Crystal of Zinc

JULES A. MARCUS
Yale University, New Haven, Connecticut*
March 10, 1947

IN 1930 deHaas and van Alphen[1] observed that the diamagnetic susceptibility of bismuth, which is independent of the field strength at ordinary temperatures, becomes a complicated periodic function of the field at temperatures of liquid hydrogen (20°K) and below. This has come to be known as the deHaas-van Alphen effect. The field dependence occurs only in a plane perpendicular to the trigonal axis. In this plane the susceptibility is anisotropic at 20°K and below but is isotropic at higher temperatures.

Subsequently, this effect was studied in greater detail by Shoenberg and Uddin[2] with respect to the influence of temperature and impurities. Blackman[3] developed a theory based on the particular electronic structure of bismuth which agrees qualitatively with these experiments but does not account for the fact that any slight change in the electronic structure caused by impurities decreases the magnitude of the effect. Blackman's theory also fails to account for the fact that the effect is not observed in antimony which has an electronic structure very similar to that of bismuth.

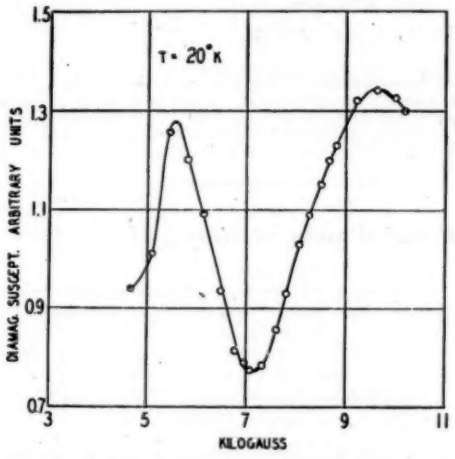

FIG. 1. Field dependence of the susceptibility parallel to the hexagonal axis of a zinc single crystal at 20°K.

In 1941 Nachimovich[4] reported an anomalous field dependence of the resistance of zinc at low temperatures. This suggested that the deHaas-van Alphen effect might occur in a single crystal of zinc since it was just such a resistance anomaly which led deHaas and van Alphen to investigate the magnetic susceptibility of bismuth.

Accordingly, the diamagnetic susceptibility of a single crystal of zinc has been measured from 20°K to 373°K in fields ranging from 4.5 to 10.5 kilogauss. It was found that at 20°K the susceptibility perpendicular to the hexagonal axis, $\chi_\perp$, is independent of the field while the susceptibility parallel to the hexagonal axis, χ_{11}, shows a marked field dependence. Figure 1 shows the variation of χ_{11} with field strength at 20°K. At 64°K this variation was only slightly larger than the experimental error and at 79°K it was no longer detectable. Figure 2 shows the variation in susceptibility with temperature at a constant field of 8.25 kilogauss. The behavior of $\chi_\perp$ is normal, being independent of temperature below 100°K and decreasing almost linearly in numerical value from 100°K to 373°K. On the other hand, χ_{11} shows anomalous behavior with pronounced maxima at approximately 40°K and 100°K and minima at 64°K and 180°K.

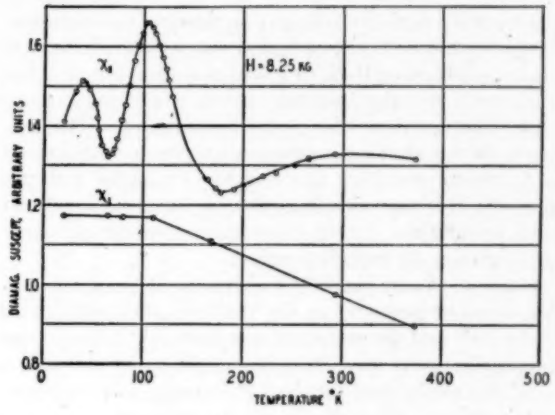

FIG. 2. Temperature variation of the susceptibility parallel and perpendicular to the hexagonal axis of a zinc single crystal at a constant field strength of 8.25 kilogauss.

Considering the difference in electronic structure between zinc and bismuth and the large difference in magnitude of the susceptibility, the similarity in the field dependence for χ_{11} in zinc and $\chi_\perp$ in bismuth is somewhat surprising. In relation to the absolute magnitude of the susceptibility at room temperature, the magnitude of the variation in χ_{11} with field for zinc is approximately twice that of $\chi_\perp$ in bismuth, although the spacing between maxima and minima is about the same in both cases.

The temperature dependence exhibited by χ_{11} for zinc does not seem to have been reported for any other metals. As the temperature variation of diamagnetism has not been worked out in detail, no comparison with theory can be made at present.

Further details of this research will be published at a later date.

The author wishes to thank Professor C. T. Lane and Dr. Henry Fairbank for their advice and assistance throughout the course of this investigation.

* Assisted by the Office of Naval Research under Contract N6ori-44.

[1] DeHaas and van Alphen, Comm. Phys. Lab. Leiden, No. 212a (1930).
[2] D. Shoenberg, Proc. Roy. Soc. **A170**, 341 (1939).
[3] Blackman, Proc. Roy. Soc. **A166**, 1 (1938).
[4] N. M. Nachimovich, J. Physiol. 6, 111 (1941). I am indebted to Professor C. T. Lane for calling my attention to this article.

Delayed Neutrons from Pu^{239}*

ROBERT R. WILSON**
Los Alamos Scientific Laboratory, Santa Fe, New Mexico
March 22, 1947

THE number of delayed neutrons from Pu^{239} relative to the number from U^{235} has been measured by means of a boron trifluoride ionization chamber immersed in a block of paraffin. The sample of Pu^{239} was placed on one end of the BF_3 chamber and the paraffin block was exposed to the direct beam of neutrons from the cyclotron target about 10 ft. away. The strong neutron intensity, with the cyclotron on, caused the grid of the first amplifier tube to drift to such a negative voltage that nothing was recorded. However, as soon as the cyclotron was turned off the grid voltage would snap back to a sensitive bias within a few milliseconds and the amplifier system would then record boron disintegrations due to delayed neutrons. The procedure, then, was to expose the block to the cyclotron beam for 5 minutes and then to count for 5 minutes with the beam off. This was sufficient time for the delays to build up to equilibrium during exposure and to die out completely during the recording period.

A sample of enriched U^{235} prepared in as nearly as possible the same geometry as the Pu^{239} was then substituted for the Pu^{239} and the procedure was repeated. To determine the contribution of the U^{238} in the sample, a disk of uranium metal was substituted for the U^{235} sample, and counts recorded. No sample at all gave no counts at all.

A comparison ionization chamber in which known amounts of Pu^{239}, enriched U^{235}, and enriched U^{238} could be placed was inserted in the paraffin block in the same position that the Pu^{239} or U^{235} sample had occupied. From the relative counts recorded and the known cross sections one can calculate that there are only 48 percent as many delayed neutrons per fission from Pu^{239} as there are from U^{235}. If one assumes the neutrons are all thermalized and applies a correction, the percentage of delayed neutrons from Pu^{239} relative to U^{235} is changed to 44 percent. However, not all the neutrons are thermal, so we can only say that the proper ratio lies within the range of 44–48 percent, and is probably about 46 percent. It is difficult to draw any conclusions about the delayed neutrons of U^{238} from the data.

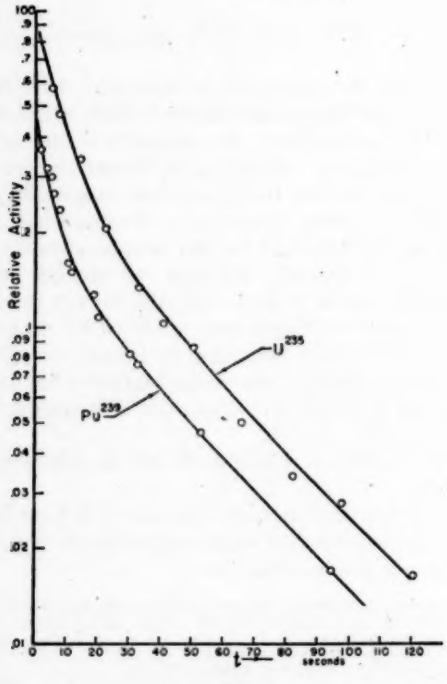

FIG. 1.

A decay curve was obtained for Pu^{239} by noting the time corresponding to each click of the scale-of-64 recorder just after the cyclotron was turned off. Similar data was taken for the U^{235} sample and the results plotted in Fig. 1. No difference between the two decay curves can be observed when the two are superimposed.

The above results indicate that the delayed neutrons observed possibly come from the same fission products in the case of Pu^{239} and U^{235}, but that the branching ratio for formation of these products for Pu^{239} is about 46 percent of that for U^{235}.

The author wishes to thank Roger B. Sutton for his assistance in taking the data.

* This letter is based on work performed in early 1944 at Los Alamos Scientific Laboratory of the University of California under Contract W-7405-eng-36 for the Manhattan Project and the information contained therein will appear in Division V of the Manhattan Project Technical Series as part of the contribution of the Los Alamos Laboratory.
** Now at Cornell University, Ithaca, New York.

Proton-Proton Scattering at 14.5 Mev

ROBERT R. WILSON*
Harvard University, Cambridge, Massachusetts
EDWARD J. LOFGREN,** J. REGINALD RICHARDSON,***
BYRON T. WRIGHT***
Radiation Laboratory, University of California, Berkeley, California
AND ROBERT S. SHANKLAND
Case School of Applied Science, Cleveland, Ohio
March 17, 1947

THE 37-inch synchro-cyclotron at the Radiation Laboratory at Berkeley has been adjusted to give a deflected beam of 14.5-Mev protons.[1] These protons have been used to study the scattering of protons by protons. The apparatus used was a coincidence counting arrangement which had been constructed at Princeton for use with the 8-Mev protons available there,[2] and which had been used for studying the scattering of the 10-Mev protons available from the Crocker cyclotron at Berkeley.[3]

The scattering foil was made of Nylon $(C_{12}H_{22}N_2O)_x$ whose thickness in the direction of the beam was equivalent to $(1.63\pm.05)10^{19}$ hydrogen atoms per cm^2. This figure was obtained from thickness measurements made with a Jamin interferometer, chemical analyses of the hydrogen content of the foil, and a knowledge of the refractive index and density of the Nylon. The solid angle subtended at the scatterer by the defining aperture of the proportional counter was known, and the total number of protons in the incident beam was measured by a current integrating system consisting of a Faraday cup, a coaxial shielded

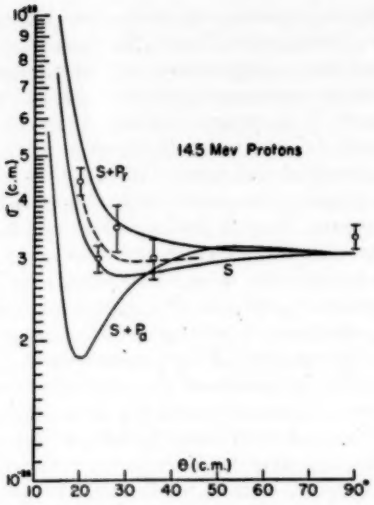

FIG. 1. The absolute scattering cross section per unit solid angle as a function of the angle. Both coordinates refer to the center of mass system.

cable, a standard condenser, and a quadrant electrometer; the whole system being calibrated.

The pulsed nature of the beam from the synchrocyclotron made the correction for accidental coincidences appreciable. The background counts were due partly to protons and partly to neutrons. Since the pulse width of the neutrons was larger than that of the protons, it was necessary to use the rather complicated correction formula

$$n_a=\frac{2\tau}{R\delta}\left[n_1n_2+\left(\frac{1}{f}-1\right)n_1{}^Pn_2{}^P\right],$$

where n_a is the number of accidentals per second, n_1 and n_2 the total counting rate in each channel, $n_1{}^P$ and $n_2{}^P$ the counting rate in each channel due to protons only, τ the resolving time of the coincidence system, R the repetition rate, δ the width of the neutron pulse, and f the ratio of the width of the proton pulse to that of the neutron pulse. The formula was derived on the assumption of square pulse shape. The lumped constant $2\tau/R\delta$ was determined to be 0.99×10^{-5} sec. by counting the neutron background counts only; i.e., proton beam cut off by a shutter. The fraction f was determined to be 0.25 by misaligning the proportional counters so that no true coincidences should occur.

The number of background counts due to protons was determined after each ten-minute run by subtracting from the total counting rate the neutron rate found by a blank run during which the proton beam was shuttered off. The average accidental correction amounted to about twenty-five percent of the observed coincidences. At the smallest angles of scattering, i.e., 10°, and 12° (laboratory system), it was necessary to add a calculated correction of 8 and 3 percent, respectively, because some of the scattered and recoil protons were geometrically unable to enter both counters.

TABLE I. Scattering cross sections of 14.5-Mev protons on protons.

θ	n	σ	ϵ
20°	12	4.4×10^{-26} cm²	$\pm0.3\times10^{-26}$ cm²
24°	20	3.0	0.2
28°	7	3.5	0.4
36°	11	3.0	0.3
90°	34	3.34	0.2

The final results obtained are given in Table I where θ is the scattering angle measured in the center of mass system, n is the number of ten-minute cyclotron runs at each angle, σ is the absolute scattering cross section per unit solid angle in the center of mass system, and ϵ is the experimental mean-square error determined from the deviations of the values given by each ten-minute run from the mean.

In Fig. 1 the experimental values of σ are compared with theoretical calculations made by L. L. Foldy[4] on the assumption of a square well of depth 10.5 Mev and width (e^2/mc^2), both for S wave scattering alone and for S plus P wave scattering with the potential for the P wave attractive (lower curve) and repulsive (upper curve). The data are definitely inconsistent with any P wave attractive effects. They are not inconsistent with pure S wave scattering or with an admixture of repulsive P wave effects. Perhaps the dotted curve of Fig. 1 is indicated; it corresponds to an admixture of P wave effects due to about one-third the repulsive interaction of the upper curve. This would be consistent with the result found at 10 Mev.[3]

We wish to express our appreciation to Professor E. O. Lawrence for making the facilities of the Radiation Laboratory available to us.

* Now at Cornell University, Ithaca, New York.
** Now at the University of Minnesota, Minneapolis, Minnesota.
*** Now at the University of California at Los Angeles, California.
[1] J. R. Richardson, K. R. MacKenzie, E. J. Lofgren and B. T. Wright, Phys. Rev. 69, 669 (1946).
[2] R. R. Wilson and E. C. Creutz, Phys. Rev. 71, 339 (1947).
[3] R. R. Wilson, Phys. Rev. 71, 384 (1947).
[4] Private communication, to be published shortly.

Neutron Cross Sections for Mercury Isotopes

MARK G. INGHRAM, DAVID C. HESS, JR., AND RICHARD J. HAYDEN
Argonne National Laboratory, Chicago, Illinois
March 10, 1947

ONE hundred twenty-five milligrams of α-phase mercuric sulfide were submitted to long bombardment by neutrons in a graphite pile. To liberate the mercury, the sample was placed in a closed system and heated while oxygen was flowing through the system. The free mercury obtained was collected at −40°C in a glass sample tube, and then transferred to the sample system of a Nier type mass spectrometer.[1] The isotopic composition of the bombarded sample was then compared with that of normal mercury. The data obtained are summarized in Table I.

Each of the values in this table is the average of 50 results. The comparative values of the cross sections as listed in the table are better than the absolute values. This is due to the fact that with a fixed neutron energy distribution the former depends only on the accuracy of the mass spectrometer measurement while the latter depends on a knowledge of the magnitude of the integrated flux.

These data show that there are two big neutron absorbers

in mercury, the isotopes at masses 196 and 199. Since the 199 is 110 times as abundant as the 196 most of the neutron absorption in normal mercury is due to the isotope of mass 199.

TABLE I. Isotopic composition of neutron irradiated mercury.

Mass No.	% Abundance normal	% Abundance bombarded	Net change	Isotopic cross sections in 10^{-24} cm²	Contribution to total section in 10^{-24} cm²
196	0.155	0.120	-0.035 ± 0.002	3100	4.8
197	<0.001	<0.001	—	—	—
198	10.12	10.17	$+0.05\pm0.05$	—	—
199	17.01	13.78	-3.23 ± 0.07	2500	425
200	23.21	26.52	$+3.31\pm0.03$	<60	<15
201	13.15	13.11	-0.04 ± 0.07	<60	<8
202	29.66	29.63	-0.03 ± 0.15	<60	<18
203	<0.001	trace	+trace	—	—
204	6.69	6.68	-0.01 ± 0.03	<60	<4
205	<0.001	<0.001	—	—	—

In the cases of the isotope of mass 198, 200, 201, 202, and 204 it was possible only to assign upper limits to the cross sections. The upper limits in the Table I were deduced by assuming only $(n-\gamma)$ reactions. There are some indications at masses 199 and 201, however, that reactions other than $(n-\gamma)$'s took place; in particular $(n-2n)$'s. The occurrence of such a reaction in this sample was possible since there was a considerable flux of fast neutrons in the pile. A much heavier flux, or a different flux distribution, would be necessary to prove this point.

No peak was detected at mass 197 so that all the mercury 197 formed by $(n-\gamma)$ reaction on mercury 196 decayed by K capture to gold 197. Thus 35 micrograms of gold were formed from the 100 milligrams of mercury.

The weak peak at mass 203 was probably caused by a long-lived $(n-\gamma)$ induced activity in mercury as it was not observed in the normal sample. This is probably the 51-day β-activity known to exist in mercury.[2]

[1] Mark G. Inghram, Phys. Rev. **70**, 653 (1946).
[2] Glenn T. Seaborg, Rev. Mod. Phys. **16**, 1 (1944).

Fine Structure of H_α

L. GIULOTTO
Istituto di Fisica "A. Volta" dell'Università di Pavia, Pavia, Italia
March 10, 1947

THE fine structure of H_α has been again examined with a Lummer plate and with a Fabry Pérot étalon. The source was a hydrogen discharge tube submerged in liquid air. Trials were made under various conditions of pressure and current density. The separation of the apparent doublet resulted in an average value of 0.310 ± 0.007 cm^{-1}. The results relative to a particular series of spectra have been examined with great care and compared with the results of Dirac's theory. The apparent doublet has been reconstructed by assigning to every theoretical component an intensity curve $\exp[-k(\nu-\nu_0)^2]$ and to k a value derived from the experimental curve.

The "reconstructed" doublet differs from the experimental one in regard to the intensities and to the distance between the two maxima, which for the "reconstructed" doublet has a value of 0.327 cm^{-1}. We have tried to establish whether these disagreements may be ascribed only to the fact that the experimental intensities of the components are not exactly in agreement with the values calculated by Dirac's theory. In order to fit well the reconstructed doublet to the experimental one without changing the separations of the components, we should triple the intensity of the third component, keeping for the others about the theoretical intensities. But such a change of intensity, affecting almost exclusively the third component, would disagree with Sommerfeld's and Unsöld's[1] suggestion according to which the deviations from the theoretical intensities are due to the fact that the $2S$ level is metastable.

The observed deviations of the separation between the two maxima of the experimental and reconstructed doublet can certainly not be attributed to the overlapping of lines of the molecular spectrum, as Drinkwater, Richardson, and Williams[2] suppose, because the intensity of the molecular spectrum near H_α under our experimental conditions was practically zero.

If in the experimental measurements a mysterious systematic error does not occur, we should conclude, in accord with C. R. Williams' observations,[3] that the separations between the components do not correspond exactly to the calculated ones on the basis of Dirac's theory. As Sommerfeld[4] has shown, using Dirac's theory also, the deviations from the coulombian field in the neighborhood of the nucleus cannot explain the deviation observed by C. R. Williams. However, it is not certain that the formalism of the quantum mechanics maintains its validity for problems involving distances of the order of the nuclear radius. Therefore, we may hope that, when a suitable formalism is found, the small observed deviations may be justified.

[1] A. Sommerfeld and A. Unsöld, Zeits. f. Physik **36**, 259 (1926).
[2] J. W. Drinkwater, O. Richardson, and W. E. Williams, Proc. Roy. Soc. London **A174**, 165 (1940).
[3] R. C. Williams, Phys. Rev. **54**, 558 (1938).
[4] A. Sommerfeld, Zeits. f. Physik **118**, 295 (1941).

A Microwave Spectrograph*

RICHARD H. HUGHES AND E. BRIGHT WILSON, JR.
Harvard University, Cambridge, Massachusetts
March 24, 1947

WE have constructed a microwave spectrograph of the wave-guide absorption cell type[1] which appears to be somewhat more sensitive than others which have been described. The basic principle is the use of a radiofrequency Stark effect field[2] which modulates the absorption by the gas so that a radio receiver can be used for detection purposes. The apparatus consists of the usual 2K33 K-band klystron oscillator tube, attenuator, a 5½-foot length of K-band wave guide, and a crystal detector, the output of which goes to a narrow-band communication receiver. The amplified output of the receiver is displayed on an oscilloscope screen. The wave guide is fitted with a central electrode insulated from the walls in the form of a brass strip inserted parallel to the broad sides of the wave guide[3] and is made gas-tight with mica windows. An oscillator supplies

a radiofrequency voltage to this electrode. In addition a d.c. potential is applied to the same electrode. The radio receiver is tuned to the same frequency as the oscillator (80 Kc has been used), or alternately (and less effectively) to various overtones of this frequency. A sawtooth voltage at about 20 cycles per second is applied to the reflector grid of the klystron and also to the horizontal plates of the cathode-ray oscillograph in order to sweep the tube through a small frequency range.

When the frequency of the klystron passes through an absorption frequency of the gas, a small part of the microwave energy is modulated because of the varying absorption of the gas as the Stark effect components are moved back and forth in frequency by the alternating Stark effect field. A radiofrequency component then appears in the crystal output and is amplified by the radio receiver and displayed on the oscilloscope screen. The shape of the curve, which is displayed when a line is present, is a complicated function of the nature of the Stark effect of the particular molecule.

The minimum detectable absorption depends upon the nature of the Stark effect of the given substance. Even with the short wave guide used, the apparatus is able to display the $J=1$, $K=1$ line of the inversion spectrum of N^{15} ammonia present in its natural proportion of 0.3 of 1 percent in ordinary ammonia.

Dr. B. P. Dailey and Mr. Robert Karplus have contributed heavily to the success of this experiment. We also wish to thank Dr. Stuart P. Cooke for the assistance rendered by himself and by other members of the Microwave Research Group. Dr. A. G. Hill of the Research Laboratory of Electronics, Massachusetts Institute of Technology, very kindly aided us through loans of apparatus.

* The research reported in this document was made possible through support extended Harvard University jointly by the Navy Department (Office of Naval Research) and the Signal Corps, U. S. Army, under Office of Naval Research contract N5ori-76.

[1] See for example, W. D. Hershberger, J. App. Physics 17, 495 (1946), W. E. Good, Phys. Rev. 70, 213 (1946), and C. H. Townes, Phys. Rev. 70, 665 (1946). We are indebted to Dr. Hershberger for giving us a detailed description of his apparatus.

[2] A principle similar to this has been used in a different way by E. M. Purcell, H. C. Torrey, and R. V. Pound, Phys. Rev. 69, 37 (1946), and by Arthur Roberts, Robert Beers, and A. G. Hill, Phys. Rev. 70, 112 (1946).

[3] As described by T. W. Dakin, W. E. Good, and D. K. Coles, Phys. Rev. 70, 560 (1946).

Conductivity of Sodium-Ammonia Solutions

D. K. C. MacDonald and K. Mendelssohn
Clarendon Laboratory, Oxford, England
and
A. J. Birch
Dyson Perrins Laboratory, Oxford, England
March 10, 1947

IN an earlier communication, two of us in collaboration with J. G. Daunt and M. Désirant[1] had reported failure to reproduce R. A. Ogg's observation[2] of superconductivity in solidified sodium-ammonia solutions. We had then worked under the assumption that the reported persistent currents had the same well-reproducible character as with established superconductors. When from a subsequent communication by Ogg[2] it became clear that the phenomena

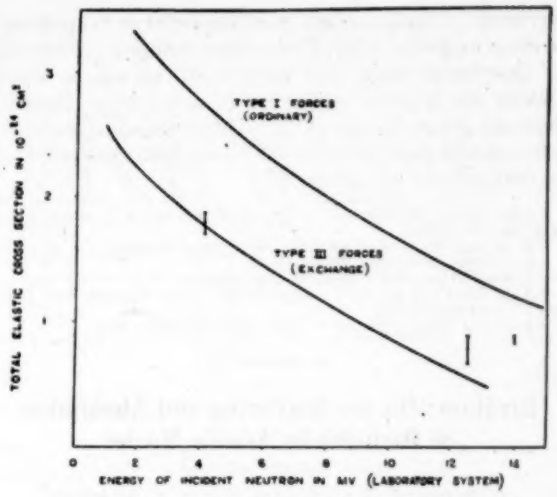

FIG. 1. Variation of resistance of a 2.1 percent ($\sim 1N$) sodium-ammonia solution.

observed by him were of a rare and transient nature, we had to admit the possibility that similar effects might have escaped our notice. In view of the importance of the possibility of superconductivity at relatively high temperatures, and also because of a confirmatory report by J. W. Hodgins,[4] a more extensive investigation of the electric, thermal, and magnetic properties of sodium-ammonia solutions was undertaken. While a full report of this work will be published elsewhere[5] a short statement of some of the conclusions reached may be of interest.

Resistivity measurements using a current-potential method were carried out on thin continuous layers of the frozen solution. In the case of $1N$ solutions, different behavior was in fact observed according to the speed with which the samples were frozen. As is shown in the accompanying figure, in general, rapid freezing yielded low resistance at low temperatures, slow freezing, high resistance. The figure illustrates the subsequent behavior on warming to higher temperatures with a very marked drop of resistivity at -114°C. In all cases, *finite conductivity* was observed throughout the experiments. As became evident from our thermal experiments, these results are readily explicable by the formation of a concentrated highly-conducting eutectic (m.p.: -114°C) (see also Ruff and Zedner[6]) which is readily supercooled.

Persistent current experiments were carried out with ring-shaped specimens similar to those used by Ogg[2] except that in all cases the formation of a continuous annulus was ensured. In the first experiments transient magnetic moments of the order described by Hodgins were indeed observed, but it was then detected that these were produced by the presence of iron objects in the laboratory or by very small vibrations of the search coil. Since the field to be detected only amounts to one-fiftieth of the vertical component of the earth's magnetic field, a slight tilting of the search coil would readily yield a false indication. Great care had therefore to be taken to avoid such disturbances and also others, as for instance would be produced by the dis-

placement of liquid oxygen (paramagnetic) in the presence of stray magnetic fields. Under these stringent conditions, 85 experiments were then carried out, no one of which yielded the slightest indication of a persistent current. Separate determination of the volume magnetic susceptibility of both rapidly and slowly frozen specimens provided no indication of any anomaly.

[1] J. G. Daunt, M. Désirant, K. Mendelssohn, and A. J. Birch, Phys. Rev. 70, 219 (1946).
[2] R. A. Ogg, Phys. Rev. 69, 243 (1946); 69, 544 (1946).
[3] R. A. Ogg, Phys. Rev. 70, 93 (1946).
[4] J. W. Hodgins, Phys. Rev. 70, 568 (1946).
[5] A. J. Birch and D. K. C. MacDonald, Trans. Faraday Soc. (submitted for publication).
[6] Ruff and Zedner, Ber. d. d. chem. Ges. 41, 1948 (1908).

Erratum: On the Scattering and Absorption of Particles by Atomic Nuclei

[Phys. Rev. 71, 145 (1947)]

H. Feshbach, D. C. Peaslee, and V. F. Weisskopf
Physics Department, Massachusetts Institute of Technology, Cambridge, Massachusetts

THE neutron scattering cross section as a function of energy in the neighborhood of a resonance as given in Fig. 3 of our paper on the Scattering and Absorption of Particles by Atomic Nuclei is correct only if the spin of the nucleus is zero. This is not true for indium whose spin $I=9/2$, for then the compound nucleus may have a spin I_c of 4 or 5. As a result, the scattering cross section for indium is found by adding the cross sections for both of these states weighting the $I_c=5$ state by $\frac{1}{2}(1+1/(2I+1))=11/20$ and the $I_c=4$ state by $\frac{1}{2}(1-1/(2I+1))=9/20$. The graph in this note shows the scattering of neutrons by indium in the neighborhood of the 1.44 ev level for the two possible assumptions 4 and 5 for the spin of the compound nucleus involved in the resonance. We have used some improved constants recently made available,[1] namely $\Gamma=0.09$ ev and $(1\pm1/(2I+1))\Gamma_n=2.5\ 10^{-3}$ ev The cross section from "potential scattering" alone, $4\pi a^2$, is $6.6\ 10^{-24}$ cm^2.

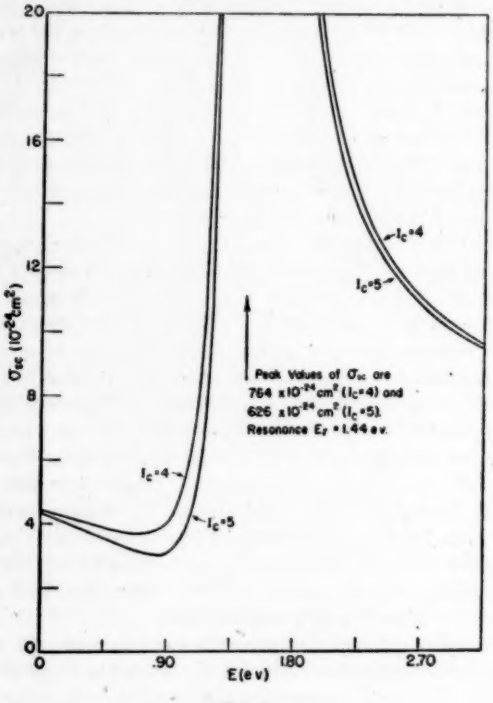

FIG. 1.

[1] B. D. McDaniel, Phys. Rev. 70, 832 (1946).

Atmospheric Temperatures from Infra-Red Emission Spectra of the Moon and Earth. I. The Ozone Layer

Arthur Adel
The McMath-Hulbert Observatory, The University of Michigan, Lake Angelus, Pontiac, Michigan
March 24, 1947

A FUNDAMENTAL and independent method of determining the temperature of the ozone layer has been applied to previously published infra-red emission spectra of the moon, the earth, and the atmosphere.[1] (The method is a general one, and is applicable as well to the atmospheric constituents H_2O, N_2O, CO_2.) The emissivity of atmospheric ozone in the band ν_3[2] at 9.6 mu is provided by the corresponding absorptivity in the lunar spectrum.[1] A gray-body comparison, in the spectral region occupied by the band, approximately 9 mu to 10 mu, is then made between the radiation intensity of the earth's surface (thermocouple) to space and the return radiation intensity of the ozone layer.[1] The method is a promising one, for even the preliminary, very low resolution spectra yield essentially correct temperatures. The temperature of the ozone layer is found to be −44°C and −53°C for the evenings of September 5, 1941 and November 3, 1941, respectively.[3]

[1] Arthur Adel, Astrophys. J. 103, 19–25 (1946).
[2] Arthur Adel and David M. Dennison, J. Chem. Phys. 14, 379–382 (1946).
[3] A connection between the comparatively high temperature of −44°C and the unusually high absorption and emission by atmospheric ozone on the night of September 5, 1941, is conjectural. The details of the calculations are contained in a paper which is scheduled to appear in a forthcoming issue of the *Astrophysical Journal*.